TAMPEREEN TEKNILLINEN YLIOPISTO
TAMPERE UNIVERSITY OF TECHNOLOGY

Jerome Geoffrey Chandraseelan

Synthetic Genetic Circuits: Plasticity and Robustness

Julkaisu 1316 • Publication 1316

Tampere 2015

Tampereen teknillinen yliopisto. Julkaisu 1316
Tampere University of Technology. Publication 1316

Jerome Geoffrey Chandraseelan

Synthetic Genetic Circuits: Plasticity and Robustness

Thesis for the degree of Doctor of Philosophy to be presented with due permission for public examination and criticism in Tietotalo Building, Auditorium TB109, at Tampere University of Technology, on the 17th of September 2015, at 12 noon.

Tampereen teknillinen yliopisto - Tampere University of Technology
Tampere 2015

ISBN 978-952-15-3560-4 (printed)
ISBN 978-952-15-3592-5 (PDF)
ISSN 1459-2045

Abstract

Living organisms have evolved to survive in a multitude of environmental conditions. This plasticity, and the robustness to environmental fluctuations, is achieved by altering gene expression levels in response to perturbations while maintaining the basic processes essential for survival. Genetic circuits, which are networks of interacting genes, are responsible for carrying out both the basic processes to sustain life, such as counting time, as well as the specific processes that provide them with adaptability to various environmental conditions while maintaining homeostasis.

Gene expression and its regulation are dynamic, stochastic processes. Namely, although gene expression was previously considered to be identical in cells arising from common ancestors, the observation of multiple, single cells expressing fluorescent proteins has shown that gene expression is noisy, which allows genetically identical cells in a homogeneous environment to behave differently, a phenomenon known as cell-to-cell phenotypic variability. Noise in gene expression arises from the fact that most of the underlying biochemical reactions involve small molecular numbers, which leads to infrequent, to some extent random in time, interactions and processes. While initially noise in gene expression was considered to be disadvantageous to the organisms, a number of recent studies suggest significant functional roles for noise in intracellular processes.

The complexity and size of natural genetic circuits hampers their detailed study at present. One approach to overcome this problem is based on design of small, and thus more tractable, artificial circuits. Aside from its small size, in such circuits, all components are known and there is less chance that they interact with unknown cellular components. This strategy offers additional advantages, such as testability of whether a certain architecture is able to generate a desired trait or function without affecting natural cellular processes e.g., by inducing other downstream effectors that affect cell functioning. Moreover, it provides an opportunity to compare different circuit designs and determine which circuit architecture is preferable. Finally, due to detailed knowledge of

their structure, the behavior of these circuits can be computationally simulated to assist, e.g., the study of their long-term behaviors, among other. Previous studies based on synthetic circuits have already provided key insights into the design principles and architecture of genetic circuits, such as how these organize genes so as to gain the ability to make decisions or track time. These circuits are also expected to become of great use in therapeutic and industrial applications.

In this thesis, we focused on the study of the phenotypic plasticity and robustness of synthetic genetic clocks. We focused on the effects of temperature, copy number and the role of components; proteins and promoters, of the circuit. For this, we made use of the well-known genetic Repressilator, a synthetic genetic clock that is also one of the simplest genetic circuits known to be functional in a living system. To assist the studies, aside from techniques from cell and molecular biology, we made use of state of the art techniques in microscopy and image analysis. From the data, we characterized, first, the phenotypic plasticity of individual genes in *Escherichia coli*, as these are the main components of the Repressilator. Next, we performed a study of the effects of temperature on the dynamics of the genetic Repressilator. Subsequently, we studied the degree of synchrony between sister cells, each containing the Repressilator, in order to evaluate the extent to which cell division affects the dynamics of this circuit. Finally, we inserted the Repressilator genetic code into a single-copy vector so as to, by comparison with the original construct, study the effects of copy numbers on the dynamics of the circuit.

Preface

First and Foremost, I express my sincere thanks to my supervisor, Andre Ribeiro, for providing me this opportunity to carry out research in the Laboratory of Biosystem Dynamics. I thank him for his constant guidance, support and motivation while carrying out the research work.

I thank Dr. Andrey Kan and Asst. Prof. Ilda Santos Sanches for reviewing the thesis and for their valuable comments and suggestions.

I thank Assistant Professor Meenakshisundaram Kandhavelu, for his support and discussions during the initial stage of this work. My sincere thanks to all the co-authors and the members of the Laboratory of Biosystem Dynamics for their support in completing this thesis.

I thank all the members of the Faculty for providing immense support. My special thanks to the Virve Larmila, Juha Peltonen and the coordinators Elina Orava and Ulla Siltaloppi, for their kind support during my studies.

Special thanks to my beloved wife Shema Angelina and my daughter Stacy Gabriella for their immense love and support.

I sincerely thank my parents, my grandmother and my brother for their everlasting love and support.

Tampere, July 2015

Jerome Geoffrey Chandraseelan

Contents

List of publications

This thesis is based on the following publications. The publications are reproduced with permission from the publishers.

1. Mäkelä, J., Kandhavelu, M., Oliveira, S. M. D., Chandraseelan, J. G., Lloyd-Price, J., Peltonen, J., Yli-Harja, O and Ribeiro, A. S. (2013). *In vivo single-molecule kinetics of activation and subsequent activity of the arabinose promoter*. Nucleic Acids Res. 41(13):6544-52.

2. Chandraseelan, J. G., Oliveira, S. M. D., Potapov, I., Häkkinen, A., Kandhavelu, M and Ribeiro, A. S. (2013). *Temperature dependence of the LacI-TetR-CI Repressilator*. Mol. Biosyst. 9(12):3117-23.

3. Chandraseelan, J. G., Oliveira, S. M. D., Häkkinen, A., Startceva, S and Ribeiro A. S. (2015). *Synchrony between Genetic Repressilators in Sister Cells in Different Temperatures*. International Science Index. 9(7). Paper presented at Proceedings of the International Conference on Computational and Molecular Systems Biology 2015, Zurich (Switzerland). World Academy of Science, Engineering and Technology.

4. Oliveira, S. M. D *., Chandraseelan, J. G *., Häkkinen, A., Goncalves, N. S. M and Ribeiro A. S. (2015). *Single-cell kinetics of the Repressilator when inserted into a single-copy plasmid*. Mol. BioSyst., 2015, 11, 1939-1945. (* equal contribution)

In this thesis we studied the phenotypic plasticity and robustness of synthetic genetic clocks. We focused on the effects of temperature, copy number, role of component proteins, and promoters of the circuit. For that we made use of the genetic Repressilator, which is one of the simplest genetic circuits known to be functional in a living system. In the following section, we describe the contribution of the scientific papers to this effort and the contribution of the author of this thesis in each of these scientific papers.

In Publication 1 (published in Nucleic Acids Research), we studied transcription dynamics from a promoter. Specifically, we studied the influence of the inducer intake kinetics and its transient effect on the kinetics of transcription. The author of the thesis contributed to this study as follows. First, the author, along with M. Kandhavelu, conducted preliminary microscopy measurements to study transcription dynamics from the promoter. Next, the author designed and conducted the qPCR measurements that validated the results obtained from the microscopy measurements. Finally, the author participated in writing of the manuscript, particularly in sections reporting the results in which the author was involved in.

In Publication 2 (published in Molecular Biosystems), we studied the effects of temperature on the dynamics of the Repressilator. For that, we subjected cells containing the Repressilator to various temperatures and measured the oscillatory dynamics, in terms of fluorescence levels, exhibited by the cells over time. Specifically, we focused on the effects of temperature on the mean period and robustness of the oscillations. From the results, it is evident that temperature has a profound effect on the dynamics of the Repressilator. Further studies on the dynamics of the CI-Cro Switch, using the MS2-GFP RNA detection method, revealed that the loss of functionality of CI, which is a component protein of both the Repressilator and the Switch, with increasing temperature leads to the observed failure of oscillations in the Repressilator at higher than optimal temperatures. The author of this thesis contributed to Publication II by, first, developing a protocol that allows the cells containing the Repressilator to produce oscillations under the microscope, and then by conducting microscopy measurements at all the temperature conditions considered in the study. The author also contributed in the preparation of the manuscript by suggesting ideas such as that CI loses functionality with increasing temperature based on previous studies.

Publication 3 (published in International Science Index, World Academy of Science, Engineering and Technology) is a follow up of the Publication 2. Here, we studied the effect of temperature on the synchrony of oscillations is sister cells following division of their mother cell. For that, we selected functional sister cells and estimated the loss of synchrony by calculating correlation coefficients between sister cells. The outcomes of

this study suggest that increases in temperature increase the loss of correlation between sister cells over time. The author of this thesis contributed to the study as follows: firstly, by conducting confocal microscopy measurements and then by performing the analysis of the images of sister cells that allowed the subsequent calculation of the degree of loss of synchrony. Finally, the author contributed in the writing of the manuscript.

In publication 4 (published in Molecular Biosystems), we studied the effects of changing the copy-number of the vector on the dynamics of the Repressilator. For that, we inserted the Repressilator in to a single-copy vector and studied the oscillatory dynamics. The study reveals that changing the copy-number of the Repressilator has strong effects on the dynamics of the Repressilator in individual cells. Namely, the results suggest that implementing the Repressilator on a single-copy vector provides this circuit with greater functionality than the original low copy Repressilator, although it causes increased mean and variability of the period of oscillations. From the analysis of the effects of temperature on the dynamics of the Repressilator, we observed also that the functionality of the single-copy Repressilator is higher at optimum and lower-than-optimal temperature conditions. Also, the single-copy Repressilator was found to be more robust than the low-copy Repressilator to external perturbations. The author of this thesis contributed to this study as follows. Firstly, the author designed and constructed the single-copy Repressilator. Next, the author performed most of the microscopy measurements and the qPCR analysis to validate the functionality of single-copy Repressilators in the cells. The author also contributed in the writing of the manuscript.

Publication 1 will be used by Jarno Mäkelä in his doctoral thesis.

Publication 2, 3 and 4 will be used by Samuel Matos Dias Oliveira in his doctoral thesis.

1 Introduction

1.1 Background and motivation

During the course of evolution, living systems have evolved adaptability to survive in a wide range of environmental conditions and compensate for the perturbations caused by changes in the environmental conditions (Cagliero *et al*., 2013; Stoebel *et al*., 2009) or by interactions with other beings. Genetic circuits, formed by a network of interacting genes, are responsible for carrying out the complex processes that provide this adaptability at a cellular level. such as counting time, responding to signals from the environment, and regulating cellular processes that perform the basic functions needed for maintaining homeostasis (Becskei *et al*., 2000).

Some of the genes in the gene regulatory networks (GRN) form 'genetic clocks' which control the timing of activity of other genes. For example, circadian oscillators, found in many living systems, control the expression of other genes in the GRN with high temporal stability. These circuits are robust to fluctuations and resilient to perturbations caused by intrinsic factors and extrinsic factors (Mihalcescu *et al*., 2004). Perturbations in the functioning of these genetic clocks has been linked to many diseases, including cancer, neural disorders, etc. (Fussenegger, 2010). Hence, understanding the regulation of these genetic circuits and their architecture is of importance for understanding several diseases and, thus, for therapeutic purposes.

Many of the elements involved in the regulation of gene regulatory networks have been identified using biochemical and molecular biological approaches. Though scientists were able to identify several of the molecules involved in gene expression regulation and, from there, produce gene interaction maps, some fundamental questions such as why a given architecture is preferred over another and how genetic circuits respond to fluctuations, still remain unanswered (Nandagopal *et al*., 2011).

Synthetic biology is an alternative approach to answer these questions. Its aim is to engineer synthetic gene networks and study how the architecture of the network influences the regulation of gene expression. In general, well-characterized genetic components are used. Also, the topologies used are derived from the design principles from electrical engineering (Guido *et al*., 2006; Miyamoto *et al*., 2013). One of the major advantages of using this approach is expected to be the enhanced predictability of the behaviour of the circuits, via the use of techniques from computational biology. A number of synthetic genetic circuits have been designed and proven to exhibit the predicted behaviour (Elowitz *et al*., 2000; Stricker *et al*., 2008). The basic components used for the construction of a synthetic genetic circuit are: the Transcription unit, which comprises of a promoter followed by a gene that encodes a protein and a downstream terminator; the Input signal, which may arise from the environment or within the cell; and the Regulators of transcription, namely activators and repressors which can be produced by the network or be external in origin (Savageau, 2001).

In this thesis, we aimed to study the phenotypic robustness and plasticity of single genes and small synthetic genetic clocks. For that, we used the Repressilator, which is one of the first built, and simplest, synthetic genetic circuits known to be functional in a living organism (Elowitz *et al*., 2000). It consists of three promoters connected together in a negative feedback loop such that transcriptional activity of one of the promoters in the loop represses the activity of the subsequent promoter (Elowitz *et al*., 2000), leading to periodic fluctuations in protein levels. These fluctuations can be visualized as oscillations in the level of Green Fluorescence Proteins (GFP) produced from a reporter plasmid, which encodes GFP under the control of one of the promoters of the Repressilator. The thesis, a compilation of works we recently published on this topic, begins with a study on

the responsiveness and phenotypic plasticity of an individual promoter at the RNA level, followed by a study on the dynamics of the Repressilator at different temperatures. Next, we present a study on the effects of temperature on the degree of synchrony of the Repressilator between sister cells. Finally, we studied the effect of the intra-cellular copy-number of the Repressilator on its dynamics.

1.2 Thesis objectives

This thesis is aimed at studying the phenotypic plasticity and robustness of a genetic circuit, namely the Repressilator. The findings of this study are expected to aid in the development of new synthetic genetic circuits. The objectives are as follows:

In objective 1, we aimed to study transcription initiation dynamics when based on the introduction in the media of an external inducer and the transcription dynamics following activation. Transcription initiation is of particular interest as most of the gene expression regulation occurs at this stage (Latchman, 2007). Moreover, it has been reported that bacterial adaptation to stress involves modifications in transcription patterns (Stoebel *et al*., 2009). Transcription initiation is a multi-stepped sequential process that comprises several rate-limiting steps. The number of rate-limiting steps differ between conditions and between different promoters (Mcclure, 1980). Relevantly, objective 1 also included the development of methods of studying transcription dynamics from time-lapse, single RNA detection.

Temperature affects gene expression regulation on a global scale, both by altering the thermodynamic rate of the underlying reactions (Gadgil *et al*., 2005; Muthukrishnan *et al*., 2012; Stricker *et al*., 2008) as well as by influencing the physical and chemical properties of the effector molecules (Hansen *et al*., 2014). The model organism used in this study, *E. coli*, is known for its ability to survive at different temperatures. Previous studies have shown that changes in temperature affect transcription dynamics in *E. coli* (Bertrand-Burggraf *et al*., 1984; Muthukrishnan *et al*., 2013). To study the effect of the temperature induced changes on the transcription dynamics on genetic circuits, in

objective 2, we studied the effect of temperature on the dynamics of the Repressilator, which exhibits oscillatory dynamics at 30^{o} C (Elowitz *et al*., 2000). Specifically, we characterized the role of one of the components, the lambda repressor cI, on the temperature-dependence of the dynamics of the Repressilator.

Synchrony of oscillations in different cells is one of the crucial traits observed in biological oscillators, which is important for performing complex, dynamic processes involving multiple cells (Kruse *et al*., 2005). Natural biological oscillators, such as circadian oscillators, exhibit synchrony with the neighboring cells as well as with the extracellular world (Dunlap., 1999). Since this is one of the desirable traits in the synthetic genetic circuit, in objective 3 we studied how temperature affects the degree of synchrony of the Repressilator between sister cells following their birth.

Copy-number of the constituent genes influences the dynamics of a gene regulatory network. For example, increasing the copy-number of circuit can lead to the relative reduction of the fluctuations in protein numbers, which, in the case of periodic oscillators, ought to affect the periodicity of the oscillations (Ribeiro *et al*., 2007; Ribeiro, 2007). The Repressilator was originally constructed on a low copy number plasmid, pZS1 (Lutz *et al*., 1997), which maintains about 3-4 copies of the plasmid per cell. All these copies dynamics are, necessarily, coupled since the proteins they code for are indistinguishable and, as such, any gene product of one of the plasmids can influence the expression of the subsequent gene in the loop in any of the other plasmids in the same cell. In objective 4, we studied the effect of copy-number on the dynamics of the Repressilator. Specifically, we inserted the Repressilator on another plasmid, BAC-2 (Bacterial Artificial Chromosome), which is known to exist as a single-copy in the cells (Gordon *et al*., 1997; Ogura *et al*., 1983), and studied how placing the Repressilator in single-copies in the cells affects its mean period and robustness. Also, we examined the effect of external perturbations in this circuit's dynamics.

1.3 Thesis outline

The structure of the thesis is as follows: chapter 2 provides an overview of the process of gene expression and its regulation, followed by a description of methods used in synthetic biology in chapter 3. In particular, we focused on the design principles and components required for construction of synthetic genetic circuits. In chapter 4, in vivo single-cell methods used to study transcription dynamics are described along with the computational and statistical methods used for segmentation of cells, quantification of single RNA molecules and inference of the number of rate-limiting steps in transcription initiation. Chapter 5 begins with an introduction to the Repressilator circuit, followed by a description of the experimental; computational and statistical methods used in this study. Finally, in chapter 6 we describe and discuss the outcomes of the study.

2 Gene expression and regulation

Gene expression can be defined as the process of conversion of the genetic information contained in the DNA (Deoxyribonucleic acid) to functional form called 'proteins'. It begins when information encoded in the DNA is transcribed to RNA (Ribonucleic acid), by the RNA polymerases, in a process called 'Transcription'. This is subsequently followed by protein synthesis by ribosomes, in a process called translation, in which information from the RNA sequence is translated into proteins (Fig. 1) (Crick, 1970).

In prokaryotes, the process of transcription and translation are coupled (Miller, 1970; Brown *et al.*, 1997). Though proteins were considered to be functional components of cells, a number of recent studies suggest that significant functional roles are played by the RNA in the regulation of many processes in gene expression (Liu *et al*., 2012; Raghavan *et al*., 2011).

The structure and function of cells are determined by their gene expression pattern. Hence, it is pivotal for a cell to regulate the expression of its genes. Commonly, the decision to initiate transcription of a particular gene is the major point of controlling its expression. In this chapter, an overview about the processes in gene expression regulation is given.

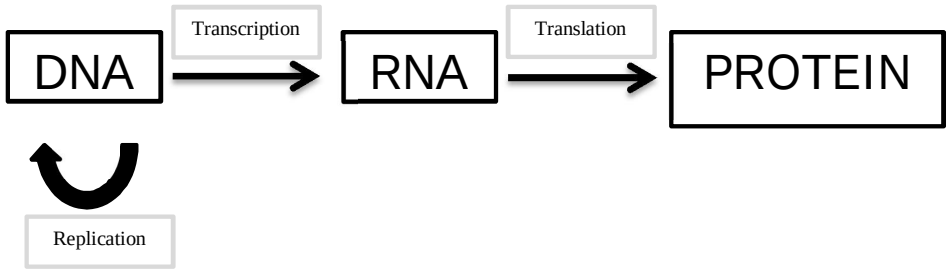

Figure 1: Schematic representation of the Central dogma of molecular biology.

2.1 Operon

In *E. coli*, several protein coding genes, which perform related functions, are organized into functional regions in the genome called operons (Fig. 2) (Jacob *et al*., 1961). The expression of the genes in an operon is under the control of a single promoter; hence activation and repression of the constituent genes of the operon are affected to the same extent, and at the same time, by the regulatory molecules. The genes encoded in the operon are transcribed together as a single poly-cistronic mRNA and either are translated together or, instead, the RNA undergoes trans-splicing to create multiple mono-cistronic mRNAs that undergo translation separately.

Typically, the promoter sequences contain both a "-10 box" and "-35 box" which, as the name indicates, are located, respectively, at about 10 and 35 base pairs (bp) upstream of the transcription start site (TSS) (Pribnow *et al*., 1975; Maniatis *et al*., 1975). The most probable sequences of these two boxes are, respectively, TATAAT and TTGACA (Siebenlist, 1979).

In general, promoters also contain operator sites, which are sites of binding of the regulatory molecules that regulate transcription, positively or negatively. In case of the Lac operon, the classic example of an operon, there are three operator sites: O1, O2 and O3. Repression is achieved when the repressor, LacI, binds to the operator O1 and prevents transcription by the RNA polymerase. Other operators are also involved in repression by binding to the repressor, though with lesser strength (Oehler *et al*., 1990

and Mueller *et al*., 1996), leading to less efficient repression. It is also reported that maximal repression is achieved by the formation of a DNA loop between the operators (Reznikoff *et al*., 1974).

The structural genes of the operon encode for proteins that perform related functions. For example, the lac operon codes for three structural genes *lacZ*, *lacY* and *lacA*, which are all involved in the metabolism of lactose, a disaccharide composed of glucose and galactose. The *lacZ* encodes the production of an enzyme, namely beta-galactosidase, which breaks lactose into glucose and galactose. *LacY* encodes a transporter protein, beta-galactoside permease, which transports lactose from the environment to the cytoplasm of the cells. Finally, *lacA* codes for an enzyme which converts galactose, produced from the breakdown of lactose to glucose, which in turn is converted into energy (Jacob *et al*., 1961).

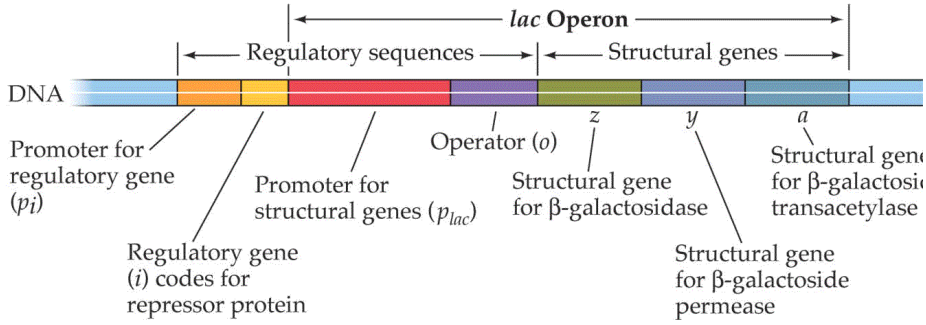

Figure 2: Schematic representation of the structural organisation of the genes of the lac operon. (Image reproduced from LIFE*: THE SCIENCE OF BIOLOGY*, seventh edition.)

2.2 Transcription

Transcription is the first step in the process of gene expression. Most of gene expression regulation occurs at this stage, ultimately controlling the rate of synthesis of the proteins (Latchman, 2007). A gene is said to be in the 'repressed' or 'off' state when the rate of

synthesis of the mRNA and the corresponding proteins is very low. Conversely, transcription of a gene is said to be in the 'active' or 'on' state when the mRNA and the corresponding proteins are produced in abundance, i.e., at high rates. Transcription begins when an RNA polymerase binds to the promoter region of a gene and initiates the synthesis of RNA (Fig. 3). The process of recognition of the promoter occurs by three-dimensional diffusion of the RNA polymerase on the DNA strand (Wang *et al*., 2013). Following promoter recognition, RNA synthesis occurs in three stages namely 'Initiation', 'Elongation' and 'Termination'.

In transcription initiation, the RNA polymerase binds to the promoter and, once finding a transcription start site, it forms a closed complex (CC). This is followed by a series of intermediate isomerization steps which, eventually, lead to the formation of the open complex (OC). Upon successful open complex formation, the promoter becomes catalytically active allowing the RNA polymerase to synthesize new RNA. During elongation, the RNA polymerase (RNAp) traverses through the template strand until the termination site, synthesizing the RNA. For successful entry into the elongation phase, the RNA polymerase has to undergo a crucial step called 'promoter clearance'; typically, a minimum of 10 base pairs synthesis should occur for the RNA polymerase to continue synthesizing the RNA. Failing to achieve this usually leads to abortive transcription (Hsu *et al*., 2003). Following promoter clearance, the polymerase starts synthesis of RNA by adding nucleotides complementary to the template strand from the 5' to 3'. This step is characterized by the release of the sigma factor from the holoenzyme, in a process called 'sigma factor recycling', while the core enzyme proceeds with the synthesis of RNA until the termination site is reached. In the final step, transcription termination, the newly formed mRNA and the RNAp are released from the elongation complex (Browning *et al*., 2004). In *E. coli*, transcription termination occurs by one of two mechanisms namely, the Rho-dependent and Rho-independent mechanisms. In the rho-dependent mechanism, a protein factor, 'Rho', destabilizes the elongation complex which releases the RNA (Ciampi, 2006), whereas in Rho-independent mechanisms, which are also called intrinsic termination mechanisms, transcription termination occurs typically by the formation of a G-C rich hairpin loop followed by a poly U-tail, which leads to the falling off of the

newly synthesized strand from the template strand, and hence the release of the RNA and RNAp from the elongation complex (Nudler *et al*., 2002).

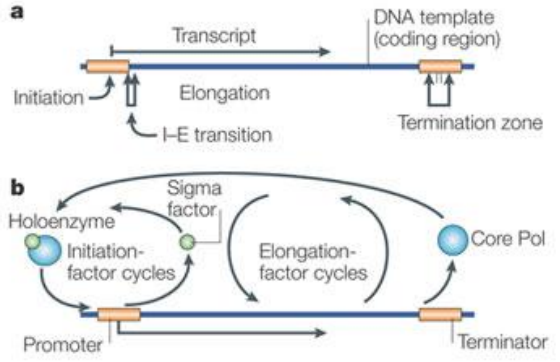

Figure 3: Steps in transcription (Reprinted by permission from Macmillan Publishers Ltd: Nature Reviews Molecular Cell Biology, Grieve et al., 2005)

2.3 Translation

In translation, information contained in the mRNA sequence is translated into proteins. This process is carried out by the ribosomes (Fig. 4). In prokaryotes, due to lack of intracellular compartmentalization of the cellular components and of a nuclear membrane, transcription and translation are coupled (Miller, 1970) (Brown *et al*., 1997); hence translation of proteins can start as soon as the ribosome binding site sequence of the RNA (RBS) is transcribed (Laursen *et al*., 2005). Like transcription, translation has three main steps (initiation, elongation and termination), with translation initiation being the most rate-limiting and regulated step. Translation initiation occurs when IF-3 (initiation factor) binds to the 30S subunit of the ribosome, leading to the dissociation of the ribosomes into subunits (Petrelli, 2001). This is followed by binding of IF-1 to the A-site (Amino-acyl site) of the ribosome, thus directing the initiator tRNA to the P-site (Peptidyl site) of the ribosome (Carter *et al*., 2001; Dahlquist *et al*., 2000). IF-1 also plays a crucial role in stimulating the activities of IF-3, hence aiding in the dissociation of the ribosomes

(Gualerzi *et al.*, 1990). Following the dissociation of the ribosomal subunits IF2, mRNA, and N-Formylmethionine (fMet-tRNA) associated with the 30S ribosomal subunit, it occurs the interaction of the Shine-Dalgarno (SD) sequence of mRNAs with the anti-SD sequence of the 16S rRNA, which leads to the positioning of the initiation codon to the P-site of the ribosome. At this point, the 30S pre-initiation complex, consisting of the three initiation factors, mRNA and the fMet-tRNA, undergoes a rate-limiting conformational change that promotes the interaction between codon and anti-codon, which leads to the formation of a stable 30S initiation complex (Pon *et al.*, 1984; Gualerzi *et al.*, 1977). Following the formation of a stable 30s initiation complex, IF-3 and IF-1 are ejected from the subunit, while IF-2 promotes the binding of the 50S ribosomal subunit to the 30S initiation complex, by undergoing hydrolysis of the GTP, leading to the formation of 70S initiation complex, which enters the elongation phase.

In elongation, a poly-peptide chain is assembled by the ribosomes from the start codon until a stop codon of the mRNA. Briefly, an aa-tRNA is first bound to the A-site and, following the establishment of proper base-pairing between the codon of the mRNA and the anticodon of the tRNA at the A-site, a peptide bond is formed with the amino acid and/or peptide, attached to the tRNA in the P-site. This is accompanied by the transfer of the peptide to the tRNA in the A-site. The peptidyl tRNA moves from the A-site to the P-site, and the deacylated-tRNA moves from the P-site to the E-site (Exit site), displacing the tRNA deacetylated in the previous cycle. The mRNA is coordinately translocated by one codon, hence retaining the correct reading frame and tRNA-mRNA base-pairing (Merrick *et al.*, 2000; Ramakrishnan, 2002). In optimal conditions, elongation proceeds at a rate of 10–15 amino acids per second and with a very low error rate (Rodnina *et al.*, 2001).

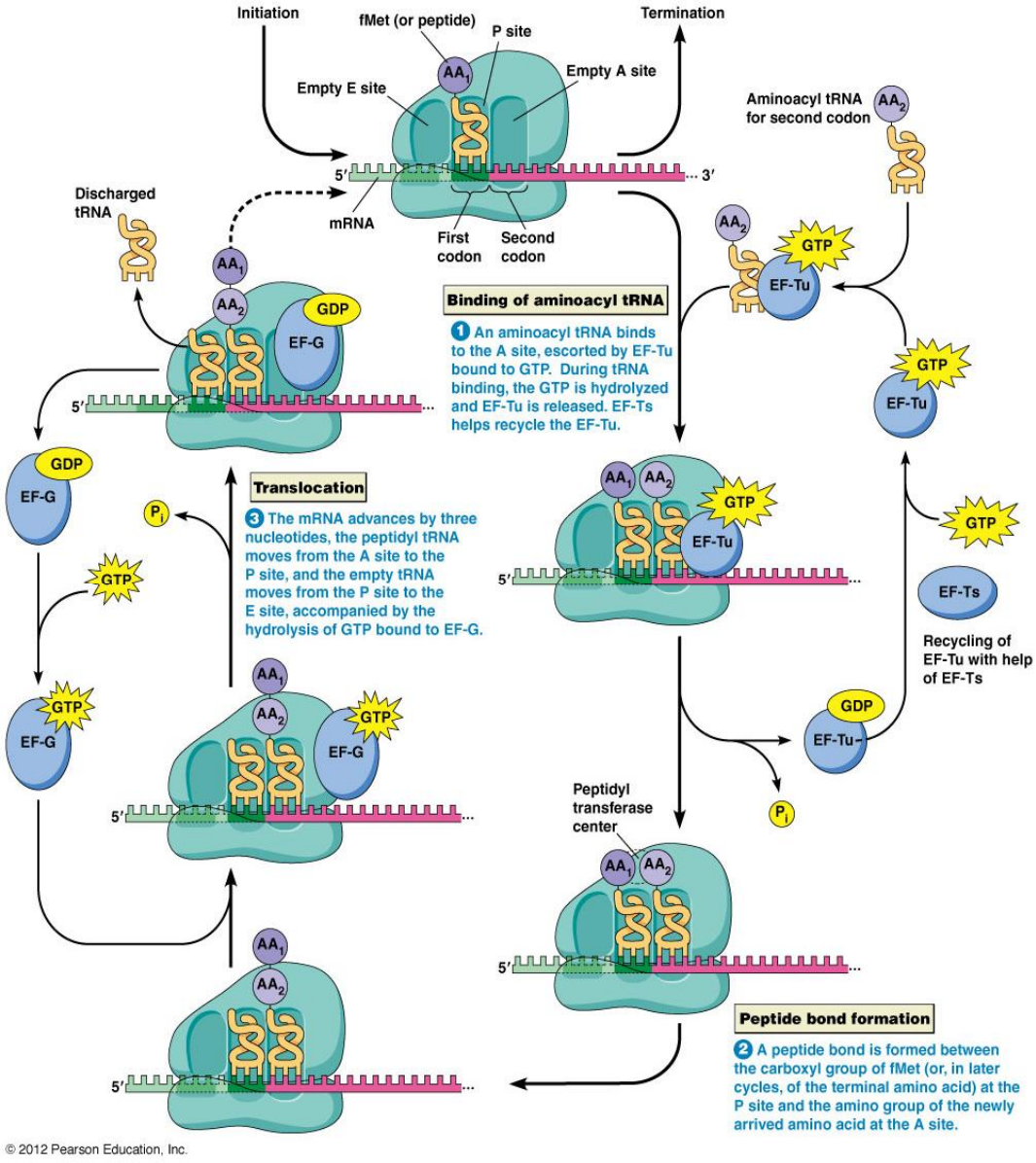

Figure 4: Steps involved in translation

(Adapted from: http://www.mun.ca/biology/desmid/brian/BIOL2060/BIOL2060-22/CB22.html).

In bacteria, the recognition of a stop codon in the mRNA in the A-site is performed by two different release factors, which belong to the 'class I' release factors, namely RF1 and RF2. RF1 recognizes the UAA and UAG stop codons while RF2 recognizes UAA and UGA. Dissociation of the nascent peptide chain occurs when a class II release factor, RF3.GDP, binds to the ribosome in the presence of a class I factor. Upon release of the nascent peptide, the GDP bound to RF3 is exchanged to GTP, accompanied by conformational changes and dissociation of the class I factor. GTP hydrolysis, in turn, causes dissociation of RF3. After termination, the ribosome is recycled by a ribosome-recycling factor, RRF, which, together with EF2, completes the process of dissociation of the two subunits (Merrick *et al*., 2000; Ramakrishnan *et al*., 2002; Kisselev *et al*., 2003).

2.4 Regulation of transcription

Gene expression in *E. coli*, aside from the genes that maintain the basic processes in the cells, occurs, in most cases, in response to different signals that may arise from internal processes or external factors, such as changes in temperature, pH, availability of nutrients etc. It is pivotal for the organism to regulate the expression of the number and the type of proteins needed to survive in a given environment, and prevent unwanted spurious production of proteins or RNA that is not required at a given time. Given the fact that transcription and translation are coupled in *E. coli* and the fact that transcription initiation is subject to stringent regulation, spurious protein productions are relatively rare, although, sporadic production events are known to occur (Cai *et al*., 2006). In this section, a brief account on the positive and negative regulation mechanisms of gene expression is provided.

2.4.1 Activation

A promoter is transcriptionally active following the successful binding of the RNA polymerase, leading to the open complex formation and hence production of RNA. Activation of gene expression from a promoter occurs in response to signals that arise from the environment or based on the intracellular needs. For example activation of the

sugar metabolizing genes occur in the presence of the respective sugars, whereas activation of genes involved in the synthesis of amino acids occur when amino acids are depleted. The strength of activation from a promoter is dependent on the sequences, which play a crucial role in the recruitment of the RNA polymerase to initiate transcription. (VonHippels *et al.*, 1984). However, this provides only static regulation, as sequence level regulation cannot be tuned to the changing conditions.

The promoter sequence also determines the selection of the sigma factor involved in transcription. Sigma factors, in addition to recognizing the promoter, are involved in the melting of the double stranded DNA to form the open complex. There are seven types of sigma factors, which are involved in transcription of specific sets of promoters based on their functions. The intracellular levels of sigma factors vary with differences in growth and stress conditions (Ishihama, 2000; Ishihama, 2010). The recognition of the promoters by sigma factors is highly sequence specific (Campbell *et al.*, 2008) and different sigma factors are involved in transcription of distinct sets of genes. For example, sigma70 is involved in the transcription of the majority of the genes active during active growth, whereas other sigma factors regulate transcription of discrete sets of genes that are required for various processes such as adaptation to different conditions. For example, sigma32 regulates the expression of genes involved in heat shock response, and sigma38 regulates genes involved in stress responses (Gruber *et al.*, 2003).

Based on their activation properties, promoters can be classified as ‘constitutive’ and ‘inducible’ promoters. In case of constitutive promoters, RNA production is always ‘ON’ or active in all circumstances. These promoters control the expression of, in general, the essential genes, such as genes that code for rRNA, RNA polymerase, etc. (Shimada *et al.*, 2014). However, overexpression of the unnecessary and harmful genes under the control of the constitutive promoter is regulated by factors like the H-NS family proteins (Oshima *et al.*, 2006). Inducible promoters, on the other hand, produce RNA upon induction with specific inducers and transcription factors. These include promoters that control the expression of genes involved in metabolizing sugars, shock response genes, etc. (Jacob *et al.*, 1961; Guisbert *et al.*, 2004). In this class of promoters, activation is achieved by de-repression of the promoters by binding of the inducer molecules to the repressor, which

leads to a conformational change in the structure of the repressor, effectively inactivating the binding of the repressor to the DNA, thus allowing the activation of transcription from the promoter. Presence of other transcription factors, such as the Catabolite Activator Protein (CAP), which binds to the CAP binding sites, further, enhance the activation of the promoters by actively recruiting RNA polymerases (Lichestein *et al*., 1987; Jacob *et al*., 1961).

2.4.2 Repression

Repression is the process of negative regulation or blocking of transcription. This is achieved by binding of the repressor to a repressor binding site, the operator site, of the promoter. The repressors specific for regulation of a particular promoter usually are coded by the operon that promoter belongs to, although its expression is under the control of a different promoter. For example, the production of the lac repressor is under the control of *lacIq*, a constitutive promoter (Jacob *et al*., 1961). Repression usually occurs when there is no inducer present, such as in case of the sugar metabolizing operons, or when the final product is present in excess, leading to repression by negative feedback as in case of the tryptophan operon (Santillan *et al*., 2000).

Repression of a promoter can be achieved in several ways. The simplest mechanism is by steric hindrance, in which the repressor binds to the DNA, physically blocking the formation of the open complex at the start site by the RNA polymerase. In other cases, repressors form DNA loops by forming oligomers and binding to multiple operators. For example AraC forms a dimer, which in the absence of arabinose, forms a DNA loop by binding to the araI1 and araO2 (Schleif, 2010). The Lambda phage repressor CI is known to form higher order oligomers up to octamers for effective repression (Dodd *et al*., 2001). 'Carbon catabolite repression' is another mechanism, and allows the bacteria to metabolize the preferred sugar when growing in an environment which contains more than one sugar (Duetscher, 2008). For example, the expression of the Lac operon is blocked when glucose is available (Lichestein *et al*., 1987; Jacob *et al*., 1961).

3 Synthetic biology

Synthetic biology is an alternative, bottom-up approach to the more traditional top-down approaches of Molecular Biology. In this approach, well characterized modular genetic components are assembled using principles derived from electrical engineering to create small synthetic genetic circuits that are capable of emulating the characteristics of the naturally occurring genetic circuits, such as oscillatory behavior and switching phenotypes, among other. Fig. 5 shows an example of how principles from electrical engineering can be used to engineer synthetic genetic circuits that emulate a natural system. Use of this strategy to construct genetic circuits offers several advantages. For example, it allows the development of an arbitrary circuit to test its efficiency in performing a desired function, without impairing or altering the basic cellular mechanisms. Also, it can be used to assess the advantages and disadvantages of different architectures that perform similar functions and hence determine the preferable architecture. Finally, this approach provides an opportunity to test the behaviour of circuits developed *in silico*. A number of synthetic genetic circuits have been developed already, which have shed light on some of the key design principles of genetic circuits (Sprinzak *et al*., 2005). In this chapter, the fundamental aspects of design and development of synthetic genetic circuits are described.

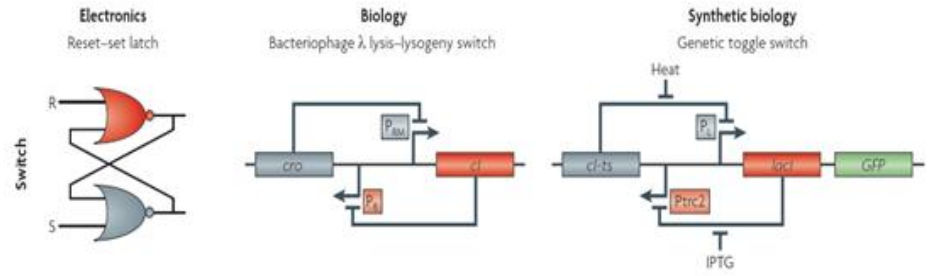

Figure 5: From left to right, the figure shows an electric circuit (a switch), a similar natural circuit (the lambda switch), and a synthetic genetic switch designed based on the principles of the electric circuit, using the components of the natural circuit. Reprinted by permission from Macmillan Publishers Ltd, Nature Reviews Genetics (Khalil *et al*., 2010).

3.1 Design principles of synthetic genetic circuits

The design principles of synthetic genetic circuits are obtained by drawing analogies between naturally occurring genetic circuits and the established techniques in electrical engineering (Miyamoto *et al*., 2013). This approach involves development of a blue print of the circuit design, which can be analyzed and tested using mathematical models and computational tools, while experimental techniques are used to construct networks according to the blue print. Recent advances in sequencing and genetic engineering aid in the design and development of these circuits, as they help in the characterization and assembly of the modular components, respectively. Logic gates, associated with their truth tables, form the basis for designing a synthetic genetic circuit, which aids in understanding the schematics of the input and output characteristics of the circuits (Weiss *et al*., 2003).

3.1.1 Logic gates

Biological networks are highly sophisticated devices, but nevertheless resemble electrical devices in the following way: they sense input signals from the environment, then perform decision making by processing the input information and, then, produce an output, similar to electrical circuits. However, biological systems are far more complicated, in that they are able to handle and benefit from the stochasticity of the underlying processes, they can receive and process multiple input signals that arise from various environmental factors such as nutrients, pH, osmotic stress, temperature etc. and, they process the input signals in parallel and respond to these inputs with little or no delays (Eldar *et al*., 2010).

Synthetic biology's design principles are drawn from electrical engineering and implemented in cells using experimental approaches. Typically, in the process of designing of an electrical device containing a circuit that produces a desired output, requires designing of a logic gate that consists of an arithmetic logic unit, the control unit, memory, and the input and output devices. The input and output characteristics are represented as Boolean logic gates. For example, in case of a binary code, the basic unit information is represented as 0 and 1 which indicate the two possible states of the circuit. A threshold is set to define the input and output range so that, depending on the value, either lower or higher than the threshold, the state of the logic circuit is denoted as 0 or 1, respectively. In digital circuits, a number of such logic elements are interconnected to create logic gates which are capable of executing Boolean logic functions. Fig. 6, shows examples of logic gates that can be used for the development of synthetic genetic circuits. A number of such modular logic gates can be networked together to make complex circuits thus making it possible to build complex circuits that can process versatile inputs (Miyamoto *et al*., 2013).

In Synthetic Biology, Boolean logic gates can also be used to design synthetic genetic circuits. In this case, chemical concentrations of proteins or inducers act as inputs and outputs for the logic gates (Lim, 2010; Morris *et al*., 2010; Slusarczyk *et al*., 2012). One crucial aspect to be considered while applying these concepts to living cells is that the

values of the thresholds of the input and output that define if these equal ‘0’ or ‘1’ must be well defined (Weiss *et al*., 2003). These thresholds are, usually, defined based on the concentration of the effector molecules; such as proteins, metabolites, and inducers, or on the rate of the chemical reactions, or on the localization of the effector biomolecules. Such characterization allows, e.g. the combinatorial synthesis of a wide variety of synthetic genetic networks with different architectures (Guet *et al*., 2002; Khalil *et al*., 2010).

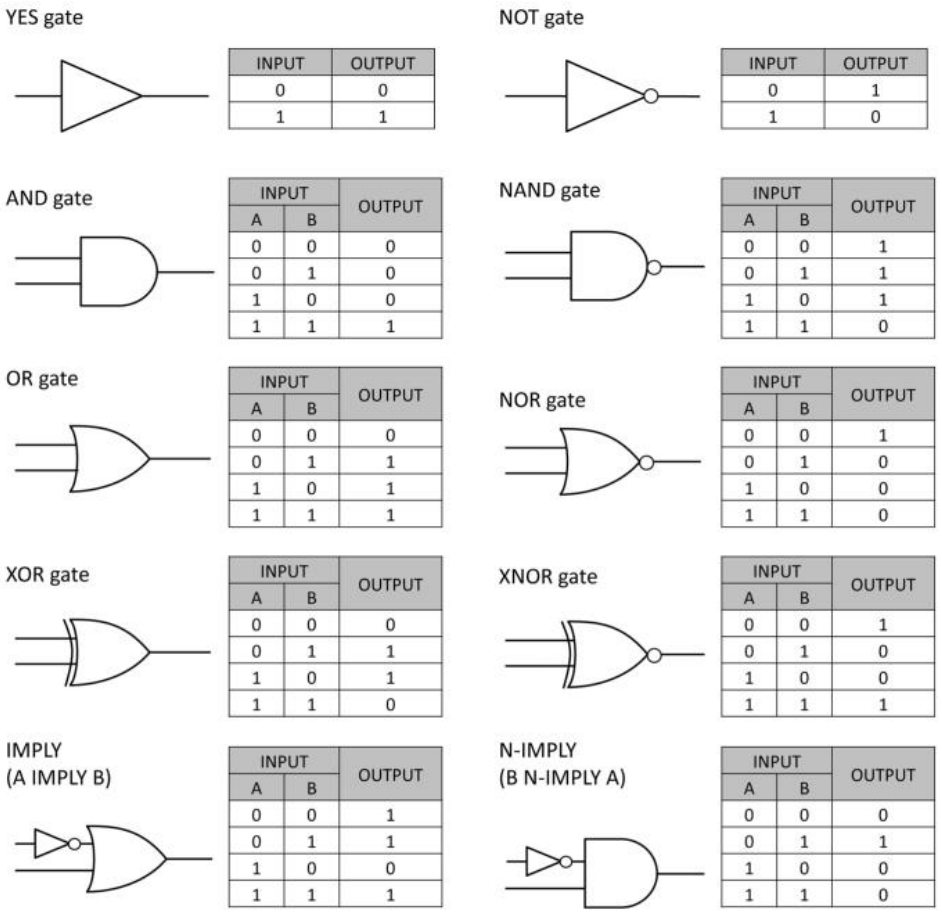

Figure 6: Boolean logic gates and the associated truth tables "Reprinted with permission from (Miyamoto *et al*., 2013). “American Chemical Society".

3.2 Components of synthetic genetic circuits

Synthetic genetic circuits are built using well characterized, modular genetic components that can act independently of other cellular processes (Sprinzak *et al*., 2005). In the following section, it is provided a brief description of the basic components required for construction of synthetic genetic circuits.

3.2.1 Transcription unit

Transcription units are the principal components of genetic circuits. They consist of DNA sequences coding for a set of coordinately regulated structural genes that encode proteins. The organization of regulators and genes of a transcription unit of a synthetic genetic circuit typically follows the organization observed in the natural systems (Nandagopal *et al*., 2011). These contain an up-stream promoter site where regulation of transcription occurs, and a down-stream terminator site where transcription ceases. Modulator sites associated with the promoter can be bound by regulatory proteins that influence the rate of transcription initiation; repressors bind operator sites that down-regulate high-level promoters, or activators bind initiator sites to up-regulate low-level promoters. These units are thus responsible for containing binding sites for regulatory molecules and for detecting such binding events. The regulatory molecules determine the production rate from a gene, whose products can be other regulatory molecules, among other (Jacob *et al*., 1961).

3.2.2 Input signal

The input signals for transcription units can arise from the environment or from within the cell. When the signal is from the environment, cells make use of cell surface receptors to detect the incoming signal. The signals from membrane-bound receptors are communicated to the inside via short signal transduction pathways (Hoch, 2000). In other systems, molecules are transported across the membrane and modified metabolically, to become signal molecules that influence transcription. Signals that arise from within the

cells are from other transcription units. These are, in most cases, regulatory proteins or regulatory non-coding RNAs (Friedland *et al*., 2009; Jacob *et al*., 1961).

3.2.3 Regulators

Regulation is achieved by factors that control gene expression by activating or by blocking the expression of a gene. Each of these two modes requires the transcription unit to have a promoter with sites for binding of the regulatory molecules. The behaviour of the circuits can be regulated by expressing the regulators constitutively and altering the functional forms of the regulators. In other cases, the regulator is always functional, and the variability in expression is achieved by regulating the rate of synthesis and degradation of the regulators (Savageau, 2001). Small non-coding RNAs have also been widely used to regulate synthetic genetic circuits (Lucks *et al*., 2011; Qi *et al*., 2014; Yuan *et al*., 2015).

3.2.4 Connectivity

Connectivity between genes allows cells to perform complex functions (Hlavacek *et al*., 1996) and it is determined by how the outputs of the transcription units are connected as inputs of other transcription units. Since these interactions can vary in function (repression or activation) and differ in strength, the number of different networks that can be formed is virtually infinite, assuming a large number of transcription units. A large number of the connections are ensured by proteins modulating the expression of the transcription unit that encoded them (Hlavacek *et al*., 1995). A number of synthetic genetic circuits that can perform a wide range of functions have been developed by connecting a wide variety of outputs to the input signal. Also, a number of oscillators have been engineered by combining promoters and transcriptional regulators (Elowitz *et al*., 2000; Gardner *et al*., 2000; Stricker *et al*., 2008).

3.2.5 Expression cascades

Expression cascades correspond to the production of output signals from transcription units. The initial signal coming from a transcription unit is an mRNA molecule that has a

sequence complementary to the DNA read. The mRNA is translated into a protein. Finally, the protein, once folded and activated, becomes an enzyme. There can be more stages in such cascades and each of these can be used for regulation. For example, in retroviruses and retrotransposons the cascade might include a stage in which RNA is used to transcribe a complementary DNA. Several mRNA molecules can be produced from the same transcription unit. Also, several proteins can be produced from the same mRNA (e.g. in bacteria) (Hlavacek *et al*., 1995). It has also been demonstrated that complex functions can be performed by integrating the transcriptional units with the output signals. In 'metabolator', oscillations are achieved by integrating transcriptional and metabolic activities (Nem *et al*., 2005). Other complex functions, exhibited by living systems, such as cell synchronization and communication between cells, have been achieved by connecting the output signals with the input signals (Bacchus *et al*., 2012; Danino *et al*., 2010).

4 Single cell, single molecule method to study dynamics of transcription

This section describes the method we used to study transcription initiation dynamics. This method is used in the publications 1 and 2. In publication 1, we used this method to study transcription dynamics from a promoter and the influence of inducer intake on the kinetic of transcription. For that, we made use of P_{BAD} promoter which controls the expression of the arabinose operon. In publication 2, this method was used to confirm that loss of functionality of the Repressilator with increasing temperature is due to the altered properties of cI. For this, we used the cI-cro switch, which is under the control of promoters, P_R and P_{RM}, respectively.

4.1 Transcription initiation dynamics

Transcription initiation is a sequential, multi-stepped process (Mcclure, 1980), which begins when an RNA polymerase (R) recognizes and binds to the promoter (P) region of the DNA, forming a closed complex (RP_c), which subsequently undergoes a series of isomerization steps (I_n) leading to the formation of the open complex (RP_o) (Fig. 7). Some of the steps in this process are rate-limiting ("slow" in Fig. 7) and the number of rate-limiting steps and their duration vary between the promoters and with conditions, such as temperature.

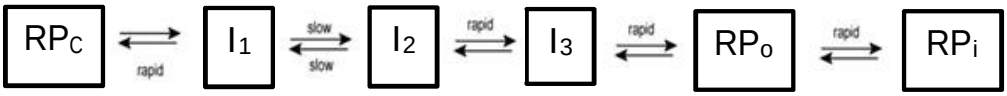

Figure 7: Steps in transcription initiation along with their relative duration. (McClure, 1983)

4.2 Measuring time intervals between consecutive RNA production events in a single cell

A number of previous studies have been done to determine the dynamics of transcription initiation in different promoters (Bertrand-Burggraf *et al*., 1984; Hawley *et al*., 1983; Mcclure, 1980). However, these studies were based on in vitro methods and fixed cells (Larson *et al*., 2011).

The MS2-GFP tagging of RNA described in (Golding *et al*., 2004), offers an opportunity to study the transcription events in vivo (a detailed description is given in the following section). Using this technique, our group has developed a method to infer the dynamics of transcription initiation, specifically the number and the duration of the rate-limiting steps (Kandhavelu *et al*., 2011; Muthukrishnan *et al*., 2012) .

4.2.1 MS2-GFP tagging method

The MS2- GFP tagging method is one of the currently used single-molecule techniques to detect RNA production in live cells with sensitivity and, thus, measure the real-time kinetics of transcription. The method was originally developed to study eukaryotic mRNA (Bertrand *et al*., 1998), and was later adapted to prokaryotes with some modifications (Golding *et al*., 2004; Golding *et al*., 2005). This method is based on the fact that MS2, the coat protein of MS2 bacteriophage, recognizes and binds to a specific RNA sequence. For RNA tagging using this technique, two plasmids are used, namely the target coding plasmid and the reporter coding plasmid. The target plasmid contains the

promoter of interest that controls the production of monomeric red fluorescent protein (mRFP-1) followed by tandem 96 binding sites for MS2. The reporter plasmid encodes the production of MS2 tagged with GFP, and is under the control of a different promoter than the target plasmid. Induction of the reporter plasmid floods the cells with MS2-GFP. Subsequently, when the promoter of interest is activated, the RNA produced can be visualized as spots under a fluorescence microscope (Fig. 8), due to the concentration of MS2-GFP molecules at the tail of the RNA produced. Time-lapse imaging of this system in multiple cells allows the extraction of a distribution of intervals between consecutive RNA productions in individual cells, from which one can extract the mean rate of RNA production and variability of the intervals between productions. From this, one can thus also assess the noise in RNA production. Further, assuming a sequential model of transcription initiation (as proposed in (McClure, 1980)), it is possible to estimate from this distribution the number of rate-limiting steps in transcription as well as their duration.

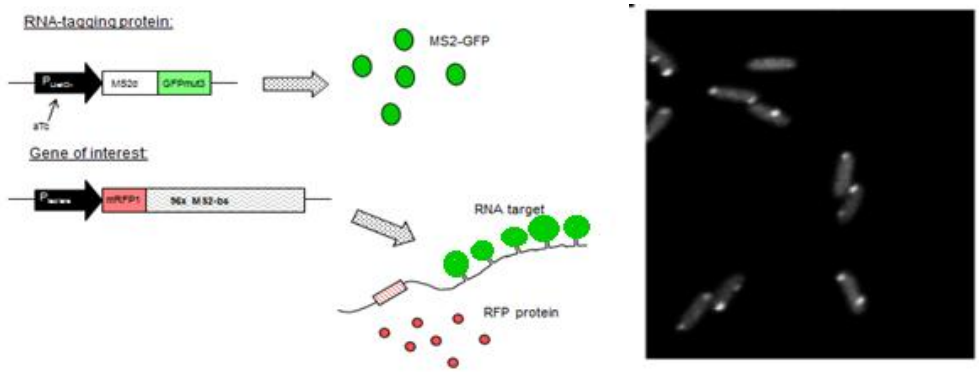

A B

Figure 8: A) Schematic representation of MS2-GFP RNA tagging B) Example image of cells containing fluorescent RNA spots.

4.2.2 Time-lapse microscopy and Image analysis

Cells containing the target and the reporter genes were grown overnight in Lysogeny broth (LB) medium with appropriate antibiotics, after which cells were sub-cultured into fresh LB medium, to an optical density (O.D.) of 0.01, incubated at 37 ℃ with shaking at 250rpm, and then grown to an O.D. of 0.3. At this point, the reporter gene, which is P_LTetO1 in both studies, was activated using 100ng/ml anhydro-Tetracycline (aTc) for at least 45 minutes followed by the induction of the target promoter. This induction was achieved differently in each case; full induction of the P_{BAD} promoter was achieved by addition of 1% arabinose to the medium, whereas no external induction is required for production of RNA by pRM as the production is constitutive in this promoter (Berthoumieux *et al*., 2013) although its rate of production is temperature dependent (Little *et al*., 2010). After induction, the cells were seeded on the imaging gel, made of LB media containing the respective inducers, and placed in a temperature controlled imaging chamber, which maintains the desired temperature during the measurements.

Next, the fluorescence images of the induced cells were acquired using a Nikon Eclipse (TE2000-U, Nikon, Japan) inverted microscope with C1 confocal laser-scanning with a 100x Apo TIRF objective. Images were acquired every minute for 2 hours. GFP fluorescence was measured using 488 nm argon ion laser (Melles-Griot) and a 515/30 nm emission filter. Images were acquired using Nikon EZ-C1 software. Independent replicates were produced to ensure reproducibility of the results.

The images were analyzed using custom programs written in MATLAB 2011b (MathWorks). The cells were detected from the fluorescence images obtained from confocal images using a semi-automatic method described in (Kandhavelu *et al*., 2012). Briefly, in time series, the area occupied by each cell was masked manually at each time point. Principal component analysis was then used to obtain the dimensions and orientation of a cell within each mask. The segmentation of the fluorescent spots in the cells was done using density estimation with a Gaussian kernel (Chen *et al*., 2008). From this, background-corrected spot intensities were calculated and summed to produce the total spot intensity in each cell, at each time moment.

4.2.3 Data analysis

The moments of appearance of new RNA molecules in each cell were obtained from the fluorescence images acquired by time-lapse microscopy by fitting the corrected total spot intensity over time in each cell to a monotone piecewise-constant function by least squares. The number of terms was selected using F-test with a P-value of 0.01. Each jump corresponds to the production of a single RNA molecule (Kandhavelu *et al*., 2011). An example of this procedure is shown in Fig. 9. Note that, in cells that do not contain target RNA molecules at the start of the measurements, the number of novel RNA molecules detected since the start of the measurements until a given moment equals the total number of RNA molecules in the cell at that moment. This is because tagged RNA molecules have a negligible degradation rate during measurements a few hours long. Nevertheless, because some cells already contained target RNA molecules at the start of the measurement, the total RNA numbers within cells at a given moment in time was obtained using a different method. Specifically, when comparing measurements using MS2d-GFP tagging and using plate reader, the total number of MS2d-GFP–tagged RNA molecules was extracted from the total spot intensity distribution, obtained from all cells in an image at a given moment after induction. For this, the first peak of the obtained distribution is set to correspond to the intensity of a single-RNA molecule. The number of tagged RNAs in each spot can be estimated by dividing its intensity by that of the first peak (Golding *et al*., 2005).

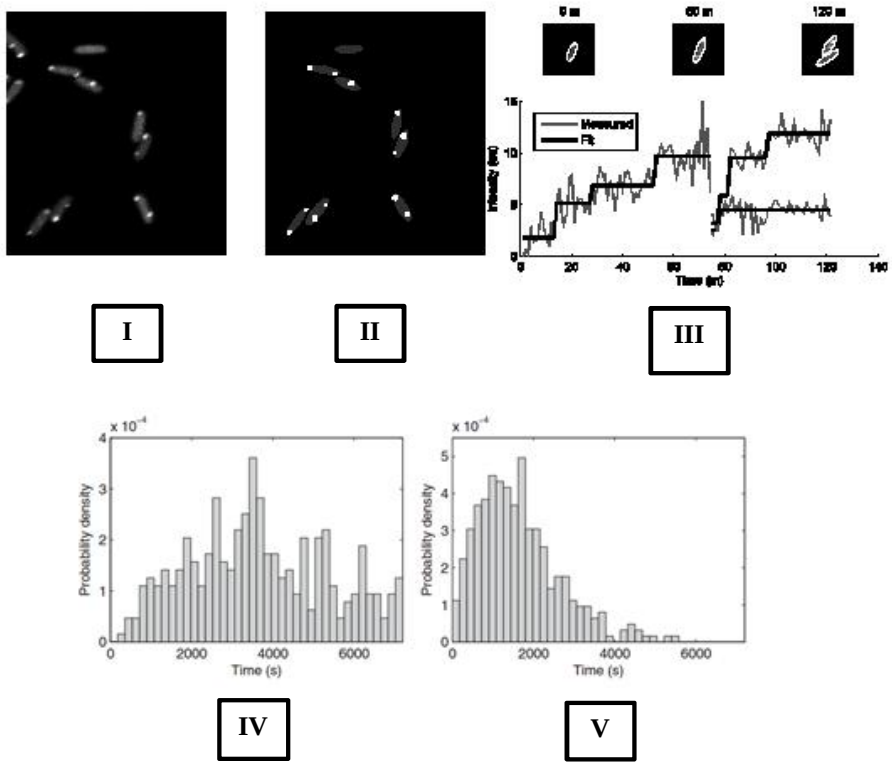

Figure 9: Example images of data extraction: Original images (I), spot detection (II) and extraction of intervals between consecutive RNA productions in individual cells from time series (III). Distributions of intervals of $P_{lac/ara-1}$ under (IV) medium and (V) strong induction as obtained from the image analysis.

4.3 Dynamics of the P_{BAD} promoter

The RNA production dynamics from the P_{BAD} promoter was studied using the method described above except that the target promoter was induced under the microscope so as to observe the first RNA production in each cell. This work was conducted using the strategies previously developed to study transcription dynamics of promoters *in vivo* (Kandhavelu *et al*., 2011; Muthukrishnan *et al*., 2012). Further, here, a method was

developed to study the inducer intake kinetics and its effect on the transient dynamics of transcription following the appearance of the inducers in the media.

Briefly, the waiting time for the appearance of the first RNA (t_0) from the P_{BAD} promoter, following induction with arabinose, and the intervals between consecutive productions (Δt) were measured as described above, namely, for each cell following induction. To verify whether the appearances of target RNA molecules are due to arabinose uptake, another promoter $P_{lac/ara-1}$, which can be induced with two inducers namely, arabinose and Isopropyl Thio-Galactosidase (IPTG) was observed. From the data, it was observed that production from both promoters is sub-poissonian ($CV^2 = 0.37$), similar to production from $P_{lac/ara-1}$ (Kandhavelu *et al.*, 2011). Moreover, the two promoters exhibit statistically indistinguishable waiting times for RNA production with mean t_0 of around 2800s, when induced with Arabinose alone. However, when induced with IPTG alone, the mean t_0 of $P_{lac/ara-1}$ is close to 2700 and less noisier (Mäkelä *et al.*, 2013). This distribution of RNA production following induction of the $P_{lac/ara-1}$ with IPTG is statistically distinguishable from the others, indicating that a different activation system is being used.

Promoter	**Inducer**	μ_{t0} **(s)**	$\mu_{\Delta t}$ **(s)**	***p*-value**
$\mathbf{P_{BAD}}$	1% arabinose	2885	532	2.83×10^{-18}
$\mathbf{P_{BAD}}$	0.1% arabinose	3519	481	4.06×10^{-21}
$\mathbf{P_{lac/ara-1}}$	1% arabinose	2832	516	2.48×10^{-26}
$\mathbf{P_{lac/ara-1}}$	1mM IPTG	2697	576	3.32×10^{-72}

Table 1: *P*-values of the Kolmogorov-Smirnov test between t_0 and Δt distributions for each promoter and induction condition

To study the kinetics of the intake process, we defined, t_{diff}, the intake time of an inducer, which differs from t_0 in that it does not include the time it takes for transcription initiation to be completed, once initiated. To obtain this quantity, the mean and variance of the Δt distribution were subtracted to the mean and variance of the t_0 distribution. This method was used due to the fact that a correlation could not be drawn between the t_0 and Δt distributions. The estimated mean and standard deviation of t_{diff} for both $P_{lac/ara-1}$ and P_{BAD}

were found to be similar (mean and standard deviation of around 1400 and 1100 s, respectively) when both are induced with 1% Arabinose, which is expected since the same intake system is used. Importantly, lac/ara-1, when induced with IPTG, exhibited a smaller standard deviation (700s), although it had a similar mean (approximately 1400s), which suggests that the intake process of arabinose is noisier than the intake process of IPTG. We also found that the mean t_{diff} is significantly affected by the concentration of arabinose in the medium (Mäkelä *et al*., 2013). Using a stochastic model of the intake process that accounts for the inducer concentration and the empirical distribution of t_0, and that assumes that transcription initiation is a 3-stepped process, we further found that the intake step likely adds variability to the RNA numbers in individual cells during the transient stage to reach the equilibrium (i.e. maximum activation possible given the inducer concentration in the medium).

4.4 Dynamics of the CI-Cro switch

The CI-Cro bistable switch, controlled by P_{RM} and P_R, present in the λ bacteriophage, controls the switching between the lytic and lysogenic states of the virus. In the lysogenic state, the CI repressor is produced in abundance, repressing P_R from producing Cro, which is required to switch from lysogenic to lytic state. In the lytic state, the production of CI from P_R is repressed by Cro (Schubert et al., 2007).

Here, we study the RNA production dynamics of the CI–Cro genetic switch as a means to indirectly validate that the observed changes with temperature in the dynamics of the genetic Repressilator are due to the temperature-dependence of the functionality of cI, a repressor of the promoter P_R.

Previous studies suggest that the activity of CI is temperature dependent (Jana *et al*., 1999). In the switch system used here, the promoter P_{RM}, which controls the expression of CI, also controls the transcription of a 96 MS2d binding array. The other promoter of the switch, P_R, controls the expression of Cro. The activity of this promoter is not followed. From previous studies, it was observed that Cro–DNA interactions do not vary

significantly between temperatures from 24–37°C (Takeda *et al*., 1992), thus, any behavioural changes observed in the switch with changing temperature in this range should arise from the changes in CI–DNA interactions. For this, time lapse microscopy was performed to obtain the RNA production intervals from the promoter for 2 hours, with images taken every minute. The measurements were conducted at 24 °C, 27 °C, 30 °C, 33 °C and 37 °C.

Table 2 shows the number of samples (i.e. intervals), mean and standard deviation of the intervals' duration in each condition. It is observed that as temperature increases, the kinetics of production of the target RNA shifts from sub-poissonian ($CV^2 < 1$) to super-poissonian ($CV^2 > 1$). From Table 2 it is also observed that as the temperature increases, the mean interval between consecutive transcription events decreases. The significance of this change was verified by comparing the distributions of intervals in consecutive temperatures with the K–S test. Table 3 shows that the distributions at 24 °C and 27 °C cannot be distinguished from one another. A similar trend was observed in case of the distributions at 33 °C and 37 °C. Meanwhile, the distributions obtained from 27 °C and 30 °C, as well as distributions from 30 °C and 33 °C differs significantly from one another. This suggests that there is a change in the dynamics of transcript production around 30 °C, which is similar to the change observed in the behaviour of the Repressilator (Results in the next chapter).

T (^{o}C)	**No. of intervals**	**μ (s)**	**σ (s)**	**CV^2**
24	157	1242	1166	0.88
27	229	1152	1191	0.67
30	88	1130	1040	0.85
33	539	788	807	1.05
37	324	714	785	1.21

Table 2: Intervals between appearances of new RNA molecules in individual cells. Table shows per condition, number of intervals, μ (s) is mean, σ (s) is standard deviation and CV^2 is coefficient of variation

T (^{o}C)	24	27	30	33
27	0.149			
30		0.06		
33			0.009	
37				0.478

Table 3: P-values of the Kolmogorov-Smirnov test between distributions of intervals between consecutive RNA production events from P_{RM}. For p-values <0.01, the hypothesis that the distributions are the same is rejected.

5 Single cell study of the dynamics of Repressilator

This chapter contains a brief introduction to the Repressilator, followed by a detailed description of the experimental and statistical methods used in the study. The Repressilator was chosen as a model for study as the dynamics of this genetic circuit is dependent on the activity of the promoters. The transcription kinetics of one of the promoters of the Repressilator has been described in Chapter 4 and it is found to be affected by temperature. In this chapter, we describe the effect of changes in temperature and copy-number on the dynamics of the Repressilator.

5.1 Repressilator

The Repressilator is one of the first built synthetic genetic circuits, which is known to be functional in a living organism. It is a negative feedback loop consisting of transcriptional regulators that are not a part of any natural biological clocks (Weiss *et al*., 2003). This is a ring-type circuit, which contains 3 promoters, each controlling the expression of a repressor that represses the activity of the subsequent promoter in the loop. As such, the expression of one of the promoters represses the activity of the next promoter leading to the expression of the third promoter, which in turn suppresses the activity of first promoter (Fig. 10). The resultant fluctuations in the level of the repressors is read-out as periodic oscillations in the green fluorescence, GFP, produced by a reporter plasmid, which is under the control of one of the promoters of the Repressilator (Elowitz *et al*.,

2000). The promoter and repressor pairs used in the construction of the repressilator are: P_LLacO1 – LacI; P_LTetO1 – TetR; and P_R – cI, and the expression of GFP from the reporter plasmid is kept under the control of P_LTetO1, which is one of the promoters of the repressilator. The proteins produced from the repressilator contain a destruction tag, *ssrA*, which makes the half-life of the proteins closer to the half-life of mRNA (Keiler *et al*., 1996).

A

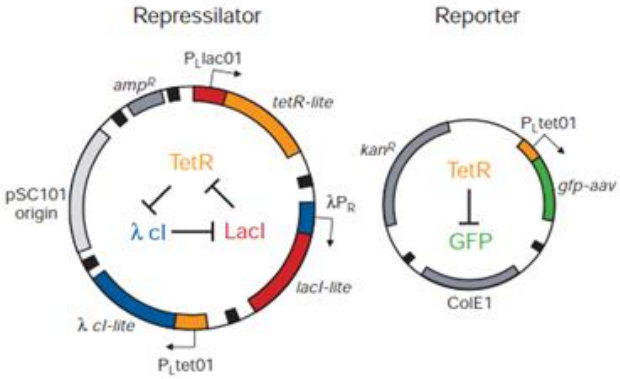

B

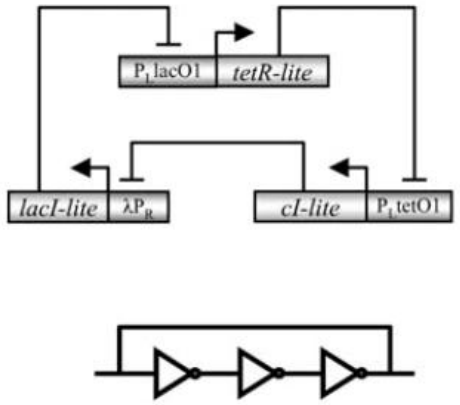

Figure 10: a) Schematic representation of the Repressilator and of the reporter (Reprinted by permission from Macmillan Publishers Ltd, Nature (Elowitz *et al*., 2000)); b) A logic circuit based representation of the repressilator. (Reprinted with kind permission from Springer Science and Business Media (Weiss *et al*., 2003).

5.2 Time lapse microscopy

E. coli cells containing the Repressilator and the reporter plasmids were grown in minimal media for up to 10 hours to an O.D. of 0.1, at 28 °C, 30 °C, 33 °C and 37 °C. The cells were then diluted in fresh media and seeded on imaging gel, made of minimal media and 0.2% low melting agarose. Fluorescent images were captured using a confocal microscope every 15 minutes for 10 hours, after which the cells enter the stationary phase and produce no oscillations (Elowitz *et al*., 2000). The temperature, during the measurement, was maintained constant using a thermal control chamber. Independent replicates were produced to ensure reproducibility of the results.

5.3 Image analysis

Fluorescent images of cells containing the Repressilator were first observed and cells that appear to produce oscillations in the levels of fluorescence were selected by inspection for further analysis. Next, the selected cells were segmented by manually masking the area the cells occupy in each frame. Using custom MATLAB based programs developed for image analysis, the total fluorescence intensities under each mask were extracted and the mean pixel intensity of cells was calculated at each time point (Fig. 11).

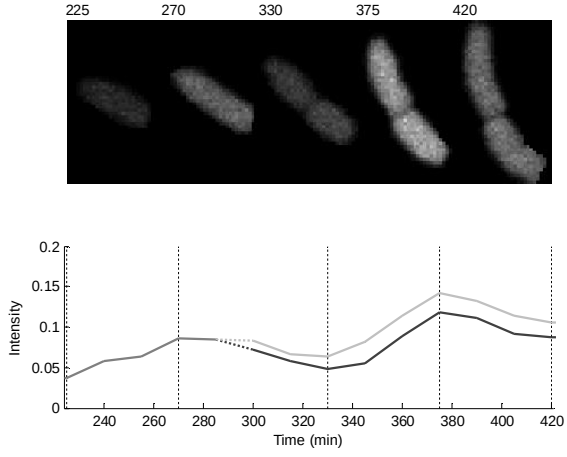

Figure 11: Example images of cells with repressilators in five different time points (top), and the

corresponding mean intensities extracted from these cells (bottom). The vertical dashed lines indicate the time points corresponding to the images.

5.4 Statistical analysis

The effect of temperature on the dynamics of the Repressilator was studied by analysing the functionality, robustness and period of oscillations from the time-series images of oscillating cells, in different temperatures. The statistical methods used in the study are as follows.

5.4.1 Functionality and estimation of periods

The functionality of the masked cells containing the Repressilator was determined using the criterion proposed in (Elowitz *et al.*, 2000). To do so, a fast Fourier transform was applied to the temporal fluorescence signal from each cell and divided by the transform of a decaying exponential with a time constant of 90 min, which is the measured lifetime of the green fluorescent protein used (GFPaav) as the reporter. Cells were classified as oscillatory when the power spectra produce peaks 4.5 times higher than the background at frequencies of 0.15–0.5 per hour. A larger bandwidth, compared to the bandwidth used in (Elowitz *et al.*, 2000), was used here, so as to include failed oscillations, which seemed to increase the period of apparent oscillations by nearly double. The apparent period, for cells that were considered functional, was estimated as follows. First, a quadratic curve in the least-squares sense was fitted to the intensity of the time series to estimate the general trend, since the measured intensity is known to be affected by different factors such as, e.g., photo bleaching. The estimated trend was subtracted from the time series and the residual was scaled to unit power, followed by computation of the autocorrelation function. From this function, the period of oscillation was estimated by locating the first and the third zeros of the autocorrelation function, and computing the distance between them (Fig. 12).

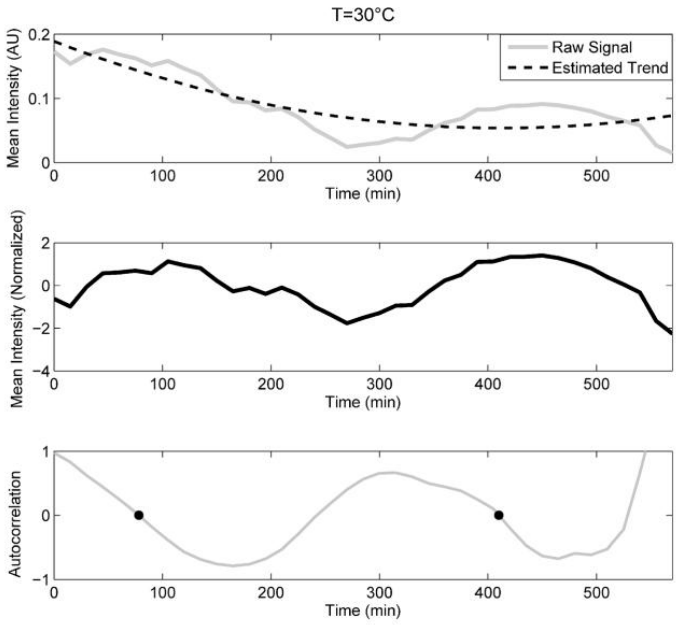

Figure 12: Estimation of the period of the Repressilator from the fluorescence intensity signal. The top panel shows the raw signal extracted from the confocal images, the dashed line show the estimated trend. In the middle panel, the trend from the raw signal was subtracted and the residual was scaled to unit power. The bottom panel shows the autocorrelation function of the treated signal. The distance between the first and the third zeros corresponds to the period of oscillation.

5.4.2 Estimation of robustness and true period of oscillations

In time series, at temperatures over 30 °C, it was observed that a certain fraction of cells, in each condition, produced oscillations followed by a brief period of no activity, in terms of fluorescence levels, which was then followed by resumption of oscillations. This can be due to, either, the failure of the reporter to produce GFP to report an oscillation or expression of reporter is repressed. However, in most cases, the signal from the reporter recovered, following the period of inactivity, thus suggesting failure of oscillations followed by recovery. The method, for estimation of the period of the Repressilator, mentioned above, relies on robust periodic behaviour and it cannot detect if a Repressilator halts its activity for a certain time and then resumes its activity. Instead, it assumes a period length that combines the periods of the true and the failed oscillations,

in which cases the measured time became double compared to other oscillations. To extract the true period, a method based on the fact that distribution of period lengths resemble a bimodal distribution when failure of oscillations occur was used (Fig. 13). Here, the mean and standard deviation of the true period in the population was estimated followed by estimation of the fraction of failed oscillations from the measured periods from each cell. For that, the maximum likelihood estimates for a single Gaussian and a mixture of two Gaussians was determined (from mean and standard deviation of the measured periods), such that the mean and the variance of the second are double than that of the first, found using an iterative expectation maximization algorithm (Dempster *et al.*, 1977). Appropriate models were selected using a likelihood ratio test with significance level of 0.01 between the two models, that is the model is selected only when the p-value of a 2-gaussian model is smaller than 0.01. Finally, the fitting was performed, using a leave-one-out-technique, with each subset of data lacking one of the measured periods, which results in N estimates, each using N-1 measure periods from which the variance of the estimates was calculated.

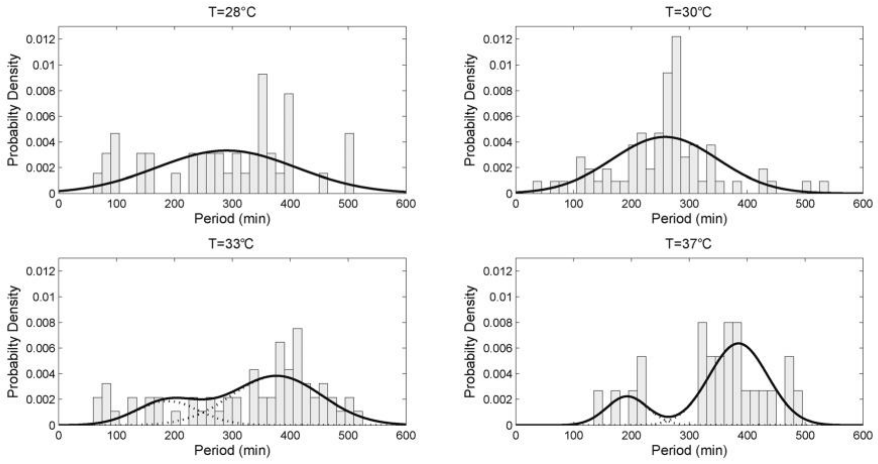

Figure 13: Distribution of periods (magnitude scaled to represent probability density) for each temperature. Solid lines represent the probability densities of the fitted model with one or two Gaussians. Dashed lines represent the densities of individual components in the case of two Gaussians. For 28 °C and 30 °C, the p-values of the likelihood ratio tests are 0.08 and 1, respectively, indicating a lack of evidence for the two-Gaussian model, whereas for 33 °C and 37

°C, the p-values are 0.0065 and 0.0015, respectively, indicating that the two-Gaussian model should be favoured over the one-Gaussian model.

5.4.3 Loss of synchrony

The effect of temperature on the loss of synchrony between sister cells was studied by detecting pairs of sister cells in which both of the sister cells were functional, and then manually following them by the criterion mentioned above. The loss of synchrony was estimated by calculating the correlation coefficients between functional sister cells. First, the likeliness of a robust cell to produce a robust sister cell, at 37 °C, was obtained. About 112, 40, and 35 pairs were found where none, one, or both of the cells were robust, respectively, suggesting that the numbers of pairs where either none or both sisters are robust are overrepresented. More specifically, there is about a 0.64 chance for a robust cell to have a robust sister, and about a 0.85 chance for a non-robust cell to have a non-robust sister (cf. 0.37). The significance of the correlations was confirmed by calculating the p-value of one-tailed Fisher's exact test with the null hypothesis. It suggests that being robust or not is independent of the sister cells, resulting in a *p*-value smaller than $1.29\times10^{-10.}$ Next, we computed the correlation between the intensity signals of each pair of sister cells. This correlation results from loss of synchrony caused both by division and variations in the behaviour of the cells over their lifetime (i.e. variations/drift in the period and noise in the intensity signal). The distributions of correlation coefficient extracted from each pair of cells are shown in Fig. 14, and the mean and standard deviation of the coefficients are shown in Table 4.

It was found that, on average, as temperature increases, sister cells lose correlation (p-values of 3.17×10^{-3} and 9.90×10^{-4} for 28 vs. 30 °C and 30 vs. 37 °C in one-tailed Welch's t-test with the null hypothesis that the means are equal). This loss of correlation may be due to the increase in the noise of the period as a function of the temperature, which appears to follow a similar pattern. Accordingly, since the non-robust cells contribute much of the variation in the 37 °C condition, the correlation is restored to a level comparable to the 30 °C condition when only the robust cells are considered. Interestingly, Fig. 14 reveals that, in each condition, most cells are very highly correlated.

However, increases in the temperature results in pairs of cells with wider range of correlation coefficients, including a sizable number of pairs whose series are strongly anticorrelated.

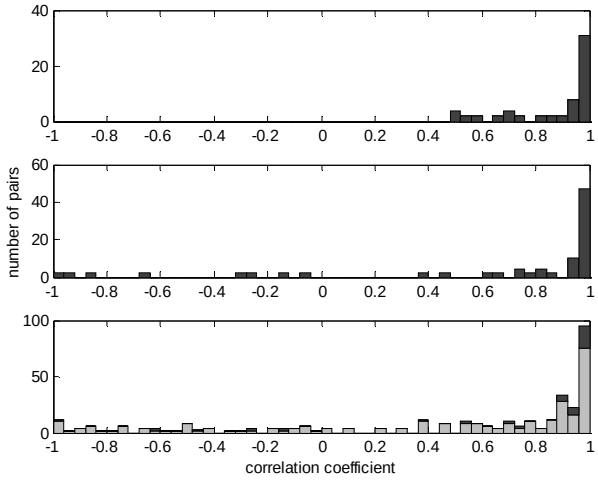

Figure 14: Distributions of correlation coefficients between functional sister cells in 28 (top), 30 (middle), and 37 °C (bottom). In the 37 °C condition, the pairs where both cells are robust are represented in dark gray bars, while the others are represented in light gray.

Statistic	**28 °C**	**30 °C**	**37 °C**	**37 °C, robust**
Correlation mean	0.87	0.66	0.42	0.63
Correlation s.d	0.16	0.58	0.66	0.58

Table 4: Correlation between sister cells in various temperatures.

5.5 Single copy Repressilator

5.5.1 Construction of single copy Repressilator

To study the effect of copy-number of genes on the dynamics of the Repressilator, we inserted the Repressilator cassette into a single copy F-plasmid, to create the single copy Repressilator (SCR) pBAC2-lTlrLLtCL. This was done by amplifying the functional repressilator cassette, flanked with SmaI restriction enzyme recognition sites, using polymerase chain reaction (PCR), from the original plasmid (generously provided by M. Elowitz, Princeton University, USA) and inserting it into an F-plasmid based single copy plasmid, pTRUEBLUEScript, which was also amplified along with SmaI restriction sites during PCR. Fig. 15 gives a schematic representation of the construction of the single copy Repressilator. The construct was validated by sequencing, and the functionality of the newly constructed Repressilator inside cells was confirmed using qPCR, in addition to the oscillations observed under the microscope. The functionality and robustness of oscillations were determined according to the above mentioned criteria.

5.5.2 Effects of plasmid copy number under optimal conditions

To study the effect of copy number on the dynamics of the Repressilator, time-lapse confocal microscopy of cells containing the SCR and the low-copy Repressilator (LCR) was performed. The experiments were carried out at 30 °C, at which the LCR exhibited shorter period of oscillations with higher functionality and robustness (Chandraseelan *et al*., 2013). The division rate of the cells under the microscope was relatively slow (division time of ~60 min), thus, it is reasonable to assume that the cells maintain one copy of the plasmid most of the time (Churchward *et al*., 1982).

Also, from the data, it is evident that the SCR cells had fewer copies of the Repressilator than the LCR, as a Kolmogorov-Smirnov (K-S) test of statistical significance, to determine whether the two sets of time lengths of oscillations could be obtained from equal distributions, show that the dynamics of the circuits differ statistically, p-value of 0.006 (*p*-values of <0.01 suggest a significant difference between two distributions).

Interestingly, the difference (particularly the higher variance) was not reflected in the robustness of the oscillations of the SCR, which was comparable to the robustness of the LCR. Surprisingly, the SCR exhibited higher functionality in cells at 30 °C than the LCR, though the mean period of oscillations from the SCR was longer and noisier (higher CV^2).

5.5.3 Dynamics at different temperatures

Following the study on the effect of temperature on the dynamics of the LCR, we studied the effect of temperature on the SCR. The measurements were conducted in a similar fashion like it was previously done in LCR (Chandraseelan *et al*., 2013). Briefly, the behaviour of the SCR was measured, using confocal microscopy, by subjecting the cells with SCR to temperatures, 28 °C, 30 °C, 33 °C, and 37 °C. Similar to LCR, the measurement period was limited to 10 hours as the cells enter stationary phase after this point, which is evident from the disappearance of oscillatory behaviour in the cells (Chandraseelan *et al*., 2013; Elowitz *et al*., 2000).

The data and image analysis were done as described above. Briefly, from the images, obtained from each condition, extracted the fraction of functional cells (F), the number of cells exhibiting oscillatory fluorescent signal, the robustness (R) of the oscillations in 'functional' cells, and the mean and standard deviation of the period (m, s) were extracted.

Results are shown in Table 5. K-S tests of statistical significance were performed to determine whether the sets of oscillations' time length from the LCR and the SCR could be obtained from equal distributions, for each temperature. From Table 6 it is evident that the two circuits differ significantly in their oscillatory dynamics in all temperatures. However, Table 5 shows that the response of both circuits to changes in temperature is similar, although not identical, in the range tested. As expected, the circuits were similar in the loss of robustness at temperatures beyond 30 °C, due to the loss of functionality of the CI repressor (Jana *et al*., 1999; Koblan *et al*., 1991a; Koblan *et al*., 1991b). One major difference observed in the response of the two circuits to temperature changes is that the functionality of the SCR suffered a steeper decrease with increasing temperature.

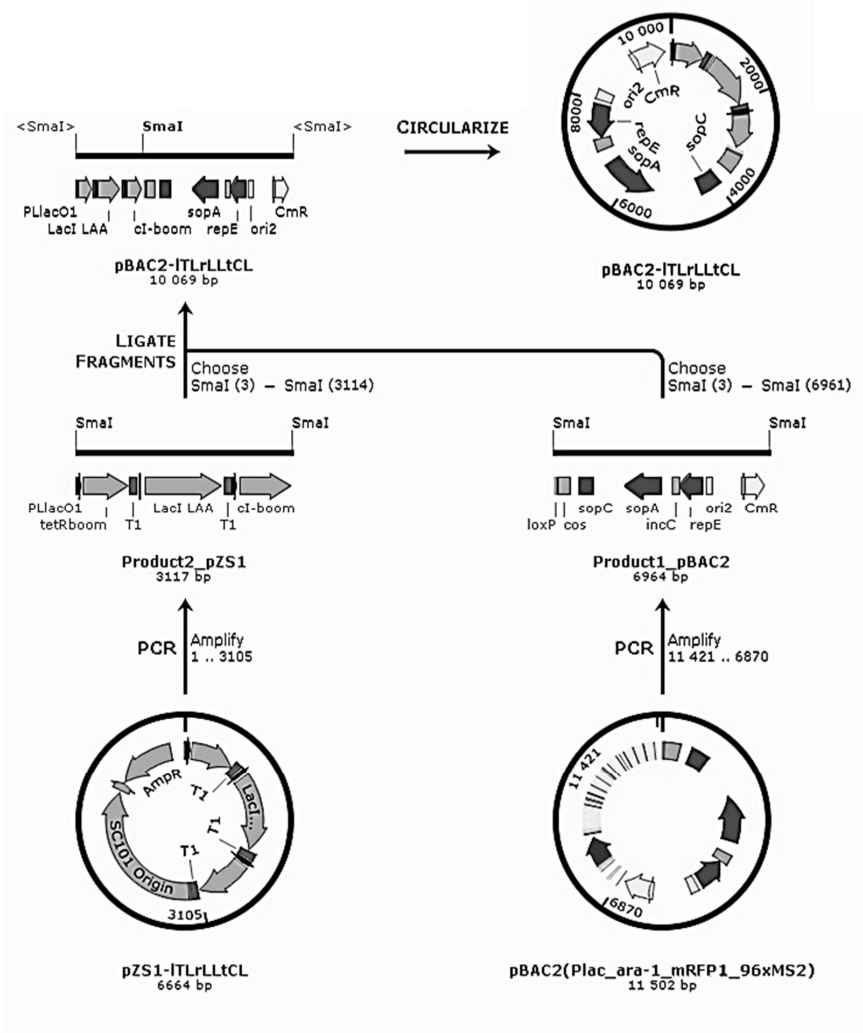

Figure 15: Construction of single copy Repressilator Plasmids used for the construction of the SCR plasmid. The pBAC2-lTlrLLtCL plasmid was engineered by linking the Repressilator system amplified region to part of the pBAC2 (Plac/ara-1-mRFP1-MS2-96x) vector (generously provided by Ido Golding of the University of Illinois, USA), containing the single-copy origin of replication (the construction history was generated and adapted using SnapGene® 1.5.2).

This is particularly interesting because it shows that the SCR's functionality is higher at lower and at optimum temperatures (28 °C and, particularly, 30 °C) but lower at higher

temperatures (33 °C and 37 °C). The other significant difference is that in the LCR the steepest change in mean period length was observed when the temperature was increased from 28 °C to 30 °C (a decrease of 142 min in length), in the SCR it was observed when temperature was increased from 30 °C to 33 °C (an increase by 51 min in length was seen). This was verified by K-S tests of statistical significance to determine whether the sets of oscillation lengths at different temperatures could be obtained from equal distributions, for the LCR and the SCR (Table 7). A *p*-value smaller than 0.01 in the LCR when comparing the data from 28 °C and 30 °C was seen, while a similar p-value was obtained in SCR when comparing the data from 30 °C and 33 °C, which is in agreement with the changes observed in the oscillations' mean period length with the changes in temperature.

Copy no.	**T (°C)**	**F (%)**	**No. cells oscillating**	**R (%)**	**m (min)**	**s (min)**
LCR	28	30	41	100	393	40
LCR	30	42	37	100	251	89
LCR	33	35	38	43	275	100
LCR	37	30	38	34	291	111
SCR	28	32	46	100	342	124
SCR	30	48	59	100	313	122
SCR	33	24	84	39	364	161
SCR	37	21	49	31	404	145

Table 5: Kinetics of LCR and SCR at different temperatures. Oscillatory signals were classified by their power spectra exhibiting peaks of more than 3 times the background at frequencies of 0.2-0.5 per hour. Temperature (T), fraction of functional cells (F), number of cells exhibiting oscillations, fraction of robust oscillations (R), mean (m) and standard deviation (s) of the period are shown.

T (°C)	28	30	33	37
***p*-value**	5.02x10-4	0.006	.36x10-4	7.04x10-7

Table 6: *P*-values of the K-S test between distributions of periods from different copy number plasmids. For *p*-values < 0.01, the hypothesis that the two distributions are the same is rejected.

Copy no.	28°C vs 30°C	30°C vs 33°C	33°C vs 37°C
LCR	3.09x10-14	0.13	0.33
SCR	0.44	6.70x10-5	0.30

Table 7: *P*-values of the Kolmogorov-Smirnov test between distributions of the LCR and SCR periods from different temperatures. For *p*-values < 0.01, the hypothesis that the two distributions are the same is rejected.

5.5.4 Effect of perturbations

The effect of perturbations with IPTG of the LCR dynamics has been described in (Elowitz *et al*., 2000). Here, to assess and compare the effect of such perturbations on the dynamics of the SCR and LCR, cells containing the SCR and LCR were subjected to external perturbations by addition of IPTG continuously into the medium. The perturbation was initiated 180 minutes after the start of the microscopy measurements, such that the cells were allowed to produce at least one cycle of oscillations. Perturbation is achieved when IPTG binds to LacI molecules (Sanchez *et al*., 2011), hence inducing constant expression of P_LLacO1, which effectively disrupts the functioning of the Repressilator, as it starts to constantly producing TetR, leading to indefinite repression of the P_LTetO1 promoter. Since P_LTETO1 is the promoter, which in addition to controlling the expression of the repressor for the next promoter also controls the expression of GFP, this leads to a loss of any fluorescence signal from the cells.

Three such experiments were performed. In the first experiment, cells with the SCR and cells with the LCR were perturbed by adding 50 μM of IPTG in the medium at 30 °C and

the robustness of the two circuits to external perturbations was compared. Next, cells with the SCR were perturbed by adding 1 mM of IPTG in the medium and the effects of 'weak' (50 µM) and 'strong' (1 mM) perturbations were compared. In all these tests, the M63 medium was pre-warmed and the desired concentration of IPTG was added, which was then supplied to the imaging chamber by a peristaltic pump at the rate of 0.3 mL/min. Images were acquired every 15 minutes for 6 hours (3 hours before perturbation and 3 hours after perturbation).

The effects of the 'weak' perturbation (50 µM of IPTG) on the dynamics of the LCR and of the SCR were compared. For that, functionality of the cells was assessed in the first 3 hours prior to the perturbation and in the subsequent 3 hours following the perturbation. The functionality of cells with the LCR was found to be equal to 93.3% during the first 3 hours, and 1.64% in the next 3 hours after perturbation (61 cells imaged) (i.e. 98% of the cells were perturbed). Interestingly, the functionality of cells containing the SCR equalled 100.0% in the first 3 hours, and 8.96% in the subsequent 3 hours after perturbation (145 cells imaged) (i.e. 91% of the cells were perturbed). This outcome suggests that the robustness of LCR is less affected by this perturbation than that of the SCR.

Next, 'strong' perturbation of the cells containing the SCR was performed by adding 1 mM of IPTG to the medium, at the end of the third hour of the measurements (112 cells imaged). Here, we observed a functionality of 100.0% in the first 3 hours as earlier, though a lower proportion of cells, 0.89%, were found to be functional in the latter 3 hours (99.1% of the cells were perturbed). From this, it can be concluded, based on predictions from simulations of models of this and similar circuits (Ribeiro *et al*, 2007), that the robustness of the SCR to external perturbations by IPTG decreases with the increase in the strength of the perturbation.

The agreement between the stochastic models and the empirical data is an indication that such models are capable of predicting the behaviour of the real circuits. As such, it is reasonable to assume that most assumptions made by such models are accurate. Therefore, it will be of interest to test, in the near future, other predictions made by such models on the long-term behaviour of the circuits, among other. Nevertheless, it is worth noted that the ability of the models to predict the behaviour of the circuits is limited. For

example, the models are unable to predict the changes in the circuit's behaviour when cells change phase (following the 10 hours under the microscope). This suggests that the causes for these changes are external to the circuit.

6 Discussion and Conclusion

In this thesis, the factors that affect the dynamics, particularly the phenotypic plasticity and robustness, of a single gene and of a small synthetic genetic circuit were studied using different methods. The study uses the Repressilator as a model circuit (Elowitz *et al.*, 2000). This genetic circuit is of particular interest because it emulates a natural circuit. Moreover, it performs the desired function, i.e., the production of oscillations. This circuit, comprised of known genetic components, has been used in various studies, although, its plasticity and robustness had not been previously studied using empirical methods.

In publication 1, we developed a method to, from the moments when RNA molecules are produced in live cells, infer the number and duration of steps involved in transcription, and also to infer how long it takes for the first RNA to appear in a cell following the appearance of the inducer in the media. Given that transcription initiation is a multi-stepped process characterized by a number of rate-limiting steps, whose duration far exceeds the duration of subsequent steps, promoter dynamics is a critical factor in the dynamics of any genetic circuit.

In this publication, the P_{BAD} and MS2-GFP tagging of RNA were used to obtain data from which one can determine the rate limiting steps in transcription and also the effect of inducer uptake kinetics on transcription initiation dynamics. The study suggests that inducer uptake kinetics plays a major role in the time it takes for the appearance of the first RNA and in the subsequent dynamics of RNA production. The results also suggest

that this waiting time is very noisy, even in a population of genetically identical cells and, as such, it plays a key role in generating cell to cell diversity in RNA numbers following changes in the environment.

Currently, this method is being used to study the dynamics of the constituent promoters that comprise the Repressilator in order to assess the importance of the dynamics of transcription initiation on the dynamics of the Repressilator, per se. Previous studies suggest that the rate of transcription initiation increases with rise in temperature, when temperature approaches 37 °C (Buc *et al*., 1985; Muthukrishnan *et al*., 2012). It was also shown that an additional rate-limiting step emerges, for lacUV5 promoter, when temperature falls below 20 °C. This finding is in agreement with the dynamics of the Repressilator with respect to temperature. At temperatures above 30 °C the circuit exhibited faster dynamics, whereas, at temperatures below 30 °C, the observed dynamics was slower (longer periods of oscillation). Future studies on the dynamics of the constituent promoters should give deeper insights on the temperature dependence of the dynamics of the Repressilator.

In publication 2, the effects of temperature on the dynamics of the Repressilator was studied (Chandraseelan *et al*., 2013). We observed that the repressor cI loses its functionality with increasing temperature. This finding is in conformity with the biology of the lambda phage. For a lambda phage to switch from lysogenic to lytic cycle, effective repression of P_{RM}, which controls the production of the lambda repressor cI, is required. This is achieved by binding of a cI octamer to the operator 3, effectively repressing the P_{RM} and causing a switch to lysogeny (Dodd *et al*., 2001). Another study indicated that oligomerization of cI is temperature dependent and production of higher order oligomers, up to octamers, occurs when the temperature approaches 37 °C (Burz *et al*., 1996). Finally, the RNA polymerase is shown to bind preferentially to P_R, rather than P_{RM}, at 37 °C (Owens, 1983). In our study, we observed that as the temperature shifts from 27 to 37 °C RNA productions by the P_{RM} promoter changes from being a sub-poissonian process to being a super-poissonian process. Further, the reduced time intervals between RNA production events suggests a brief period of increased production, followed by no production at the end of the measurements (data not shown). This has

consequences in the dynamics of the repressilator. At 30 °C, the repressilator's functionality was unaffected, but with increase in temperature the functionality was eventually lost; as it is evident from the bimodal distribution of the periods and failed oscillations, due to the altered properties that lead to deficient repression by cI and preferable binding of RNA polymerase to P_R (Fig 4, Chandraseelan *et al*., 2013). Meanwhile, the loss- of- functionality at lower temperatures are due to slower rate of the reactions (Buc *et al*., 1985; Muthukrishnan *et al*., 2012; Stricker *et al*., 2008). The outcomes of this study suggest that replacing the lambda repressor and the promoter, cI and P_R respectively; by less a temperature-dependent protein and promoter can make this circuit more functional at temperatures above 30 °C.

The study of effect of temperature on the synchrony of oscillations between sister cells, in publication 3, reveals that temperature has a profound influence in enhancing loss of synchrony between sister cells containing the Repressilator. Analysis of whether a robust cell is likely to have a robust sister cell suggested that it is more likely to have a robust sister cell than not, but the chance for a non-robust cell to have a non-robust sister cell is much higher. We also found that sister cells lose correlation as temperature increases. This effect can be explained with the increase in the noise of the period as a function of the temperature. Since non-robust cells are responsible for much of the behaviour variability at 37 °C, elimination of non-robust cells from the analysis restored correlation to a level comparable to that of 30 °C. Finally, we found that increasing temperature leads to pairs of cells with wider range of degrees of correlation.

Copy number is expected to be one of the key factors controlling the expression dynamics of simple genetic networks. Changes in the number of copies of the genes can result in behaviour switching of the network to different equilibrium points (Mileyko *et al*., 2007). In study 4, we studied the effect of copy number on the dynamics of the Repressilator by comparing the SCR with the LCR. It was observed that the SCR and the LCR are similar in terms of functionality and robustness to internal fluctuations. However, the dynamics of the SCR differed from that of the LCR in that it exhibited stronger fluctuations in the duration of each oscillation and a longer mean period length. It was also observed that, while the response of the two systems to temperature changes is not identical, as the

dynamics of the SCR varies more widely, in both the cases, the minimum period length was observed when setting temperature to 30 °C.

The higher mean period length of the SCR (30 °C or higher) is explained by the fact that, in general, in cells with LCR, when gene 'A' is in the 'ON' state, the system will evolve to gene 'B' being in the ON state, following the production of proteins from the several copies of gene 'C'. This behaviour is expected from the models, provided that a protein produced by a single copy of a gene is sufficient to repress all the promoter copies of the subsequent gene in the loop (Golding *et al.*, 2005).

Meanwhile, the shorter mean period length of the SCR at 28 °C can be explained as the opposite effect occurring at low temperatures, as each gene produces less proteins when 'ON', also the binding rate of the proteins to promoters is reduced, so a single gene being 'ON' is no longer sufficient to turn 'OFF' all the subsequent promoters in the loop. This possibly explains the longer mean period in length in cells at 28°C, so presence of multiple copies of a gene may be needed to activate the progression to the next stage of the cycle (Golding *et al.*, 2005). These hypotheses can be tested in the future, by implementing the Repressilator on, e.g., a medium copy plasmid (MCR). If the hypotheses are correct, the differences in behaviour between MCR and LCR, at temperatures between 30 °C to 37 °C, should be similar to the differences between the SCR and LCR, and it is also expected that there should be no significant differences between the LCR and MCR at 28 °C in period length.

Interestingly, the period of the SCR, at 30 °C, was observed to be longer and noisier (higher CV^2) than the period of the LCR. This could be due to the fact that in the LCR the variability in period lengths is reduced by expression of one copy of a gene going 'ON' producing enough repressors to turn 'OFF' all the copies of the subsequent gene in the loop, consistent with the findings, based on simulations of (Mileyko *et al.*, 2007), which suggest that copy-number acts as a proxy in coupling of the system and, hence, maintain oscillations effectively. It was also noted that the LCR and SCR robustness to internal fluctuations do not differ. Similar to the LCR, loss of robustness was observed with increasing temperature, which has been shown (Chandraseelan *et al.*, 2013) to be due to the loss of ability of CI to repress beyond 30 °C (Jana *et al.*, 1999; Koblan *et al.*, 1991a;

Koblan *et al*.,1991b). This can be the effect of similar fraction of hampered CI proteins with increasing temperature in LCR and SCR cells are similar.

The functionality of both SCR and LCR were found to be maximized at 30 °C, although the effects of changing temperature on the functionality appeared to differ to a greater extent between the two systems. The functionality was higher in the SCR than in the LCR at 28 °C and 30 °C, but lower at 33 °C and 37 °C. The reasons as to why not all Repressilators (LCR and SCR) are functional in a cell are not known and, at this stage, it is not possible to explain the changes in functionality with temperature, however, these differences may offer clues to understand the mechanisms that underlie the functionality of the circuit.

Another interesting observation in the SCR worth discussing is the robustness of the SCR to external perturbations. The robustness of LCR to a constant perturbation (50 µM of IPTG in the medium) was found to be less than the SCR. This is perhaps surprising but can be explained by the dynamic coupling of all the copies of Repressilator in the LCR system; perturbing one of the copies of the repressilator (e.g. causing the operator sites of one of the promoters to become vacant, thus allowing its expression) may be sufficient to disrupt the activity of all other repressilators in the cells due to coupling. Since the cells with LCR have more copies of repressors, for a perturbation of identical 'strength', it is more likely that at least one copy will be perturbed in cells with LCR than in cells with SCR.

The outcomes of this study suggest significant differences in robustness to internal and external perturbations as well as the differences in the dynamics of the two circuits. Also, it emphasizes the need for a single-copy version of the synthetic Repressilator which is, for example highly robust to external perturbations and highly functional at lower temperatures that will be a new building block in Synthetic Biology to engineer single copy based artificial genetic circuits. Our findings might also be initial clues to explain why the variation in copy-number of genes has been linked to a number of altered phenotypes, including many diseases (Stranger *et al*., 2007). Further studies on the regulation of the dynamics of the SCR and LCR and its effects on the phenotypic

differences in cells will give deeper insights about how cells alter phenotypes with respect to changing copy numbers of genes.

Although a number of synthetic genetic circuits have been developed, development of a genetic circuit with significant complexity that resemble the natural genetic circuits is still a complex task owing to the complexity of the biological systems and the stochasticity of genetic processes. For the development of complex synthetic circuits, it is of importance to characterise the components and their functioning in the system. In this work, we quantified the effect of different factors on the dynamics of the Repressilator. The outcomes of the study reemphasise the need for characterisation of genetic components that can be used to build genetic circuits with significant functions and complexity. It was also observed, in agreement with previous studies, cell to cell diversity in the populations observed which again supports the notion that noise is a key component of genetic circuits. Finally, we observed that copy-number of genes is a significant factor on the dynamics of the circuit.

Overall, from this study, it is evident that the phenotypic plasticity and robustness of simple genetic circuits can be affected by temperature, copy-number, etc. The methods used in this study, can be used in the future to study other genetic circuits, synthetic and natural, which will enable the development of new synthetic genetic circuits capable of performing complex tasks in cells.

References

Bacchus, W., Lang, M., El-Baba, M. D., Weber, W., Stelling, J., & Fussenegger, M. (2012). Synthetic two-way communication between mammalian cells. *Nature Biotechnology*, 30, 991–6.

Becskei, A., & Serrano, L. (2000). Engineering stability in gene networks by autoregulation. *Nature*, 405, 590–593.

Berthoumieux, S., de Jong, H., Baptist, G., Pinel, C., Ranquet, C., Ropers, D., & Geiselmann, J. (2013). Shared control of gene expression in bacteria by transcription factors and global physiology of the cell. *Molecular Systems Biology*, 9, 634.

Bertrand, E., Chartrand, P., Schaefer, M., Shenoy, S. M., Singer, R. H., & Long, R. M. (1998). Localization of ASH1 mRNA Particles in Living Yeast, *Molecular cell*, 2, 437–445.

Bertrand-Burggraf, E., Lefevre, J. F., & Daune, M. (1984). A new experimental approach for studying the association between RNA polymerase and the tet promoter of pBR322. *Nucleic Acids Research*, 12, 1697–1706.

Brown, J. R., & Doolittle, W. F. (1997). Archaea and the Prokaryote-to-Eukaryote Transition. M*icrobiology and Molecular Biology Reviews : MMBR*, 61, 456–502.

Browning, D. F., & Busby, S. J. (2004). The regulation of bacterial transcription initiation. *Nature Reviews. Microbiology*, 2, 57–65.

Buc, H., & McClure, W. R. (1985). Kinetics of open complex formation between *Escherichia coli* RNA polymerase and the lac UV5 promoter. Evidence for a sequential mechanism involving three steps. *Biochemistry*, 24, 2712–2723.

Burz, D. S., & Ackers, G. K. (1996). Cooperativity mutants of bacteriophage λ cI repressor: Temperature dependence of self-assembly. *Biochemistry*, 35, 3341–3350.

Cagliero, C., & Jin, D. J. (2013). Dissociation and re-association of RNA polymerase with DNA during osmotic stress response in *Escherichia coli*. *Nucleic Acids Research*, 41, 315–26.

Cai, L., Friedman, N., & Xie, X. S. (2006). Stochastic protein expression in individual cells at the single molecule level. *Nature*, 440, 358–62.

Campbell, E. a, Westblade, L. F., & Darst, S. a. (2008). Regulation of bacterial RNA polymerase sigma factor activity: a structural perspective. *Current Opinion in Microbiology*, 11, 121–7.

Carter, A. P., W. M. Clemons, Jr., D. E. Brodersen, R. J. Morgan-Warren, T. Hartsch, B. T. Wimberly, and V. Ramakrishnan. 2001. Crystal structure of an initiation factor bound to the 30S ribosomal subunit. *Science*, 291, 498–501.

Chandraseelan, J. G., Oliveira, S. M. D., Häkkinen, A., Tran, H., Potapov, I., Sala, A., … Ribeiro, A. S. (2013). Effects of temperature on the dynamics of the LacI-TetR-CI repressilator. *Molecular BioSystems*, 9, 3117–23.

Chen, T.-B., Lu, H. H.-S., Lee, Y.-S., & Lan, H.-J. (2008). Segmentation of cDNA microarray images by kernel density estimation. *Journal of Biomedical Informatics*, 41, 1021–7.

Ciampi, M. S. (2006). Rho-dependent terminators and transcription termination. *Microbiology* (Reading, England), 152, 2515–28.

Crick, F. (1970). Central dogma of molecular biology. *Nature*, 227, 561- 563.

Dahlquist, K. D., and J. D. Puglisi. 2000. Interaction of translation initiation factor IF1 with the *E. coli* ribosomal A site. *J. Mol. Biol*, 299, 1–15.

Danino, T., Mondragón-Palomino, O., Tsimring, L., & Hasty, J. (2010). A synchronized quorum of genetic clocks. *Nature*, 463, 326–30.

Dempster, A. P., Laird, N. M., & Rubin, D. B. (1977). Maximum likelihood from incomplete data via the EM algorithm. *JSTOR*, 39, 1–38.

Dodd, I. B., Perkins, A. J., Tsemitsidis, D., & Egan, J. B. (2001). Octamerization of CI repressor is needed for effective repression of P RM and efficient switching from lysogeny, *Genes and development*, 15, 3013–3022.

Duetscher, J. (2008). The mechanisms of carbon catabolite repression in bacteria. *Curr Opin Microbiol*, 11, 87-93.

Dunlap, J. C. (1999). Molecular Bases for Circadian Clocks Review. *Cell*, 96, 271–290.

Eldar, A and Elowitz, M. B. (2010). Functional roles for noise in genetic circuits. *Nature*, 467, 167-173.

Elowitz, M. B., & Leibler, S. (2000). A synthetic oscillatory network of transcriptional regulators. *Nature*, 403, 335–338.

Friedland, A. E., Lu, T. K., Wang, X., Shi, D., Church, G., & Collins, J. J. (2009). Synthetic gene networks that count. *Science*, 324, 1199–202.

Fussenegger, M. (2010). Synchronized bacterial clocks. *Nature*, 463, 301–302.

Gadgil, M., Kapur, V., & Hu, W. (2005). Transcriptional Response of *Escherichia coli* to Temperature Shift. *Biotechnol. Prog*, 21, 689–699.

Gardner, T. S., Cantor, C. R., & Collins, J. J. (2000). Construction of a genetic toggle switch in *Escherichia coli*. *Nature*, 403, 339–342.

Golding, I., & Cox, E. C. (2004). RNA dynamics in live *Escherichia coli* cells, *Proc. Nat. Acad. Sci. USA*, 101, 11310-11315.

Golding, I., Paulsson, J., Zawilski, S. M., & Cox, E. C. (2005). Real-time kinetics of gene activity in individual bacteria. *Cell*, 123, 1025–1036.

Gordon, G. S., Sitnikov, D., Webb, C. D., Teleman, A., Straight, A., Losick, R., … Wright, A. (1997). Chromosome and Low Copy Plasmid Segregation in *E . coli* : Visual Evidence for Distinct Mechanisms. *Cell*, 90, 1113–1121.

Gruber, T.M and Gross, C. A. (2003). Multiple sigma subunits and the partitioning of bacterial transcription space. *Annu. Rev. Microbiol*, 57, 441 - 66

Gualerzi, C., G. Risuleo, and C. L. Pon. (1977). Initial rate kinetic analysis of the mechanism of initiation complex formation and the role of initiation factor IF-3. *Biochemistry*, 16, 1684–1689.

Gualerzi, C. O., and C. L. Pon. (1990). Initiation of mRNA translation in prokaryotes. *Biochemistry*, 29, 5881–5889.

Guet, C. C., Elowitz, M. B., Hsing, W and Leibler, S. (2002). Combinatorial synthesis of genetic networks. *Science*, 296, 1466-1470.

Guido, N. J., Wang, X., Adalsteinsson, D., McMillen, D., Hasty, J., Cantor, C. R., … Collins, J. J. (2006). A bottom-up approach to gene regulation. *Nature*, 439, 856–60.

Guisbert, E., Herman, C., Lu, C.Z and Gross, C. A. (2004). A chaperone network controls the heat shock response in *E. coli*. *Genes & Dev*, 18, 2812-2821

Hansen, H., Bjelland, A. M., Ronessen, M., Robertsen, E., & Willassen, N. P. (2014). LitR is a repressor of syp genes and has a temperature-sensitive regulatory effect on biofilm formation and colony morphology in vibrio (Aliivibrio) salmonicida. *Applied and Environmental Microbiology*, 80, 5530–41.

Hawley, D. K., & Mcclure, W. R. (1983). Nucleic Compilation and analysis of *Escherichia coli* promoter DNA sequences. The DNA sequence of 168 promoter regions (-50 to + 10) for *Escherichia coli* RNA polymerase were compiled . The complete listing. *Nucleic Acids Research*, 11, 2237–2255.

Hlavacek W S and M A Savageau (1995), Subunit structure of regulator proteins influences the design of gene circuitry: Analysis of perfectly coupled and completely uncoupled circuits, *J. Mol. Biol,* 248, 739–755.

Hlavacek W S and M A Savageau (1996), Rules for coupled expression of regulator and effector genes in inducible circuits, *J. Mol. Bio,* 255, 121–139

Hoch, J. A. (2000). Two-component and phosphorelay signal transduction. *Current Opinion in Microbiology*, 3, 165–170.

Hsu, L. M., Vo, N. V, Kane, C. M., & Chamberlin, M. J. (2003). In Vitro Studies of Transcript Initiation by *Escherichia coli* RNA Polymerase . 1 . RNA Chain Initiation , Abortive Initiation , and Promoter Escape at Three. *Biochemistry*, 42, 3777–3786.

Ishihama, A (2000) Functional modulation of *Escherichia coli* RNA polymerase.*Annu Rev Microbiol,* 54, 499–518.

Ishihama, A (2010) Prokaryotic genome regulation: Multi-factor promoters, multi-target regulators and hierarchic networks. *FEMS Microbial Rev*, 34, 628–645.

Jacob, F. J., & Monod. (1961). Genetic Regulatory Mechanisms in the synthesis of proteins. *Journal of Molecular Biology*, 3, 318–356.

Jana, N. K., & Roy, S. (1999). Amino acid changes in the repressor of bacteriophage lambda due to temperature-sensitive mutations in its cI gene and the structure of a highly temperature-sensitive mutant repressor, *Protein engineering*, 12, 225–233.

Kandhavelu, M., Häkkinen, A., Yli-Harja, O., & Ribeiro, A. S. (2012). Single molecule dynamics of transcription of the lar. *Physical Biology*, 9, 026004 – 026016.

Kandhavelu, M., Mannerström, H., Gupta, A., Häkkinen, A., Lloyd-Price, J., Yli-Harja, O., & Ribeiro, A. S. (2011). In vivo kinetics of transcription initiation of the lar

promoter in *Escherichia coli*. Evidence for a sequential mechanism with two rate-limiting steps. *BMC Systems Biology*, 5, 149.

Kauffman S A, The Origins of Order: Self-Organization and Selection in Evolution (Oxford University Press, New York, 1993).

Keiler, K.C., Waller., P:R and Sauer, R.T. (1996). Role of peptide tagging system in degradation of proteins synthesised from damaged messenger RNA. *Science,* 271, 998-993.

Khalil, A. S and Collins, J. J. (2010). Synthetic Biology: Applications Come of Age. *Nat Rev Genet*, 11, 367–379.

Kisselev, L., Ehrenberg, M and Frolova, L.(2003). Termination of translation: interplay of mRNA, rRNAs and release factors? *EMBO J*, 22, 175–182.

Koblan, K. S., & Ackers, G. K. (1991a). Cooperative Protein-DNA Interactions : Effects of KC1 on X cI Binding to OR +, *Biochemistry*, 7822–7827.

Koblan, S., & Ackers, G. K. (1991b). Quantitative Study of Protein Association at Picomolar Concentrations : The X Phage cl Repressor, *Analytical biochemistry*, 75, 69–75.

Kruse, K., & Jülicher, F. (2005). Oscillations in cell biology. *Current Opinion in Cell Biology*, 17, 20–6.

Kurten K E and H Beer. (1997). Inhomogeneous Kauffman models at the borderline between order and chaos, *J. Stat. Phys.* 87, 929–935.

Larson, D. R., Zenklusen, D., Wu, B., Chao, J. a, & Singer, R. H. (2011). Real-time observation of transcription initiation and elongation on an endogenous yeast gene. *Science* (New York, N.Y.), 332, 475–8.

Latchman, D. S. (2007). Transcription Factors. In Encylclopedia of life sciences (pp. 1–5). John Wiley and sons.

Laursen, B. S., Sørensen, H. P., Mortensen, K. K., & Sperling-petersen, H. U. (2005). Initiation of Protein Synthesis in Bacteria. *Microbiology and Molecular Biology Reviews : MMBR*, 69, 101–123.

Lichestein, H. S., Hamilton, E. P and Lee, N. (1987). Repression and Catabolite Gene Activation in the araBAD Operon. *Journal of bacteriology*, 169, 811 -822.

Lim, W. a. (2010). Designing customized Cell signaling circuits. *Nature Reviews. Molecular Cell Biology*, 11, 393–403.

Little, J. W., & Michalowski, C. B. (2010). Stability and instability in the lysogenic state of phage lambda. *Journal of Bacteriology*, 192, 6064–76.

Liu, H., Wang, X., Wang, H.-D., Wu, J., Ren, J., Meng, L., … Shan, G. (2012). Escherichia coli noncoding RNAs can affect gene expression and physiology of Caenorhabditis elegans. *Nature Communications*, 3, 1073.

Lucks, J. B., Qi, L., Mutalik, V. K., Wang, D., & Arkin, A. P. (2011). Versatile RNA-sensing transcriptional regulators for engineering genetic networks. *Proc. Nat. Acad. Sci. USA*, 108, 8617–22.

Lutz, R and Bujard, .(1997). Independent and tight regulation of transcriptional units in *E.coli* via the LacR/o, TetR/O and AraC/I1-I2 regulatory elements. *Nucleic acids research*, 25, 1203-1210.

Maniatis, T., Jefferey, A and Kleid, D.G. (1975). NucleotideSequenceof the Rightward Operator of Phage lambda. *Proc. Nat. Acad. Sci. USA*. 1184-1188

Mcclure, W. R. (1980). Rate-limiting steps in RNA chain initiation. *Proc. Nat. Acad. Sci. USA*, 77, 5634–5638.

Mihalcescu, I., Hsing, W., & Leibler, S. (2004). Resilient circadian oscillator revealed in individual cyanobacteria. *Nature*, 430, 81–85.

Mileyko, Y., Joh, R. I., & Weitz, J. S. (2007). Small-scale Copy Number Variation and Large-scale Changes in Gene Expression. *Proc. Nat. Acad. Sci. USA*, I, 1– 11.

Miller (1970) Electron Microscopic Visualization of Transcription *Cold Spring Harb Symp Quant Biol*, 3, 505-512.

Miyamoto, T., Ravazi, S., DeRose, R and Inoue, T. (2013). Synthesizing Biomolecule-based Boolean Logic Gates. *ACS Synth Biol*. 15, 2, 72–82.

Morris, M. K., Saez-Rodriguez, J., Sorger, P. K., & Lauffenburger, D. (2010). Logic-based models for the analysis of cell signaling networks. *Biochemistry*, 49, 3216–24.

Mueller, J., Oehler, S and Mueller-Hill, B. (1996). Repression of lac Promoter as a Function of Distance, Phase and Quality of an Auxiliary lac Operator. *J. Mol. Biol.*, 257, 21–29.

Muthukrishnan, A.-B., Kandhavelu, M., Lloyd-Price, J., Kudasov, F., Chowdhury, S., Yli-Harja, O., & Ribeiro, A. S. (2012). Dynamics of transcription driven by the tetA promoter, one event at a time, in live *Escherichia coli* cells. *Nucleic Acids Research*, 40(17), 8472–83.

Mäkelä, J., Kandhavelu, M., Oliveira, S. M. D., Chandraseelan, J. G., Lloyd-Price, J., Peltonen, J., Yli-Harja, O and Ribeiro, A. S. (2013). In vivo single-molecule kinetics of activation and subsequent activity of the arabinose promoter. *Nucleic Acids Res.* 41, 6544-52.

Nandagopal, N., & Elowitz, M. B. (2011). Synthetic biology: integrated gene circuits. *Science* (New York, N.Y.), 333, 1244–1248.

Nem, M. N., Fung, E., Wong, W. W., Suen, J. K., & Bulter, T. (2005). A synthetic gene – metabolic oscillator, *Nature*, 435, 118–122.

Nudler, E., & Gottesman, M. E. (2002). Transcription termination and anti-termination in *E . coli*, *Genes to cells*, 755–768.

Oehler, S., Eismann, E. R., Krämer, H and Müller-Hill B. (1990). The three operators of the lac operon cooperate in repression. *EMBO J*, 9, 973–979.

Oshima, T., Ishikawa, S., Kurokawa, K., Aiba, H and Ogasawara, N. (2006). *E. coli* histone-like protein H-NS preferentially binds to horizontally acquired DNA in association with RNA polymerase. *DNA Res*, 31, 141-53.

Ogura, T., & Hiraga, S. (1983). Mini-F plasmid genes that couple host cell division to plasmid proliferation. *Proc. Nat. Acad. Sci. USA*, 80, 4784–4788.

Owens, E. M and Gussin, G.N.(1983). Differential binding of RNA polymerase to the pRM and pR promoters of bacteriophage lambda. *Genes*, 23, 157-166.

Petrelli, D., A. LaTeana, C. Garofalo, R. Spurio, C. L. Pon, and C. O. Gualerzi. (2001). Translation initiation factor IF3: two domains, five functions, one mechanism? *EMBO J*, 20, 4560–4569.

Pon, C. L., and C. O. Gualerzi. (1984). Mechanism of protein biosynthesis in prokaryotic cells. Effect of initiation factor IF1 on the initial rate of 30 S initiation complex formation. *FEBS Lett*, 175, 203–207.

Pribnow, D. (1979) In biological regulation and development (Goldberger, R.R., ed) vol.1, 219 – 269, Plenum Press, New York.

Qi, L. S., & Arkin, A. P. (2014). A versatile framework for microbial engineering using synthetic non-coding RNAs. *Nature Reviews. Microbiology*, 12, 341–54.

Raghavan, R., Groisman, E. A., & Ochman, H. (2011). Genome-wide detection of novel regulatory RNAs in *E . coli*. *Genome Research*, 21, 1487–1497.

Reznikoff, W.S., Winter, W.B and Hureley, C.K. (1974) The location of repressor binding sites in the lac operon. *Proc. Nat. Acad. Sci. USA*, 71,2314-2318.

Ribeiro, A. (2007). Effects of coupling strength and space on the dynamics of coupled toggle switches in stochastic gene networks with multiple-delayed reactions. *Physical Review E*, 75, 061903.

Ribeiro, A. S., & Kauffman, S. a. (2007). Noisy attractors and ergodic sets in models of gene regulatory networks. *Journal of Theoretical Biology*, 247, 743–55.

Sanchez, A., Osborne, M. L., Friedman, L. J., Kondev, J., & Gelles, J. (2011). Mechanism of transcriptional repression at a bacterial promoter by analysis of single molecules. *The EMBO Journal*, 30, 3940–6.

Santillan, M and Mackey, M.C. (2000). Dynamic regulation of the tryptophan operon: A modeling study and comparison with experimental data. *Proc. Nat. Acad. Sci. USA*, 98, 1364 - 1369.

Savageau, M. a. (2001). Design principles for elementary gene circuits: Elements, methods, and examples. *Chaos*, 11, 142–159.

Schleif, R. (2010). AraC protein, regulation of the l-arabinose operon in Escherichia coli, and the light switch mechanism of AraC action. *FEMS Microbiology Reviews*, 34, 779–96.

Schubert, R. A., Dodd, I. B., Egan, J. B and Shearwin, K, E (2007) Cro's role in the CI Cro bistable switch is critical for {lambda}'s transition from lysogeny to lytic development. *Genes Dev* 21: 2461–2472

Siebenlist, U. (1979). Nuckotide sequence of the three major early promoters of bacteriophage T7. *Nucl. Acids Res.* 6, 1895-l907.

Shimada, T., Yamazaki, Y., Tanaka, K and Ishihama, A.(2014). The Whole Set of Constitutive Promoters Recognized by RNA Polymerase RpoD Holoenzyme of *Escherichia coli. PLoS one.* e100908.

Slusarczyk, A. L., Lin, A., & Weiss, R. (2012). Foundations for the design and implementation of synthetic genetic circuits. *Nature Reviews. Genetics.* 13, 406–20.

Sprinzak, D., & Elowitz, M. B. (2005). Reconstruction of genetic circuits. *Nature*, 438, 443–448.

Stoebel, D. M., Hokamp, K., Last, M. S., & Dorman, C. J. (2009). Compensatory evolution of gene regulation in response to stress by Escherichia coli lacking RpoS. *PLoS Genetics*, 5, e1000671.

Stranger, B. E., Forrest, M. S., Dunning, M., Ingle, C. E., Thorne, N., Redon, R., … Bari, B. (2007). Relative impact of nucleotide and copy number variation on gene expression phenotypes. *Science*, 315, 848–853.

Stricker, J., Cookson, S., Bennett, M. R., Mather, W. H., Tsimring, L. S., & Hasty, J. (2008). A fast, robust and tunable synthetic gene oscillator. *Nature*, 456, 516–519.

Takeda, Y., Rosst, P. D., & Muddt, C. P. (1992). Thermodynamics of Cro protein-DNA interactions. *Proc. Natl. Acad. Sci. USA*, 8180–8184.

Thieffry D, H Salgado, A M Huerta, and J Collado-Vides (1998), Prediction of transcriptional regulatory sites in the complete genome sequence of *Escherichia coli* K-12, *Bioinformatics*, 14, 391–400.

VonHippels, P. H., Bear, D. G., Morgan, W. D and McSwiggen, J. A. (1984). Protein-Nucleic acid interactions in transcription: A molecular Analysis. *Ann. Rev.Biochem.* 53, 389 - 446.

Wang, F., Redding, S., Finkelstein, I.J. , Gorman, J., Reichman, D.R., & Greene, E. C (2013). The promoter search mechanism of *E. coli* RNA polymerase is dominated by three–dimensional diffusion. *Nat Struct Mol Biol*. 20, 174-81

Weiss, R. O. N., Basu, S., & Hooshangi, S. (2003). Genetic circuit building blocks for cellular computation, communications, and signal processing, *Natural computing*, 47–84.

Yuan, Y., Liu, B., Xie, P., Zhang, M. Q., Li, Y., Xie, Z., & Wang, X. (2015). Model-guided quantitative analysis of microRNA-mediated regulation on competing endogenous RNAs using a synthetic gene circuit. *Proc. Nat. Acad. Sci. USA*, 112, 3158–3163.

Publications

Publication I

Mäkelä, J., Kandhavelu, M., Oliveira, S. M. D., Chandraseelan, J. G., Lloyd-Price, J., Peltonen, J., Yli-Harja, O and Ribeiro, A. S. (2013). *In vivo single-molecule kinetics of activation and subsequent activity of the arabinose promoter*. Nucleic Acids Res. 41(13):6544-52.

Nucleic Acids Research Advance Access published May 3, 2013

Nucleic Acids Research, 2013, 1–9
doi:10.1093/nar/gkt350

In vivo single-molecule kinetics of activation and subsequent activity of the arabinose promoter

Jarno Mäkelä[1], Meenakshisundaram Kandhavelu[1], Samuel M. D. Oliveira[1], Jerome G. Chandraseelan[1], Jason Lloyd-Price[1], Juha Peltonen[1], Olli Yli-Harja[1,2] and Andre S. Ribeiro[1,*]

[1]Laboratory of Biosystem Dynamics, Computational Systems Biology Research Group, Department of Signal Processing, Tampere University of Technology, FI-33101 Tampere, Finland and [2]Institute for Systems Biology, 1441N 34th Street, Seattle, WA 98103-8904, USA

Received March 21, 2013; Revised April 11, 2013; Accepted April 13, 2013

ABSTRACT

Using a single-RNA detection technique in live *Escherichia coli* cells, we measure, for each cell, the waiting time for the production of the first RNA under the control of P_{BAD} promoter after induction by arabinose, and subsequent intervals between transcription events. We find that the kinetics of the arabinose intake system affect mean and diversity in RNA numbers, long after induction. We observed the same effect on $P_{lac/ara-1}$ promoter, which is inducible by arabinose or by IPTG. Importantly, the distribution of waiting times of $P_{lac/ara-1}$ is indistinguishable from that of P_{BAD}, if and only if induced by arabinose alone. Finally, RNA production under the control of P_{BAD} is found to be a sub-Poissonian process. We conclude that inducer-dependent waiting times affect mean and cell-to-cell diversity in RNA numbers long after induction, suggesting that intake mechanisms have non-negligible effects on the phenotypic diversity of cell populations in natural, fluctuating environments.

INTRODUCTION

Transcription in *E. coli* is, at a genome-wide scale, a relatively rare stochastic event (1–3). Further, many genes only become active in response to external stimuli (4–7), via processes that are also stochastic (7). Although much is known on the noise in gene expression at the single-cell level (1–3,7–10), most of our present knowledge concerning the kinetics of response, in terms of gene activity, to external signals concerns the average behaviour of cell populations alone (11). However, to characterize the dynamics and the underlying steps of intake processes, it is necessary to observe their effects in individual live cells (12). This observation should inform also on the robustness of cellular response mechanisms by informing on the degree of change in the responses of a single cell to multiple occurrences of the same stimulus, as well as the difference in responses to different stimuli.

One of the most well-known gene activation mechanisms is the arabinose utilization system of *E. coli*. This system imports arabinose into the cell by AraFGH, an arabinose-specific high-affinity ABC transporter (11,13–15), and by a low-affinity transporter, AraE, which binds to the inner membrane and makes use of electrochemical potential to intake the arabinose (11,16,17). This system exhibits wide variability in the timing of activation and in the rates of accumulation of inducer molecules (18). It has been hypothesized that this is due to the cell-to-cell variability in the numbers of proteins responsible for the intake of arabinose (18). Interestingly, if the intake gene *araE* is placed under the control of a constitutive promoter the intake rates become more homogenous (19–21), suggesting that the diversity in the number of intake proteins is a non-negligible source of cell-to-cell variability in the kinetics of the arabinose utilization system (12).

Evidence suggests that when the intracellular concentration of arabinose exceeds a threshold, the dimeric AraC protein activates the genes that code for the proteins responsible for the intake (AraE and AraFGH) and for the catabolism of arabinose (*araBAD*) (11,22). In the absence of arabinose, AraC binds two half-sites on the DNA (I_1 and O_2) and promotes the formation of a DNA loop that prevents access of RNA polymerases to the promoters in that region (P_C and P_{BAD}). When bound by arabinose, AraC binds instead to the adjacent I_1 and I_2 half-sites. The resulting configuration promotes transcription initiation at P_{BAD} (11).

Transcription initiation is a complex, multi-stepped process (23,24). *In vitro* measurements suggest that this process has at least two to three rate limiting steps (25,26). It starts when the RNA polymerase binds to the

*To whom correspondence should be addressed. Tel: +358408490736; Fax: +358331154989; Email: andre.ribeiro@tut.fi

promoter region of the DNA molecule, forming the closed complex, which is followed by the open complex formation and promoter escape (27,28). The RNA polymerase then elongates the nascent RNA (28). Evidence suggests that, in general, initiation is much longer in duration than elongation (26,29). Recent *in vivo* measurements of the kinetics of initiation of $P_{lac/ara-1}$ and P_{tetA} promoters have shown that RNA production under the control of these promoters is a sub-Poissonian process (8–10). These studies also support the existence of multiple steps at the stage of initiation, significantly limiting the rate of RNA production, as suggested by *in vitro* measurements (30).

Here, we investigate the degree of contribution of the process of intake of arabinose and of the process of transcription under the control of P_{BAD} to the cell-to-cell diversity in RNA production. Namely, we report measurements of the *in vivo* kinetics of induction and transcript production of P_{BAD} with single-molecule sensitivity, making use of the MS2d-GFP tagging of RNA in *E. coli* (31). For that, in each cell, we measure the waiting time until the first RNA is produced after induction and the subsequent intervals between consecutive transcript productions. For comparison, we conduct the same measurements for $P_{lac/ara-1}$ when induced by either of its two inducers, arabinose and IPTG.

MATERIALS AND METHODS

Strains and plasmids

Escherichia coli strain DH5α-PRO was generously provided by I. Golding, University of Illinois and contains the construct PROTET-K133, carrying $P_{LtetO-1}$-MS2d-GFP (31), along with a new construct, pMK-BAC (P_{BAD}-mRFP1-MS2-96bs), which is a single-copy F-based vector carrying a sequence coding for a monomeric red fluorescent protein (mRFP1) followed by a 96 binding site array under the control of P_{BAD} (cloning information provided in Supplementary Methods) (see also Supplementary Figures S1 and S2). The strain with plasmids $P_{LtetO-1}$-MS2d-GFP and pIG-BAC ($P_{lac/ara-1}$-mRFP1-MS2-96bs) (32) was used as well. The DH5α-PRO strain [identical to Z1 (31)] is a genuine producer of AraC (33). No modifications were made to the chromosome of this strain in our experiments.

Media and growth conditions

Cells were grown overnight at 30°C with aeration and shaking in Luria-Bertani (LB) medium, supplemented with antibiotics according to the plasmids. The cells were diluted in fresh M63 medium and allowed to grow until an optical density of $OD_{600} \approx 0.3$–0.5. To attain full induction of the MS2d-GFP reporter, cells were pre-incubated for 40 min with 100 ng/ml anhydrotetracycline (aTc, IBA GmbH). The same protocol was used for each strain.

Microscopy

For microscopy measurements, cells were pelleted and re-suspended in ~50 µl of fresh M63 medium. Afterwards, few microlitres of cells were placed between a 3% agarose gel pad made with medium and a glass coverslip before assembling the imaging chamber (FCS2, Bioptechs). Before the starting of the experiment, the chamber was heated to 37°C.

Cells were visualized in a Nikon Eclipse (TE2000-U, Nikon, Japan) inverted microscope with C1 confocal laser-scanning system using a ×100 Apo TIRF objective. A flow of fresh, pre-warmed M63 medium containing the inducer was provided with a peristaltic pump at a rate of 1 ml/min. Images were taken once per minute for 2 h, and the laser shutter was open only during the exposure time to minimize photobleaching. The peristaltic pump was initialized at the same time as the collection of the time series. For image acquisition, we used Nikon EZ-C1 software. GFP fluorescence was measured using a 488 nm argon ion laser (Melles-Griot), 515/30 nm emission filter and a pixel dwell time of 3.36 µs (total image acquisition time of 3.5 s).

An interacting multiple model filter-based autofocus strategy (34) was used to correct focus drift in time series acquisitions. The method estimates the focal drift using an interacting multiple model filter algorithm to predict the focal drift at time t based on the measurement at t-1. It allows reducing the number of required images at different z-planes for drift correction, thus minimizing photobleaching.

Data and image analysis

Data and images were analysed using custom software written in MATLAB 2011b (MathWorks). Cells were detected from fluorescence images by a semi-automatic method described previously (8). In time series, the area occupied by each cell was manually masked. Principal component analysis was used to obtain the dimensions and orientation of the cells within each mask. Fluorescent spots in the cells were automatically segmented using density estimation with a Gaussian kernel (35) and Otsu's thresholding (36). Finally, background-corrected spot intensities were calculated and summed to produce the total spot intensity in each cell.

Moments of appearance of novel target RNA molecules in each cell were obtained from time-lapse fluorescence images by fitting the corrected total spots intensity over time in each cell to a monotone piecewise-constant function by least squares (37). The number of terms was selected using the F-test with a P-value of 0.01. Each jump corresponds to the production of a single RNA molecule (37). An example of this procedure is shown in Figure 1D. For more details on the image analysis see (8). Note that, in cells that do not contain target RNA molecules at the start of the measurements, the number of novel RNA molecules detected since the start of the measurements until a given moment equals the total number of RNA molecules in the cell at that moment.

Because some cells already contained target RNA molecules at the start of the measurement, the total RNA numbers within cells at a given moment in time is obtained using a different method. Specifically, when

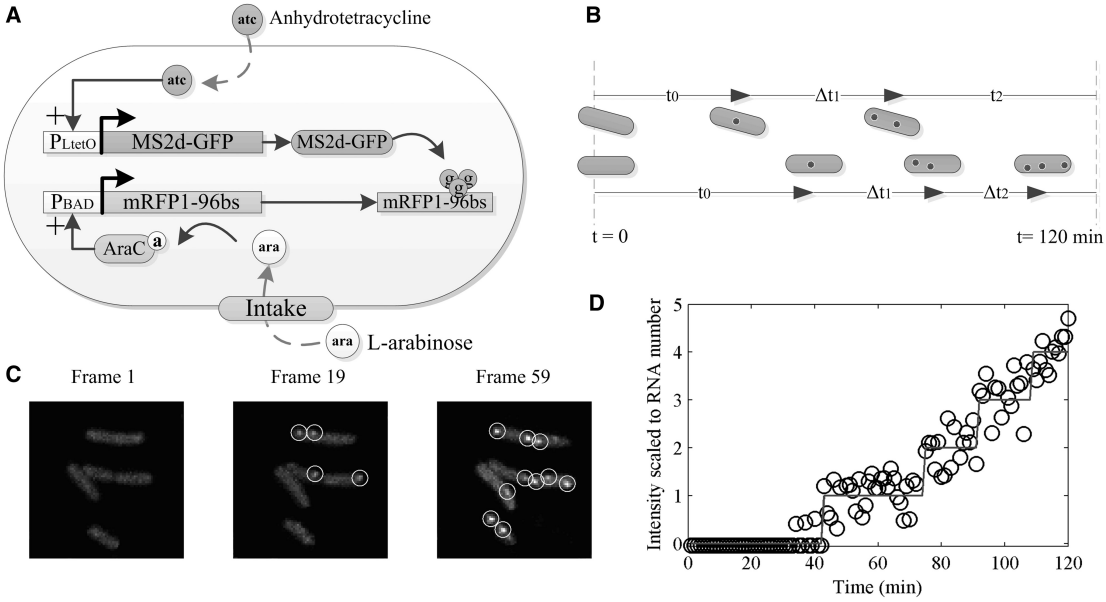

Figure 1. Measurement system. (**A**) Components of the detection system. The expression of the tagging protein, MS2d-GFP, is controlled by P_{LtetO} (33) and is inducible by anhydrotetracycline (aTc). The target RNA contains an mRFP1 coding region, followed by an array of 96 MS2d-binding sites. Expression of the target RNA is controlled by P_{BAD} whose activity is regulated by AraC and the inducer L-arabinose. The target construct is on a single-copy F-plasmid. The tagging construct is on a medium-copy vector. (**B**) Figurative description of the waiting time for the first RNA production (t_0) and intervals between subsequent productions (Δt). Images are taken once per minute for 2 h. (**C**) Example of *E. coli* cells expressing MS2d-GFP and target RNA. GFP-tagged RNA molecules are marked by circles. (**D**) Time course of total intensity of spots in a cell (circles) and monotone piecewise-constant fit (line).

comparing measurements using MS2d-GFP tagging and using plate reader (Supplementary Figure S4), the total number of MS2d-GFP–tagged RNA molecules was extracted from the total spot intensity distribution, obtained from all cells in an image obtained at a given moment after induction. For this, the first peak of the obtained distribution is set to correspond to the intensity of a single-RNA molecule. The number of tagged RNAs in each spot can be estimated by dividing its intensity by that of the first peak (32).

RESULTS

Experimental design

To study the kinetics of expression of P_{BAD}, we detect individual RNA molecules, as these are produced in live cells and register when these events occur. For this, we placed the P_{BAD} promoter on a single-copy F-plasmid, followed by a coding region for mRFP1 and an array of 96 binding sites for MS2d-GFP–tagging proteins (32) (Figure 1A). The expression of MS2d-GFP is controlled by P_{TetO}, which is activated before the gene of interest so that sufficient MS2d-GFP proteins are present when target RNA molecules appear. Induction of P_{BAD} and image acquisitions is initialized simultaneously (Figure 1B). For this, we use a temperature-controlled imaging chamber and a peristaltic pump for introducing inducers and fresh media. From the fluorescence images, using semi-automated cell segmentation and tracking (Figure 1C) (8), we measure in each cell the time for the first RNA to appear (named 'waiting time', t_0), as well as the subsequent intervals between consecutive RNA productions, Δt, until cell division occurs or until the end of the measurement period (Figure 1D).

Given that values of t_0 can only be obtained from cells of the first generation (i.e. cells already on the slide when the measurement begins), and as cells that do not divide in the first 2 h will not, in general, divide afterwards, we limited the measurement period to 2 h for simplicity. This was possible, as this period also proved to be sufficient to acquire enough samples of Δt.

From cells born during the measurement period, we only extract intervals between consecutive RNA productions, not waiting times, as these contain inducers by inheritance. We detected no difference in the distributions of intervals obtained from such cells and cells already present when induction is initiated. Finally, we observed ~0.2 RNA molecules per cell, at the moment preceding induction, because of spurious transcription events. Cells where a target RNA was already present at the start of the measurement were also not used to obtain values of t_0.

First, we compared by quantitative polymerase chain reaction the RNA production from the F-plasmid and from the native gene under the control of P_{BAD} (Supplementary Methods). Using 16S rRNA as reference

gene, we observe similar trend in activity over time in the native promoter and in the one on the F-plasmid (Supplementary Figure S3).

We next compare expression levels of the target gene, when assessed by independent methods, for two induction levels, namely, 0.1 and 1% L-arabinose (Supplementary Methods). In Supplementary Figure S4A and B, we show the temporal variation after induction in mean numbers of MS2d-GFP–tagged RNA molecules in cell populations and in the fluorescence intensity of RFP measured by plate reader, respectively.

The plate reader measurements of mRFP1 levels, 2 h after induction in liquid culture, show a fold change of 1.67 times when L-arabinose is increased from 0.1 to 1%. The MS2d-GFP *in vivo* detection method shows a fold change of 1.74 between these same conditions, showing that the results from the two methods are in accordance. From this and the previous experiment, we also conclude that the MS2d-GFP tagging method accurately detects RNA production of the target gene, and that the target gene behaves similarly to the natural system.

We also assessed for what range of inducer concentrations is the target gene under full induction. We measured with the plate reader its expression for varying inducer concentration, 2 h after induction. From Supplementary Figure S5, maximum induction is achieved for 1% arabinose. Here onwards, unless stated otherwise, we use this concentration to assess the kinetics of RNA production under the control of P_{BAD}.

First RNA and intervals between consecutive RNA molecules in individual cells

From the time-lapse images acquired with confocal microscopy, after induction, we measure in each cell both t_0 and subsequent values of Δt. t_0 is expected to include the time for arabinose to enter the cell via the intake mechanism, the time to find the promoter and release the repressor and also the time for the recruitment of the RNA polymerase and subsequent production of the first target RNA. The latter process includes events such as the closed and the open complex formation at the promoter region, as well as the elongation time. Both the elongation time and the time for MS2d-GFP to bind to a target RNA are expected to be negligible in comparison with the duration of the intake and of transcription initiation (8,12,31). Meanwhile, Δt should depend only on the events in transcription initiation (37).

The distribution of values of the waiting times, t_0, is shown in Figure 2A. Cells were induced in the gel with fresh media and 1% arabinose. The distribution is broad, as the waiting times spread through the measurement time and has a mean of 3071 s.

The distribution of intervals between consecutive productions of target RNA molecules (Δt) is shown in Figure 2B. This production is a sub-Poissonian process, as the normalized variance (σ^2/μ^2) of the distribution is 0.37. Similar conclusions were obtained from measurements of the *in vivo* kinetics of RNA production under the control of $P_{lac/ara-1}$ and P_{tetA} (9,10).

The distributions in Figure 2A and B differ significantly. We verified this with a statistical testing of equality of two empirical distributions, the Kolmogorov–Smirnov (K–S) test. We obtained a *P*-value of 2.8×10^{-18}, much smaller than 0.05, which allows rejecting the null hypothesis of similarity. We conclude that in the case of P_{BAD} and the arabinose intake mechanism, the time of intake of inducers affects significantly both mean and standard deviation of RNA numbers in individual cells, long after induction. Finally, note that the difference between the distributions of t_0 and Δt provides evidence that the activity of P_{BAD} changes significantly with induction. Otherwise, these two distributions should not differ significantly, as they would both result, e.g. from spurious transcription events alone.

One recent study (12) also focuses on the *in vivo* induction kinetics of P_{BAD}. This study uses measurements of GFP levels in cell populations, whose expression is controlled by P_{BAD} (inserted into a medium-copy vector) and a model to extrapolate the mean activation time of the promoter, after induction. Assuming a threshold for GFP levels to consider the promoter as active, the mean appearance time of GFP after induction was ~960 s. By considering several features of the measurement system, including the mean maturation time of GFP, a value was then extrapolated for the expected activation time of the promoter, namely, ~250 s. This does not include the time for transcription to be completed, once the closed complex is formed. This study thus predicts a faster mean initiation time than what our direct measurements indicate (~3000 s). Two main reasons exist for this difference. First, in the mutant used previously (12), the chromosomal *araBAD* operon is deleted, avoiding the negative feedback mechanism, which likely fastens the response time significantly. Additionally, gene expression was assessed from a medium-copy vector, which should respond much faster than the single-copy vector system used here, as its response time depends on the fastest of the response times of several promoter copies. Thus, we find that the results reported previously (12) and ours are in agreement. For example, while observing mean waiting times one order of magnitude longer, we do observe RNA molecules appearing in some of the cells within a time scale of 200–400 s after induction. Therefore, provided the usage of a multi-copy vector instead of the single-copy vector used here, we expect mean waiting times one order of magnitude smaller and thus in agreement with the measurements described previously (12).

Correlations between consecutive processes

To study whether the durations of the processes of intake and of transcription initiation are correlated, we first assessed whether consecutive intervals of Δt in individual cells are correlated. We measured the Pearson correlation from 101 pairs of consecutive intervals, and found it to be 0.16. We obtained a *P*-value of 0.11, assuming no correlation as the null hypothesis, which implies that we cannot prove that the correlation is significant. This is in agreement with previous studies of $P_{lac/ara-1}$ kinetics, which also

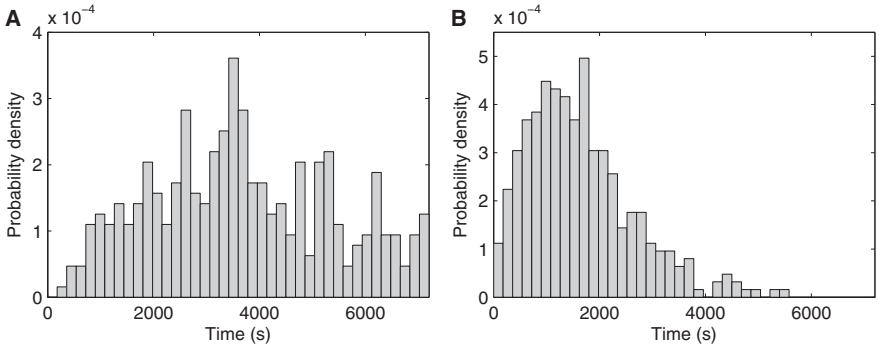

Figure 2. Kinetics of the intake and production. (**A**) Probability density distribution of waiting times ($\mu = 3071$ s, $\sigma = 1711$ s) for the first RNA to be produced in cells induced by 1% L-arabinose (354 data points). (**B**) Probability density distribution of intervals between transcription events for P_{BAD} when induced by 1% L-arabinose ($\mu = 1672$ s, $\sigma = 1012$ s) (347 data points).

indicate inexistence of correlation between durations of consecutive intervals between RNA productions (8).

We next assessed whether the distributions of t_0 and values of Δt (Figure 2A and B) are correlated. Note that t_0 and the Δt are of similar order of magnitude as the measurement period. This introduces artificial correlations between t_0 and Δt of individual cells, as, e.g. a cell with a large t_0 is expected to exhibit smaller than average Δt values, as larger intervals would not be detected during the measurement period as likely as in cells with smaller values of t_0. To remove these artificial correlations between t_0 and Δt of individual cells, in this assessment, we only considered RNA productions for a certain window size (Supplementary Methods and Supplementary Figure S6). This window is set so as to maximize the number of data points that can be extracted from the measurements.

From the windowed data, we calculated the Pearson correlation between t_0 and Δt values in individual cells to be -0.15. We calculated a *P*-value of 0.18 assuming no correlation as the null hypothesis, which implies that we cannot prove that the correlation is significant. This result is in line with (12), which reports a lack of correlation between initiation of protein expression and subsequent rate of protein synthesis in individual cells.

Dynamics of induction and of transcription initiation under different induction schemes

The distinctiveness of the distributions of t_0 and Δt of P_{BAD}, as assessed by the K–S test, suggests that they are, partially, the result of different processes. Although t_0 ought to depend on the kinetics of intake of arabinose and on the first transcription initiation event, Δt values ought to depend mostly on the kinetics of transcription initiation events alone.

These assumptions arise from the following. First, *in vitro* and *in vivo* measurements (26,38) suggest that transcription initiation (including closed and open complex formation) is a long-duration, multi-step process, usually taking 10^2–10^3 s in bacterial promoters (10,25,26,37,38). Other events that need to occur before the appearance of a target RNA because of the tagging of the MS2d-GFP are not expected to affect Δt significantly. These are transcription elongation and the tagging by multiple MS2d-GFP. Elongation of the target RNA was measured to take only tens of seconds (31). Also, the tagging occurs at a rate that makes the RNA visible during elongation or shortly after (31).

To test the two assumptions, we measured the distributions of t_0 and Δt for another promoter, $P_{lac/ara\text{-}1}$, in two conditions. $P_{lac/ara\text{-}1}$ can be induced either by IPTG or by arabinose (as P_{BAD}), or by both inducers simultaneously (9). According to our assumption, the distribution of t_0 of P_{BAD} is expected to be similar to that of $P_{lac/ara\text{-}1}$ when the latter is induced by arabinose, because of depending on the same intake mechanism, whereas it should differ significantly when $P_{lac/ara\text{-}1}$ is induced by IPTG, given the different intake mechanisms of IPTG.

We measured the distributions of t_0 and Δt for $P_{lac/ara\text{-}1}$ when induced by IPTG alone and when induced by arabinose alone (Table 1). We used the same concentration of arabinose as when inducing P_{BAD}. The IPTG concentration used is the one required for maximum induction of $P_{lac/ara\text{-}1}$ (33). Results in Table 1 follow the windowing procedure described earlier in the text. The table shows mean, standard deviation and square of the coefficient of variation (μ^2/σ^2) of t_0 and of Δt for the two promoters, each of which in two induction schemes.

We first assessed the distinctiveness of the distributions of t_0 and Δt by the K–S test, for each promoter in each condition (Table 2). In all cases, these two distributions differ in a statistical sense. This is in agreement with the assumption that although both Δt and t_0 depend on the kinetics of initiation at the promoter, only t_0 depends on the kinetics of intake of inducers.

We next performed statistical tests to assess the distinctiveness between the induction kinetics (t_0) of the two promoters (Table 3), when subject to the same inducer and when subject to different inducers. Also, we compared the effects of a different inducer concentration in the case of P_{BAD}. From Table 3, when P_{BAD} and $P_{lac/ara\text{-}1}$ are induced with 1% arabinose, they exhibit distributions of t_0 that cannot be distinguished. However, when $P_{lac/ara\text{-}1}$ is

Table 1. Measurements of t_0 and Δt

Promoter	Inducer	No. of samples (Δt)	$\mu_{\Delta t}$ (s)	$\sigma_{\Delta t}$ (s)	σ^2/μ^2	No. samples (t_0)	μ_{t0} (s)	σ_{t0} (s)	σ^2/μ^2
P_{BAD}	1% arabinose	102	1440.6	532.8	0.14	84	2885.0	1159.8	0.16
P_{BAD}	0.1% arabinose	78	1475.4	481.2	0.11	70	3519.4	1236.2	0.12
$P_{lac/ara\text{-}1}$	1% arabinose	149	1516.5	516.0	0.12	125	2832.5	1184.6	0.17
$P_{lac/ara\text{-}1}$	1 mM IPTG	485	1314.4	576.0	0.19	286	2697.0	913.6	0.11

The table shows the mean (μ), the standard deviation (σ) and the normalized variance (σ^2/μ^2) of the measured distributions of t_0 and Δt.

Table 2. *P*-values of the Kolmogorov–Smirnov test between t_0 and Δt distributions for each promoter and induction condition

Promoter	Inducer	*P*-value
P_{BAD}	1% arabinose	2.83×10^{-18}
P_{BAD}	0.1% arabinose	4.06×10^{-21}
$P_{lac/ara\text{-}1}$	1% arabinose	2.48×10^{-26}
$P_{lac/ara\text{-}1}$	1 mM IPTG	3.32×10^{-72}

For $P < 0.05$, it is generally accepted that the hypothesis that the two distributions are the same should be rejected.

Table 3. *P*-values of the Kolmogorov–Smirnov test between t_0 distributions for each promoter and induction condition

	P_{BAD} 1% arab	P_{BAD} 0.1% arab	$P_{lac/ara\text{-}1}$ 1% arab	$P_{lac/ara\text{-}1}$ IPTG
P_{BAD} 1% arab	1			
P_{BAD} 0.1% arab	5.93×10^{-4}	1		
$P_{lac/ara\text{-}1}$ 1% arab	0.8533	1.10×10^{-4}	1	
$P_{lac/ara\text{-}1}$ IPTG	0.0126	4.49×10^{-12}	0.0049	1

For $P < 0.05$, it is generally accepted that the hypothesis that the two distributions are the same should be rejected.

induced with IPTG, the resulting t_0 distribution is statistically distinguishable from that of P_{BAD}, when induced by either 0.1 or 1% arabinose. It is also distinct from its own t_0 distribution when induced by 1% arabinose. This statistically significant difference supports the hypothesis that the distributions of t_0 are dependent on the kinetics of the intake system of the inducers, and that these differ for IPTG and arabinose.

Finally, we observed that the distributions of t_0 of P_{BAD}, when induced by 0.1% and by 1% arabinose, are distinct. This is expected as the time for inducers to 'first reach the promoter' ought to depend on the inducer's concentration.

Kinetics of the intake process

The intake time of an inducer, here named 't_{diff}', differs from t_0 in that it does not include the time for the first transcription initiation event to occur. Because of this, t_{diff} cannot be measured directly with the MS2-GFP–tagging method. We thus estimate the mean and variance of the distribution of values of t_{diff} by subtracting the means and variances of the Δt distribution from the t_0 distribution. This method is based on the fact that we were unable to establish the existence of a correlation between the values of t_0 and Δt. Given this, and as they are, at most, weakly correlated (Pearson correlation of -0.15), we assume that they are independent so as to be able to estimate the standard deviation of the duration of the intake process alone (note that the mean of this quantity can be estimated as described later in the text, regardless of the existence of dependence).

The estimated mean and a standard deviation of t_{diff} are similar for P_{BAD} and for $P_{lac/ara\text{-}1}$, when induced with 1% arabinose. Namely, in both cases, we obtained a mean of $\sim$1400 s and a standard deviation of $\sim$1100 s. This is expected, given the usage of the same intake mechanism and inducer concentration. Importantly, when $P_{lac/ara\text{-}1}$ is induced by IPTG, the standard deviation of t_{diff} is much smaller ($\sim$700 s), whereas the mean is similar to when induced by arabinose ($\sim$1400 s). This suggests that the intake of arabinose is a noisier process (concerning the uncertainty of the intake time) than the intake of IPTG. Finally, we find that in the case of P_{BAD}, the concentration of arabinose affects the mean of t_{diff} significantly, as it equals $\sim$2000 s for 0.1% arabinose.

Effect of the intake process on the temporal cell-to-cell diversity in RNA numbers

Because of being stochastic and thus variable in duration from one event to the next (i.e. it differs from one cell to the next), the intake process impacts on the diversity in RNA numbers of a cell population. This impact should decrease with time, after induction. We estimated the time during which the effect is tangible for each measurement condition. For this, we assume that values of t_0 depend mostly on the intake of arabinose and on the first transcription initiation event at the start site of P_{BAD}. Meanwhile, the distribution of intervals between consecutive RNAs is assumed to depend solely on the kinetics of transcription initiation (8,10,37).

The events determining Δt as well as t_0 are modelled as *d*-step processes, each step with an exponentially distributed duration (Supplementary Methods) (37). From this assumption, it is possible, for a given number of steps, to find the duration of each step that best fits the measurements. We assume transcription initiation to be a three-step process, namely, the closed complex formation, the open complex formation and promoter escape (27,38), as evidence suggests that these are the most rate-limiting steps in normal conditions, i.e. the ones most contributing to the intervals between production of consecutive RNA molecules (26). This assumption also relies on recent

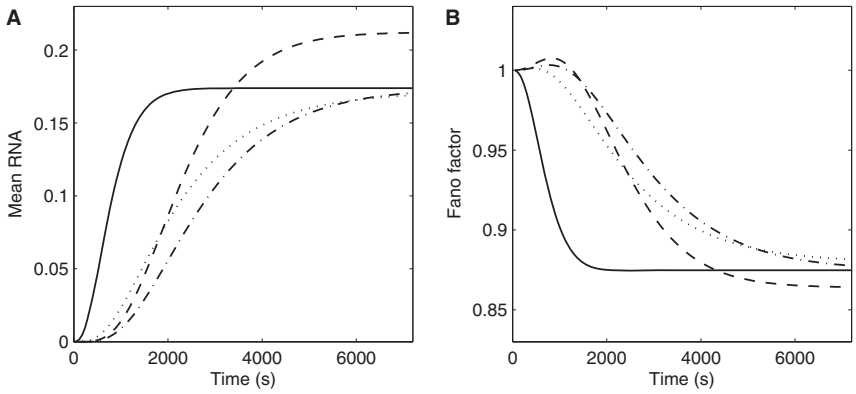

Figure 3. Mean and Fano factor of transient times for different models of intake and subsequent RNA production kinetics. Mean (**A**) and Fano factor (**B**) of RNA numbers as obtained by CME models of activation and expression. The models shown are that of $P_{lac/ara-1}$ with 1 mM IPTG (dashed line), $P_{lac/ara-1}$ with 1% arabinose (dotted line), P_{BAD} with 1% arabinose (dash-dotted line) and P_{BAD} with 1% arabinose and infinitely fast intake (solid line).

studies (37) that indicate that assuming this number of steps suffices to generate distributions that cannot be distinguished, in a statistical sense, from measurements with accuracy and quantity of data similar to the measurements reported here. Finally, we assume the intake to be a two-step process, namely, the binding of extracellular arabinose to an uptake protein and, once bound, its translocation to the cytoplasm (12). The combination of the two processes (intake followed by transcription initiation) is, consequently, assumed to be a five-step process.

Assuming these numbers of steps and stable conditions (e.g. induction level), we searched for models that fit the distributions accurately enough so that the K–S test does not find differences between model and measurements. The *P*-values of these tests are shown in Supplementary Table S1 and show that in all but one case, it is possible to find a model that cannot be distinguished from the empirical distribution, in a statistical sense.

The case for which we could not find a model that fits the measurements is that of P_{BAD} at 0.1% arabinose induction. This may be due to lack of sufficient data or because the model is unsuitable. Future studies are required to assert this. One explanation may be that, in this case, the distribution of intake times results from two distinct kinetics, one being the productions under induction and the other being spurious productions by promoters in the 'non-induced' state.

Given the models aforementioned and provided a rate of RNA degradation, it is possible to estimate the time it takes for the mean RNA numbers of a model cell population to reach equilibrium, as this time depends solely on the rate of degradation of RNAs and t_0. We do not have measurements of the degradation rate of the target RNA, as the tagging with MS2d-GFP 'immortalizes' it for the duration of the measurements (32). Instead, the models in Figure 3 assume an RNA degradation rate of $5\,min^{-1}$, which is within realistic intervals for *E. coli* (1).

From all of the aforementioned data, we estimated the mean times for RNA numbers to reach near-equilibrium, as well as the Fano factor of this quantity since the start of the simulations. Results are shown in Figure 3, as estimated for each of the models. Also shown is an estimation that assumes the model of transcription initiation of P_{BAD} when induced by 1% arabinose, coupled with an infinitely fast intake.

In all cases, reaching equilibrium in mean RNA numbers takes >1 h, except when assuming infinitely fast intake, in which case the time to reach equilibrium is <0.5 h. Thus, for a time length as long as 1–2 h, the intake process has a non-negligible contribution on the mean and the on the cell-to-cell diversity in RNA numbers of the cell populations. From Figure 3A, one also observes different shapes in the curves of $P_{lac/ara-1}$ when induced by IPTG (dashed line) and when induced by arabinose (dotted line), because of differing intake kinetics.

From Figure 3B, the contribution of the intake kinetics on the cell-to-cell variability in RNA numbers is also significant. For example, the kinetics of intake causes an increase in the Fano factor in the initial moments not observable in the case of infinitely fast intake.

We also tested models of P_{BAD} induced by 1% arabinose (normal and infinitely fast intake) with other RNA degradation rates (Supplementary Figure S7), within realistic intervals (1). Aside from assessing the degree of dependency on the intake time and degradation rate, one also observes from the figure that although the latter determines the rate at which the system reaches equilibrium, the former acts as a delay towards reaching the numbers at equilibrium. Further, one can see that the intake step adds diversity to the RNA numbers in the cells, during the transient to reach equilibrium.

DISCUSSION

We measured, at the single-cell level, how long it takes for the first RNA under the control of P_{BAD} to be produced, followed the introduction of the inducer in the media. Also, we measured the subsequent intervals between

consecutive RNA productions. From the intervals between transcription events, we determined that RNA production under the control of P_{BAD} is a sub-Poissonian process. Two recent studies reached similar conclusions for $P_{lac/ara-1}$ and P_{tetA}, for all induction conditions tested (9,10). We hypothesize that this may be a common phenomenon because of the kinetic properties of the process of transcription initiation in bacteria, in particular, because of its multi-stepped nature.

From the distributions of the time, it takes for the appearance of the first RNA in each cell when under the control of P_{BAD} and of $P_{lac/ara-1}$, for different induction conditions, we assessed the effect of the kinetics of the intake process on the mean and cell-to-cell diversity in RNA numbers of cell populations. Relevantly, this effect was found to be tangible for a long period after induction. Also, we verified that different intake mechanisms differ significantly not only in mean but also in the degree of variability of the intake time, and that this has a non-negligible effect on RNA population statistics.

Given the aforementioned data, and considering that natural environments are fluctuating, we expect the kinetics of cellular intake mechanisms to have a significant effect on the degree of phenotypic diversity of cell populations. Finally, we expect the methodology used here to assess the *in vivo* kinetics of intake of arabinose and of IPTG to be applicable to any gene of interest. Such studies should provide valuable insight into the adaptability of prokaryotic organisms to environmental changes and stress. They should also provide a better understanding of the observed cell-to-cell phenotypic diversity in *E. coli* when in fluctuating environments.

SUPPLEMENTARY DATA

Supplementary Data are available at NAR Online: Supplementary Table 1, Supplementary Figures 1–7, Supplementary Methods and Supplementary References [39–43].

FUNDING

The Academy of Finland [257603 to A.S.R.]; the Finnish Funding Agency for Technology and Innovation [40226/12 to O.Y.-H.]; the Foundation for Science and Technology, Portugal [PTDC/BBB-MET/1084/2012 to A.S.R.]. Funding for open access charge: Academy of Finland [257603, 2012 to A.S.R.].

Conflict of interest statement. The funders had no role in study design, data collection and analysis, decision to publish, or preparation of the manuscript.

REFERENCES

1. Bernstein,J.A., Khodursky,A.B., Lin-Chao,S. and Cohen,S.N. (2002) Global analysis of mRNA decay and abundance in *Escherichia coli* at single-gene resolution using two-color fluorescent DNA microarrays. *Proc. Natl Acad. Sci. USA*, **99**, 9697–9702.
2. Yu,J., Xiao,J., Ren,X., Lao,K. and Xie,X.S. (2006) Probing gene expression in live cells, one protein molecule at a time. *Science*, **311**, 1600–1603.
3. Taniguchi,Y., Choi,P.J., Li,G.-W., Chen,H., Babu,M., Hearn,J., Emili,A. and Xie,X.S. (2010) Quantifying *E. coli* proteome and transcriptome with single-molecule sensitivity in single cells. *Science*, **329**, 533–538.
4. Weickert,M.J. and Adhya,S. (1993) The galactose regulon of *Escherichia coli*. *Mol. Microbiol.*, **10**, 245–251.
5. Skerra,A. (1994) Use of the tetracycline promoter for the tightly regulated production of a murine antibody fragment in *Escherichia coli*. *Gene*, **151**, 131–135.
6. Schleif,R. (2000) Regulation of the L-arabinose operon of *Escherichia coli*. *Trends. Genet.*, **16**, 559–565.
7. Choi,P., Cai,L., Frieda,K. and Xie,X. (2008) A stochastic single-molecule event triggers phenotype switching of a bacterial cell. *Science*, **322**, 442–446.
8. Kandhavelu,M. and Häkkinen,A. (2012) Single-molecule dynamics of transcription of the lar promoter. *Phys. Biol.*, **9**, 026004.
9. Kandhavelu,M., Lloyd-Price,J., Gupta,A., Muthukrishnan,A.B., Yli-Harja,O. and Ribeiro,A.S. (2012) Regulation of mean and noise of the *in vivo* kinetics of transcription under the control of the lac/ara-1 promoter. *FEBS Lett.*, **586**, 3870–3875.
10. Muthukrishnan,A.B., Kandhavelu,M., Lloyd-Price,J., Kudasov,F., Chowdhury,S., Yli-Harja,O. and Ribeiro,A.S. (2012) Dynamics of transcription driven by the tetA promoter, one event at a time, in live *Escherichia coli* cells. *Nucleic Acids Res.*, **40**, 8472–8483.
11. Schleif,R. (2010) AraC protein, regulation of the l-arabinose operon in *Escherichia coli*, and the light switch mechanism of AraC action. *FEMS Microbiol. Rev.*, **34**, 779–796.
12. Megerle,J.A., Fritz,G., Gerland,U., Jung,K. and Rädler,J.O. (2008) Timing and dynamics of single cell Gene expression in the arabinose utilization system. *Biophys. J.*, **95**, 2103–2115.
13. Hogg,R.W. and Englesberg,E. (1969) L-arabinose binding protein from *Escherichia coli* B/r. *J. Bacteriol.*, **100**, 423–432.
14. Schleif,R. (1969) An l-arabinose binding protein and arabinose permeation in *Escherichia coli*. *J. Mol. Biol.*, **46**, 185–196.
15. Horazdovsky,B.F. and Hogg,R.W. (1989) Genetic reconstitution of the high-affinity L-arabinose transport system. *J. Bacteriol.*, **171**, 3053–3059.
16. Lee,J.H., Al-Zarban,S. and Wilcox,G. (1981) Genetic characterization of the araE gene in Salmonella typhimurium LT2. *J. Bacteriol.*, **146**, 298–304.
17. Stoner,C. and Schleif,R. (1983) The araE low affinity L-arabinose transport promoter. Cloning, sequence, transcription start site and DNA binding sites of regulatory proteins. *J. Mol. Biol.*, **171**, 369–381.
18. Siegele,D.A. and Hu,J.C. (1997) Gene expression from plasmids containing the araBAD promoter at subsaturating inducer concentrations represents mixed populations. *Proc. Natl Acad. Sci. USA*, **94**, 8168–8172.
19. Khlebnikov,A., Risa,O., Skaug,T., Carrier,T.A. and Keasling,J.D. (2000) Regulatable arabinose-inducible gene expression system with consistent control in all cells of a culture. *J. Bacteriol.*, **182**, 7029–7034.
20. Khlebnikov,A., Datsenko,K.A., Skaug,T., Wanner,B.L. and Keasling,J.D. (2001) Homogeneous expression of the P-BAD promoter in *Escherichia coli* by constitutive expression of the low-affinity high-capacity AraE transporter. *Microbiology*, **147**, 3241–3247.
21. Morgan-Kiss,R.M., Wadler,C. and Cronan,J.E. (2002) Long-term and homogeneous regulation of the *Escherichia coli* araBAD promoter by use of a lactose transporter of relaxed specificity. *Proc. Natl Acad. Sci. USA*, **99**, 7373–7377.
22. Johnson,C.M. and Schleif,R.F. (1995) In vivo induction kinetics of the arabinose promoters in *Escherichia coli*. *J. Bacteriol.*, **177**, 3438–3442.
23. Walter,G., Zillig,W., Palm,P. and Fuchs,E. (1967) Initiation of DNA-Dependent RNA synthesis and the effect of heparin on RNA polymerase. *Eur. J. Biochem.*, **3**, 194–201.
24. Chamberlin,M.J. (1974) The selectivity of transcription. *Annu. Rev. Biochem.*, **43**, 721–775.
25. Buc,H. and McClure,W.R. (1985) Kinetics of open complex formation between *Escherichia coli* RNA polymerase and the lac

UV5 promoter. Evidence for a sequential mechanism involving three steps. *Biochemistry*, **24**, 2712–2723.
26. Lutz,R., Lozinski,T., Ellinger,T. and Bujard,H. (2001) Dissecting the functional program of *Escherichia coli* promoters: the combined mode of action of Lac repressor and AraC activator. *Nucleic Acids Res.*, **29**, 3873–3881.
27. Hsu,L.M. (2002) Promoter clearance and escape in prokaryotes. *Biochim. Biophys. Acta*, **1577**, 191–207.
28. DeHaseth,P.L., Zupancic,M.L. and Record,M.T. (1998) RNA polymerase-promoter interactions: the comings and goings of RNA polymerase. *J. Bacteriol.*, **180**, 3019–3025.
29. Greive,S.J. and Von Hippel,P.H. (2005) Thinking quantitatively about transcriptional regulation. *Nat. Rev. Mol. Cell Biol.*, **6**, 221–232.
30. McClure,W.R. (1985) Mechanism and control of transcription initiation in prokaryotes. *Annu. Rev. Biochem.*, **54**, 171–204.
31. Golding,I. and Cox,E.C. (2004) RNA dynamics in live *Escherichia coli* cells. *Proc. Natl Acad. Sci. USA*, **101**, 11310–11315.
32. Golding,I., Paulsson,J., Zawilski,S.M. and Cox,E.C. (2005) Real-time kinetics of gene activity in individual bacteria. *Cell*, **123**, 1025–1036.
33. Lutz,R. and Bujard,H. (1997) Independent and tight regulation of transcriptional units in *Escherichia coli* via the LacR/O, the TetR/O and AraC/I1-I2 regulatory elements. *Nucleic Acids Res.*, **25**, 1203–1210.
34. Chowdhury,S., Kandhavelu,M., Yli-Harja,O. and Ribeiro,A.S. (2012) An interacting multiple model filter-based autofocus strategy for confocal time-lapse microscopy. *J. Microscopy*, **245**, 265–275.
35. Chen,T.B., Lu,H.H., Lee,Y.S. and Lan,H.J. (2008) Segmentation of cDNA microarray images by kernel density estimation. *J. Biomed. Inform.*, **41**, 1021–1027.
36. Otsu,N. (1979) A threshold selection method from gray-level histograms. *IEEE Trans. Sys. Man Cybern.*, **9**, 62–66.
37. Kandhavelu,M., Mannerström,H., Gupta,A., Häkkinen,A., Lloyd-Price,J., Yli-Harja,O. and Ribeiro,A.S. (2011) *In vivo* kinetics of transcription initiation of the lar promoter in *Escherichia coli*. Evidence for a sequential mechanism with two rate-limiting steps. *BMC Syst. Biol.*, **5**, 149.
38. McClure,W.R. (1980) Rate-limiting steps in RNA chain initiation. *Proc. Natl Acad. Sci. USA*, **77**, 5634–5638.
39. Skaletsky,H.J. (2000) Primer3 on the WWW for general users and for biologist programmers. In: Krawetz,S. and Misener,S. (eds), *Bioinformatics Methods and Protocols: Methods in Molecular Biology*. Humana Press, Totowa, NJ, pp. 365–386.
40. Livak,K.J. and Schmittgen,T.D. (2001) Analysis of relative gene expression data using real-time quantitative PCR and the 2(-Delta Delta C(T)) method. *Methods*, **25**, 402–408.
41. Daruwalla,K.R., Paxton,A.T. and Henderson,P.J.F. (1981) Energization of the transport systems for arabinose and comparison with galactose transport in *Escherichia coli*. *Biochem. J.*, **200**, 611–627.
42. Gillespie,D.T. (1976) A general method for numerically simulating the stochastic time evolution of coupled chemical reactions. *J. Comput. Phys.*, **22**, 403–434.
43. Munsky,B. and Khammash,M. (2006) The finite state projection algorithm for the solution of the chemical master equation. *J. Chem. Phys.*, **124**, 044104.

Supplementary Information

In vivo single-molecule kinetics of activation and subsequent activity of the arabinose promoter

Jarno Mäkelä[1], Meenakshisundaram Kandhavelu[1], Samuel M.D. Oliveira[1], Jerome G. Chandraseelan[1], Jason Lloyd-Price[1], Juha Peltonen[1], Olli Yli-Harja[1,2] and Andre S. Ribeiro[1,*]

[1] Laboratory of Biosystem Dynamics, Department of Signal Processing, Tampere University of Technology, P.O. Box 553, 33101 Tampere, Finland.
[2] Institute for Systems Biology, 1441N 34th St, Seattle, WA, 98103-8904, USA

* Corresponding author: andre.ribeiro@tut.fi (Andre S. Ribeiro)

Supplementary Methods

Chemicals

Bacterial cell cultures were grown in two media, namely Luria-Bertani (LB) and M63. The chemical components of LB broth (Tryptone, Yeast extract and NaCl) were purchased from LabM (UK). For M63 media, the following components were used: 2 mM $MgSO_4.7H_20$ (Sigma-Aldrich, USA), 7.6 mM $(NH_4)_2SO_4$ (Sigma Life Science, USA), 30µM $FeSO_4.7H_2O$ (Sigma Life Science, USA), 1 mM EDTA (Sigma Life Science, USA), 60 mM KH_2PO_4 (Sigma Life Science, USA), Glycerol 0.5 % (Sigma Life Science, USA), and Casaminoacids 0.1 % (Fluka Analytical, USA). Isopropyl β-$_D$-1-thiogalactopyranoside (IPTG), $_L$-(+)-Arabinose and anhydrotetracycline (aTc) used for induction of the cells and the antibiotics (100 mg/ml kanamycin and 35 mg/ml chloramphenicol) were purchased from Sigma-Aldrich (USA). Agarose (Sigma Life Science, USA) was used for the microscopic slide gel preparation.

Bacterial Strain

Cloning and expression experiments were performed in *E. coli* DH5α-PRO strain (Clontech; identical to DH5α-Z1 (31). The strain information is: deoR, endA1, gyrA96, hsdR17($r_{k-}m_{k+}$), recA1, relA1, supE44, thi-1, Δ(lacZYA-argF)U169, Φ80δlacZΔM15, F-, λ-, P_{N25}/tetR, P_{lacIq}/lacI, and Sp^R. Frag1A: F-, rha-, thi, gal, $lacZ_{am}$, ΔacrAB::kan^R, P_{N25}/tetR, P_{lacIq}/lacI, and Sp^R. Frag1B: F-, rha-, thi, gal, $lacZ_{am}$, P_{N25}/tetR, P_{laciq}/lacI, and Sp^R. The P_{N25}/tetR, P_{laciq}/lacI, Sp^R cassette was transferred from *DH5αPRO* to Frag1 to generate Frag1B by P1 transduction. The ΔacrAB:kan^R cassette was transferred from KZM120 to Frag1B, so as to generate Frag1A.

Construction of the pMK-BAC vector

To construct the pMK-BAC (P_{BAD}-mRFP1-96 binding site (96 BS) array, the following plasmids were used: a plasmid with mRFP1 plus 96bs array region in the BAC vector, originally designed and generously provided by Prof. Ido Golding ($P_{lac/ara-1}$- mRFP1-96 bs) (32). To amplify the construct containing the AraC and pBAD promoter region from the pGLO vector (Biorad), a primer set was designed as follows:

Ara_AatII-Fw-5´CCTAAGACGTCATCGATGCATAATGTGCC 3´
Ara_AatII-Rv-5´CCTTGATGACGTCATGTATATCTCCTTCTTAAAGTTA3´

The target BAD promoter region along with AraC coding region from the pGLO vector was amplified and inserted into the pIG-BAC vector by standard molecular biology techniques. The construct was verified by sequencing with the appropriate primers and transformed into the *E. coli* DH5α-PRO strain carrying the bacterial expression vector pPROTET.E (Clontech) coding for MS2d–GFP. For more details see Supplementary Figures 1 and 2.

Plate reader experiment

The mean fluorescence of RFP under the control of P_{BAD} was measured with a microplate fluorometer (Fluoroskan Ascent, Thermo Scientific). 200 ml of cells at OD600 ≈ 0.5 were induced with 0.1 % or 1 % L-arabinose and placed on 96 well microplate. From this, cells were measured for 2 hours for relative fluorescence levels of mRFP1 protein (excitation and emission wavelengths were 584 nm and 607 nm, respectively). The cell density was kept identical in all wells of the plate for all conditions.

Quantitative PCR for mean mRNA quantification

The change in the rate of transcription of genes araB and mRFP was studied using qPCR. *E. coli* DH5α-PRO cells containing the constructs were grown as described in the section describing the microscopy measurements. Cells were grown overnight at 30°C with aeration, diluted into fresh medium and allowed to grow at the appropriate temperature of the experiment until an optical density of OD_{600} ≈ 0.3-0.5 was reached. For the experiment, 5 ml of cells were pre-incubated with 100 ng/ml of aTc to induce the expression of MS2d-GFP. 1 % $_L$-arabinose was used for induction of the BAD promoter, 30 minutes after induction, the first sample was taken. From then onwards, samples were taken at an interval of 60 minutes. Rifampicin was added to the samples immediately, so as to prevent further transcription and the cells were fixed with RNA protect reagent immediately followed by enzymatic lysis using Tris-EDTA lysozyme buffer (pH 8.3). RNA was purified from each sample by RNeasy mini-kit (Qiagen). The total RNA was separated by electrophoresis through a 1 % agarose gel and stained with SYBR Safe DNA Gel Stain. The RNA was found intact with discreet bands for 16 S and 23 S ribosomal RNAs. To ensure purity of the RNA samples, they were subject to treatment with DNase free of RNase, to remove residual DNA. The yield of RNA obtained was 0.4 – 0.6 mg/ml. Approximately 40 ng of RNA was used for cDNA synthesis using iSCRIPT reverse transcription super mix (Biorad) according to the manufacturer's instructions.

Quantification of cDNA was performed by real-time PCR using SYBR-green supermix with primers for the amplification of target and reference genes at a concentration of 200nM. Primers specific to AraB (Forward: 5' GGTACTTCCACCTGCGACAT 3', Reverse: 5' CAACCTGACCGCAAATACCT 3') and mRFP genes (Forward: 5' TACGAC GCCGAGGTCAAG 3' and Reverse: 5' TTGTGGGAGGTGATGTCCA 3') were designed using PRIMER3 (39), the length of the amplicon for the target and reference were maintained at 90bp. The sequence of the primers for the reference gene 16S rRNA (EcoCyc Accession Number: EG30090) (Forward: 5' CGTCAGCTCGTGTTGTGAA 3' and Reverse: 5' GGACCGCTGGCAACAAAG 3') and the primers were obtained from Thermo Scientific. The level of 16s rRNA was used to normalize the expression data of each target gene. 10 ng of cDNA was used as a template. The cycling protocol used was 94 °C for 15 s, 51 °C for 30 s, and 72 °C for 30 s, up to 39 cycles. The amplification was monitored in real time by measuring the fluorescence intensities at the end of each cycle. The experiment was performed in triplicates along with the No-RT and no template controls. The volume used for each reaction was 25 µl in low-profile tube strips in a MiniOpticon Real time PCR system (Biorad). The Cq values were obtained from the CFX ManagerTM Software and the fold change of expression of the target gene was analysed by normalizing against the reference gene according to the Livak method (40). See Supplementary Figure 3 for the results.

Normalization between samples of the distributions of time intervals

The observation time for the production of RNAs is two hours. In some cells, the intervals between transcription events (Δt) are of this order of magnitude. This causes shorter intervals to be 'favored'. This is more likely to occur in cells where the waiting time for the first RNA to be produced (t_0) is longer, since the remaining observation time is shorter. This introduces an artificial anti-correlation between t0 and Δt in individual cells. Similar correlations are introduced by different division times as well, i.e., shorter division times hamper the collection of longer Δt samples.

Thus, prior to determine if any real correlation exists between t_0 and Δt in individual cells, it is necessary to remove these artificial sources of anti-correlation due to the limits in the measurement period. For this, in all cells, all intervals between consecutive RNAs were collected only for a time window of size t_c after the previous production. The value of t_c is identical in all cells. This causes the probability of appearance of the next RNA molecule during that period to be uniform for all cells, if the underlying process is in fact identical in all cells.

This restriction in the collection of values of Δt is made when assessing correlations between t_0 and Δt and when comparing these two distributions between conditions. When imposing the restriction, we thus consider only cells that produce at least 2 RNA molecules during their life time and measurement period. The value of t_c was selected so as to maximize the number of data points collectable from the data sets. Here, t_c was set to 39 minutes (see Supplementary Figure S6).

Fitting the empirical distributions to a sum of *d*-exponential variates

The arabinose intake mechanism can be described by a single Michaelis-Menten function (41). Since the backward reaction of the intake process is slower than the forward reaction (12), the intake process is modeled, roughly, by a sequence of non-reversible reactions. Interestingly, we found from the measurements and the inference procedure, evidence of two steps at this stage (exponential in duration), which is in agreement with the number of forward steps assumed in other studies for this process (12). Finally, transcription initiation, which follows the intake process, can also be modeled by a 3-step exponential model according recent in vivo measurements (9, 10). Thus, we fit the measured distributions of t_0 to a 5-step exponential model.

To fit the empirical distribution with a sum of *d*-exponential variates (of possibly unequal rates), we select the exponential rate parameters $\lambda_1, \ldots, \lambda_d$ such that the Kolmogorov-Smirnov (K-S) statistic is minimized. That is, parameters are selected as $\hat{\theta} = \arg\max_{\theta=\lambda_1,\ldots,\lambda_d} \sup_x |F_\theta(x) - G(x)|$, where $F_\theta(x)$ is the cumulative distribution function (CDF) of a sum of d exponentials with parameters $\theta = (\lambda_1, \ldots, \lambda_d)$, and $G(x)$ is the CDF of the empirical distribution.

$$F_{\theta=L_1,\ldots,L_d}(X) := \sum_{i=1}^{d} \left((1 - e^{-L_i x}) \prod_{\substack{j=1 \\ j \neq i}}^{d} \frac{L_j}{L_j - L_i} \right)$$

The parameter values θ are found using a nonlinear numerical optimizer. This method is convenient, since if the K-S test was rejected for the parameters $\hat{\theta}$, such a test would also be rejected for any other set of parameters θ in this family of fitted distributions, indicating that these distributions are inappropriate models of the data. The results of the fitting are shown in Table S1.

As a final note, the model assumed above can be considered as the simplest possible, i.e., each step is an elementary reaction of the form $A \xrightarrow{c} B$, with a constant probability of occurring per unit time. This entails that the distributions of intervals between steps are exponential (42). Notably, the inferred distributions and the experimental data are statistically indistinguishable by the K-S test, which implies that there is no evidence to assume that the model is wrong (see Table S1).

CME solution

To estimate the effect of the intake on the cell-to-cell diversity in RNA numbers we made use of direct integration of the Chemical Master Equation (CME) of the model described in the previous section, using the Finite State Projection algorithm (43). This method truncates the infinite state space of the CME such that the amount of probability outside the truncated region is negligible. In all cases, we truncated the state space at 20 RNA molecules. This number sufficed for this space to contain virtually all of the total probability in the system. The probability mass vector at each time moment is then solved by numerically integrating the truncated CME. From this distribution over time, we calculate mean, variance, and Fano factor of RNA molecules of a model at each moment.

Supplementary Figures

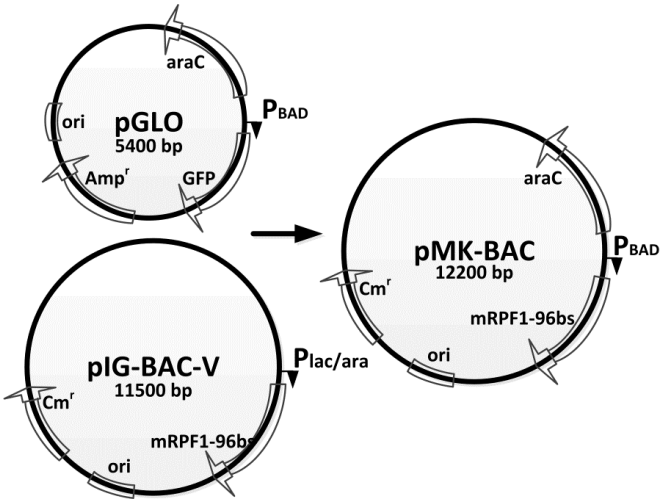

Figure S1. Plasmids used for the pMK-BAC construction. The pMK-BAC(P_{BAD}-mRFP1-96bs) plasmid was engineered by linking the amplified region, containing the P_{BAD} promoter and the araC gene, obtained from pGLO, to the pIG-BAC expression vector, without the lac/ara-1 promoter, obtained from pIG-BAC($P_{lac/ara-1}$- mRFP1-96 bs)-V.

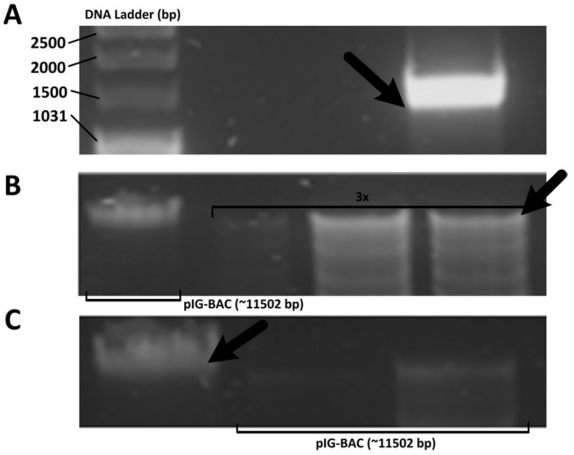

Figure S2. Split gels of the plasmid construction. (A) The PCR fragment of 1347bp amplified from pGLO with the appropriate primers. (B) Lanes containing pIG-BAC-V without the $P_{lac/ara-1}$ promoter region (10849bp), and the pIG-BAC-V expression plasmid (11502bp. (C) The pMK-BAC plasmid (12196bp) containing the araC-P_{BAD} amplified fragment inserted to the BAC expression vector, and the pIG-BAC-V (11502bp). Note the black arrows indicating the bands.

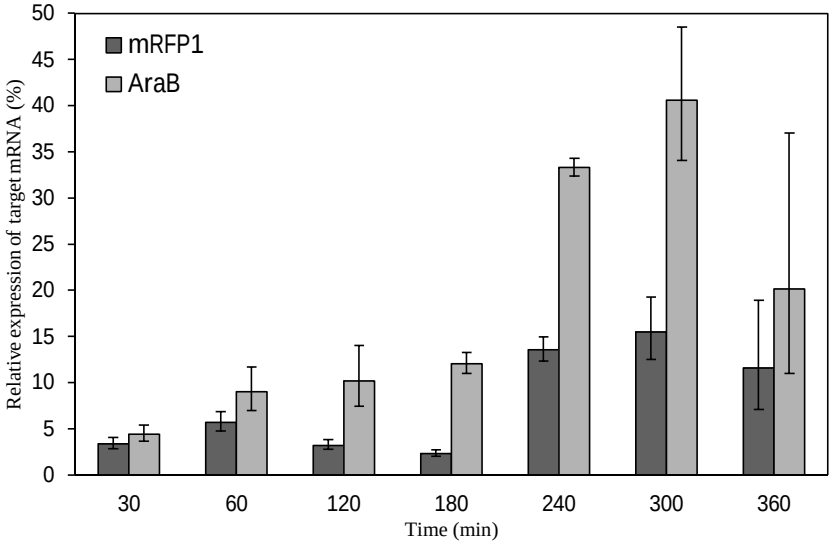

Figure S3. Q-PCR of the native and of the target gene. Q-PCR of RNA expression of the native, integrated AraB gene and of the mRFP1 probe in the F-plasmid, as a function of time, when subject to induction by 1% L-arabinose in liquid culture. The standard deviation bars are from three independent experiments.

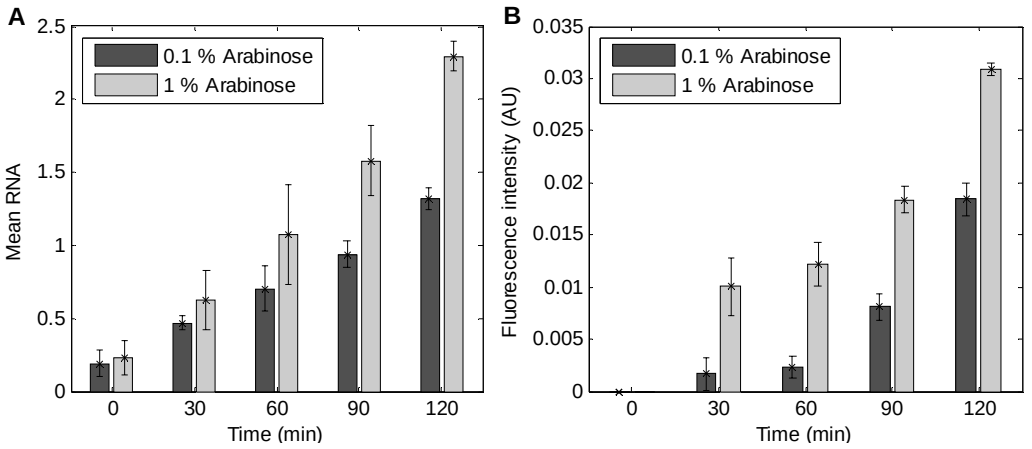

Figure S4. MS2-GFP measurement of RNA numbers compared with Plate reader results. (A) RNA numbers over time measured in vivo with the MS2-GFP method for 0.1 % and 1 % L-arabinose. Mean and standard deviation of RNA numbers in individual cells were calculated for each sample separately. Error bars show the standard error of the mean from independent measurements (3 measurements) (B) Fluorescent intensity of RFP over time for 0.1 % and 1 % L-arabinose as measured by Plate reader. Error bars show the standard error of the mean obtained from 8 wells.

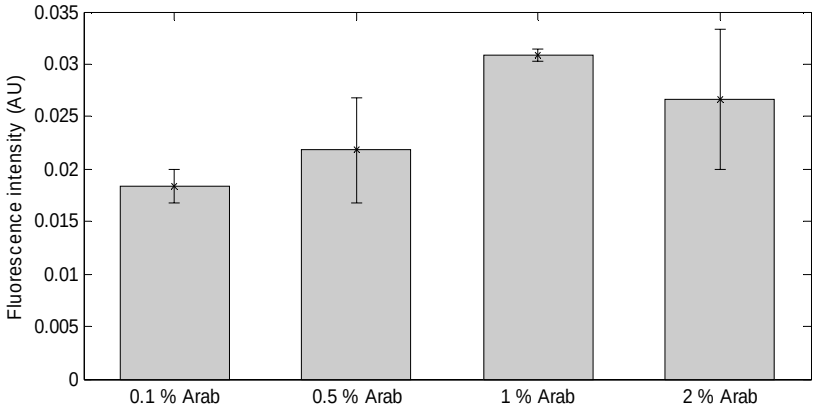

Figure S5. Gene expression as measured by Plate Reader. Comparison of different inducer concentrations by plate reader measurements, 2 hours following induction. Maximum induction is achieved with 1 % L-arabinose. Error bars show the standard error of the mean obtained from 8 wells.

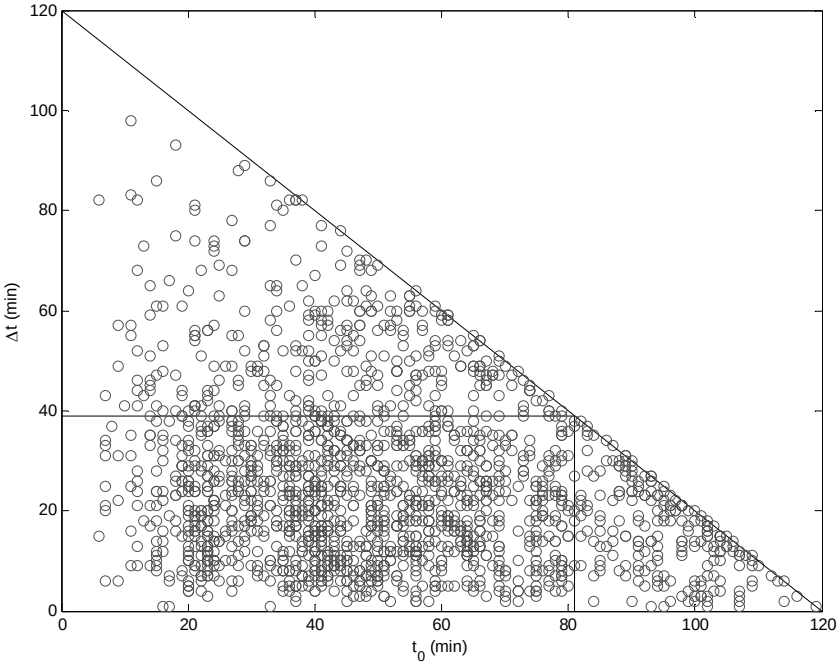

Figure S6. Normalization of the data. The values of t_0 and the corresponding values of the first Δt in each cell. The diagonal line is the total observation time (120 min). Vertical and horizontal (t_c = 39 min) lines define the intervals that meet the requirements for un-biasedness.

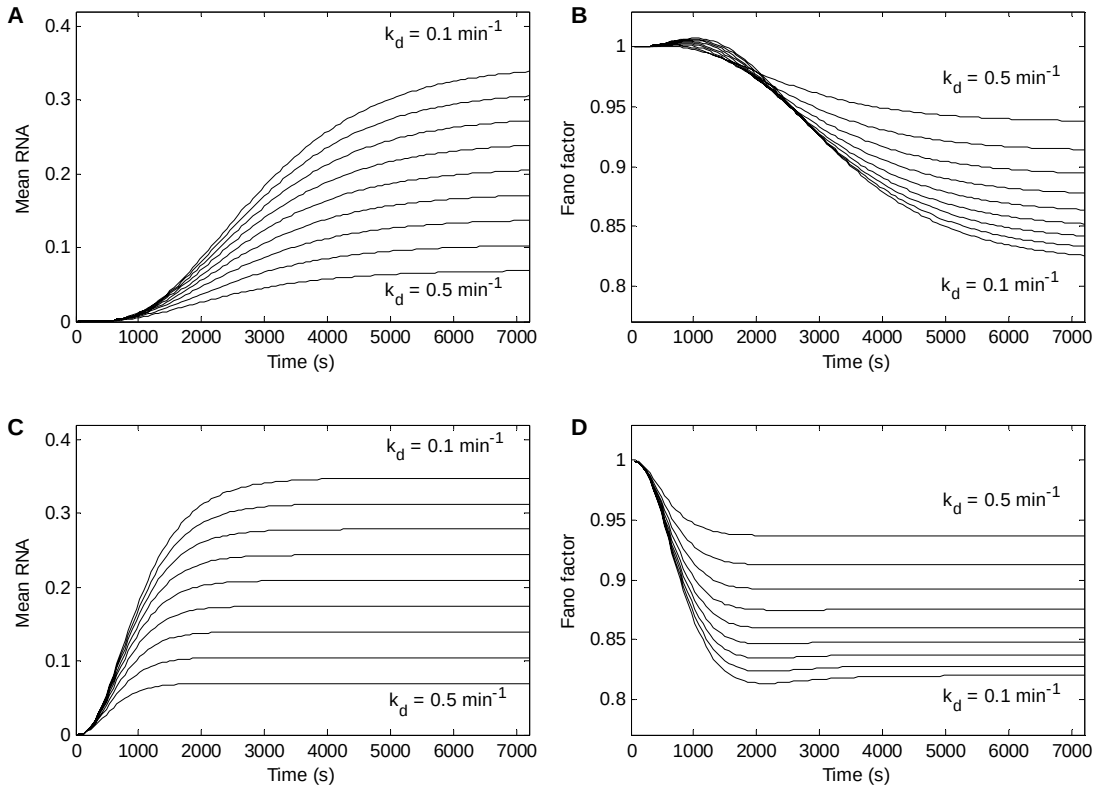

Figure S7. Models with different degradation rates. The degradation rate was set to the following values: 0.1 min^{-1}, 0.111 min^{-1}, 0.125 min^{-1}, 0.143 min^{-1}, 0.167 min^{-1}, 0.2 min^{-1}, 0.25 min^{-1}, 0.333 min^{-1}, 0.5 min^{-1}. In the figures, only the highest and the lowest values are marked. Mean RNA numbers shown for (A) P_{BAD} with 1 % Arabinose and for (C) P_{BAD} with 1 % Arabinose and infinitely fast intake. Fano factors of RNA numbers are shown for (B) P_{BAD} with 1 % Arabinose and, (D) P_{BAD} with 1 % Arabinose and infinitely fast intake.

Supplementary Table

	p-value for t_0	p-value for Δt
P_{BAD} 1 % arabinose	0.2613	0.8930
P_{BAD} 0.1 % arabinose	0.0020	0.5728
$P_{lac/ara-1}$ 1 % arabinose	0.1759	0.3826
$P_{lac/ara-1}$ 1 mM IPTG	0.1155	0.2413

Table S1. Results of the K-S fitting. Asymptotic p-values of the Kolmogorov-Smirnov goodness-of-fit test when fitting the empirical distribution with a sum of 5-exponential variates in the case of t_0 and of 3-exponential variates in the case of Δt. We compare these p-values with a standard value of 0.05.

Publication II

Chandraseelan, J. G., Oliveira, S. M. D., Potapov, I., Häkkinen, A., Kandhavelu, M and Ribeiro, A. S. (2013). Temperature dependence of the LacI-TetR-CI Repressilator. Mol. Biosyst. 9(12):3117-23.

Available online on the Royal Society of Chemistry's website, DOI: 10.1039/C3MB70203K

Molecular BioSystems

RSC Publishing

PAPER

Effects of temperature on the dynamics of the LacI-TetR-CI repressilator

Cite this: *Mol. BioSyst.*, 2013, **9**, 3117

Jerome G. Chandraseelan, Samuel M. D. Oliveira, Antti Häkkinen, Huy Tran, Ilya Potapov, Adrien Sala, Meenakshisundaram Kandhavelu and Andre S. Ribeiro*

Received 31st May 2013,
Accepted 27th September 2013

DOI: 10.1039/c3mb70203k

www.rsc.org/molecularbiosystems

We studied the behaviour of the repressilator at 28 °C, 30 °C, 33 °C, and 37 °C. From the fluorescence in each cell over time, we determined the period of oscillations, the functionality (fraction of cells exhibiting oscillations) and the robustness (fraction of expected oscillations that occur) of this circuit. We show that the oscillatory dynamics differs with temperature. Functionality is maximized at 30 °C. Robustness decreases beyond 30 °C, as most cells exhibit 'failed' oscillations. These failures cause the distribution of periods to become bimodal, with an 'apparent period' that is minimal at 30 °C, while the true period decreases with increasing temperature. Based on previous studies, we hypothesized that the failures are due to a loss of functionality of one protein of the repressilator, CI. To test this, we studied the kinetics of a genetic switch, formed by the proteins CI and Cro, whose expression is controlled by P_{RM} and P_R, respectively. By probing the activity of P_{RM} by *in vivo* detection of MS2-GFP tagged RNA, we find that, beyond 30 °C, the production of the CI-coding RNA changes from sub-Poissonian to super-Poissonian. Given this, we suggest that the decrease in efficiency of CI as a repressor with temperature hinders the robustness of the repressilator beyond 30 °C. We conclude that the repressilator is sensitive but not robust to temperature. Replacing CI for a less temperature-dependent protein should enhance robustness.

Introduction

Natural genetic circuits can efficiently perform various tasks, such as time counting,[1] state holding,[2] and signal filtering,[3] while maintaining robustness to environmental changes. This is necessary for them to be able to regulate complex cellular processes under various conditions[4–6] or to efficiently determine cells' response to environmental shifts and signals. Much effort has been made to reproduce their behaviour in synthetic circuits.[6–8] Once proven reliable, these synthetic circuits should have a wide range of applications.[9–12] For example, synthetic genetic clocks promise to be of use as regulators of intracellular processes. For that, they will need to be robust to environmental changes, similarly to natural circuits.

One of the most famous synthetic circuits is the 'repressilator', engineered by Elowitz *et al.*[7] This circuit has three genes, whose interactions form a negative feedback loop. Namely, the three genes form a cycle, with each gene expressing a protein that represses the next gene in the cycle. At 30 °C, the repressilator exhibits periodic oscillations,[7] visible in time-lapse measurements of a green fluorescent protein (GFP) reporter that is under the control of a promoter that is also present in the 3-gene circuit.

Temperature affects the dynamics of most cellular processes, including gene expression.[13] Evidence suggests that natural, time-keeping circuits, such as circadian oscillators, evolved robustness to temperature fluctuations.[14–16] Similar robustness is desired in synthetic circuits designed for time keeping.

The degree of robustness of the repressilator to temperature is unknown, but studies on some of its components suggest that its behaviour is bound to be strongly affected by small changes in temperature. For example, one of its proteins, the wild-type CI,[7] has temperature-dependent DNA-binding stability.[17] Namely, it is maximized at ~30 °C and is gradually lost as temperature increases, becoming ~50% weaker at 42 °C.[17] This decrease may arise from the fact that the ability of CI to discriminate between operator sites depends on ion binding/release reactions[18] and/or from the temperature-dependence of the CI's dimerization process.[19]

Here, we investigate how temperature affects the dynamics of the repressilator. Afterwards, we search for causes. Motivated by previous evidence that CI's functionality is temperature-dependent, we also study the temperature-dependence of another circuit, the CI–Cro switch. After comparing the effects of temperature on the kinetics of the two circuits, we propose

Computational Systems Biology Research Group, Tampere University of Technology, P.O. Box 553, 33101 Tampere, Finland. E-mail: andre.ribeiro@tut.fi

modifications to the repressilator that may enhance its robustness to temperature fluctuations.

Methods

Repressilator: strain, plasmid, and microscopy

Cells of *E. coli* lac$^-$ strain MC 4100 with the repressilator (pZS1-lTlrLLtCL) and the reporter plasmid (pZE21-GFPaav) were generously provided by M. Elowitz, Princeton University, NJ, USA. Minimal media were prepared with 2 mM $MgSO_4 \cdot 7H_2O$ (Sigma-Aldrich, USA), 7.6 mM $(NH_4)_2SO_4$ (Sigma Life Science, USA), 30 μM $FeSO_4 \cdot 7H_2O$ (Sigma Life Science, USA), 1 mM EDTA (Sigma Life Science, USA), 60 mM KH_2PO_4 (Sigma Life Science, USA) pH 6.8 with Glycerol 0.5% (Sigma Life Science, USA) and Casaminoacids 0.1% (Fluka Analytical, USA).

E. coli cells with the repressilator and reporter plasmids were grown in minimal media overnight at 28 °C, 30 °C, 33 °C or 37 °C with shaking at 300 rpm, to an optical density (OD) of 0.1 at 600 nm. Next, cells were diluted into fresh media and a few μl of the culture was placed between a cover-slip and a slab of 2% low melting agarose in minimal media, 0.75 mm thick. During time lapse microscopy, the temperature of the samples was kept stable by a control chamber (Bioptechs, FCS2, Pennsylvania, USA). Images were obtained every 15 minutes for 10 hours by a Nikon Eclipse (TE2000-U, Nikon, Tokyo, Japan) inverted C1 confocal laser-scanning system with a 100× Apo TIRF (1.49 NA, oil) objective. GFP fluorescence was measured using a 488 nm laser (Melles-Griot) and a 515/30 nm detection filter. For image acquisition, we used Nikon software EZ-C1.

Switch: strain, plasmid, and microscopy

E. coli CZ071 with a reporter plasmid PLtetO-1-MS2d-GFP and a target plasmid pIG-BAC (P_{RM}-limm(rexAB::bs48)) were generously provided by I. Golding (University of Illinois, USA). The target plasmid is a single-copy F-plasmid with a genetic switch coding for CI, under the control of P_{RM}, and Cro,[20] under the control of P_R. Further, the plasmid contains the immunity region of wild-type λ.,[21] where the rexA and rexB genes were replaced by a 48 binding site array for MS2d proteins, so as to detect individual RNAs whose production is controlled by P_{RM}. Depending on the occupation of the sites OR1, OR2 and OR3, one of the two promoters will be in a repressed state.[32,33] Note that OR3 is absent in the repressilator. Nevertheless, the existence of oscillations[7] shows that CI still achieves repression of P_R.

Cells were grown in Luria–Bertani (LB) medium with the following components: 10 g L^{-1} of Tryptone (Sigma Aldrich, USA), 5 g L^{-1} of yeast extract (LabM, UK) and 10 g L^{-1} of NaCl (LabM, UK), with addition of 34 μg ml^{-1} of Kanamycin and 34 μg ml^{-1} of Chloramphenicol (both antibiotics from Sigma Aldrich, USA). Cells were grown overnight with shaking at 260 rpm, in an orbital shaker (Labnet), at 30 °C for 12–16 h to an optical density (OD) of 0.1 at 600 nm. Thereafter, cells were grown until they reached an OD of ≈0.01 and diluted to 1 : 10 in LB medium with antibiotics. Then, they were grown at 37 °C with shaking at 260 rpm for a few hours, until they reached the exponential phase and an OD of ≈0.3.

The reporter gene, TetO1-MS2d, was activated using 10 ng ml^{-1} of anhydrotetracycline (aTc) (IBA GmbH, Germany), for at least 45 minutes, to allow the production and maturation of enough reporter MS2-GFP proteins. For acclimatization, cells were grown at room temperature for 1 hour. Afterwards, they were transferred to a microscope chamber, for image acquisition.

Cells were kept at 24 °C, 27 °C, 30 °C, 34 °C, or 37 °C during microscopy in a thermal chamber (Bioptechs, FCS2, Pennsylvania, USA). We poured 100 μl of melted agarose-medium with 1% agarose (Sigma life science, USA), LB medium, and aTc (10 ng ml^{-1}), into a microscope slide with a glass coverslip on top. After waiting for the gel-pad to solidify, prior to adding cells, we removed the coverslip and left the gel-pad to dry for 2–5 minutes at room temperature. Finally, we added 5–8 μl of cell suspension into the gel and placed this sandwich in the thermal chamber for image acquisition.

Cells were visualized in a Nikon Eclipse (TE2000-U, Nikon, Japan) inverted microscope with C1 confocal laser-scanning and a 100× Apo TIRF objective. Images were taken every minute for 2 hours. GFP fluorescence was measured using 488 nm argon ion laser (Melles-Griot) and a 515/30 nm emission filter. Images were acquired with Nikon EZ-C1 software and were analysed by custom software written in MATLAB 2011b (MathWorks).

Image analysis

Images of cells with the repressilator and with the switch were analysed differently. To detect cells with the repressilator from images (Fig. 1), we segment them by manually masking the area each occupies in each frame. Next, the total fluorescence intensity in each mask is extracted and the mean pixel intensity of each cell is calculated for each time moment.

For cells containing the switch, thus expressing MS2-GFP and its target RNA, the region occupied by each cell over time was manually masked. In each mask, principal component analysis (PCA) was used to obtain dimensions and orientation of the cell at each moment. By kernel density estimation using a Gaussian kernel[22] and Otsu's thresholding,[23] fluorescent spots were automatically segmented. To obtain the intensity of each spot, the cell background was subtracted. Finally, RNA numbers in each cell were obtained from the time series of the corrected total spot intensity by a least squares fit of a monotone piecewise-constant curve (Fig. 2b).[24] The number of terms in the curve was selected by an *F*-test with a *p*-value of 0.01. Each jump corresponds to the production of one RNA[24] (Fig. 2, for details see ref. 25).

Assessing functionality and apparent period of oscillations

To determine if a repressilator is 'functional' during a time series, we use the criterion used in Elowitz *et al.*[7] A fast Fourier transform is applied to the temporal fluorescence signal from

Fig. 1 Cell exhibiting oscillatory fluorescence. 5 frames are shown, along with time stamps in minutes. In this case, the images were taken at 30 °C.

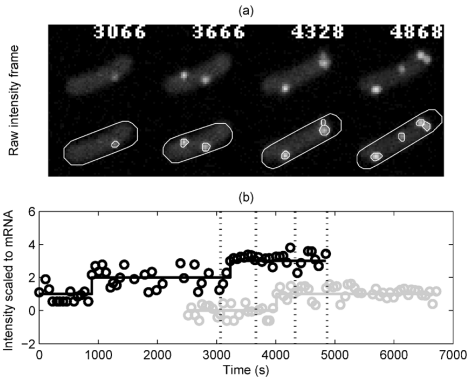

Fig. 2 MS2-GFP tagged RNAs in *E. coli* cells. Unprocessed and segmented cells and RNA spots (a). Moments when images were taken are indicated in each frame. Examples of time series in cells with scaled intensity levels (circles) and estimated RNA numbers (solid lines) (b).

each cell and divided by the transform of a decaying exponential with a time constant of 90 min, the measured lifetime of the fluorescent protein used (GFPaav).[7] Power spectra with peaks 4.5 times higher than the background at frequencies of 0.15–0.5 per hour were classified as oscillatory. The bandwidth used here is larger than in ref. 7 so as to include failed oscillations that should cause apparent oscillations with close to double period.

For cells considered functional, we estimated the 'apparent period' as follows. First, we fit a quadratic curve in the least-squares sense to the intensity time series, to estimate the general trend (Fig. 3, top panel) since the measured intensity is affected by, *e.g.*, photo-bleaching. After subtracting the estimated trend, the residual is scaled to unit power (Fig. 3, middle panel), and then the autocorrelation function is computed (Fig. 3, bottom panel). From this function, we estimate the period by locating the first and the third zeros of the autocorrelation function and computing their distance (Fig. 3, bottom panel, black circles).

Detecting failed oscillations and estimating the true period

The above method of period estimation relies on robust periodic behaviours. If a repressilator halts its activity for a while and then resumes it, the above method cannot detect it. Instead, it assumes an oscillation length that includes the halting and the 'true' oscillation. We observed by inspection that, in some cells, the GFP reporter failed to report an oscillation, either because the oscillation itself failed or because the reporters' expression failed. In general, the reporter signal 'recovered' in the next cycle. In these cases, the measured time was double that between other consecutive oscillations.

To extract the 'true period', we employed a method that relies on the fact that the distributions of period lengths, when failures occur, resemble bimodal distributions. Namely, we estimate the mean and standard deviation of the true period in the population and the fraction of failed oscillations from

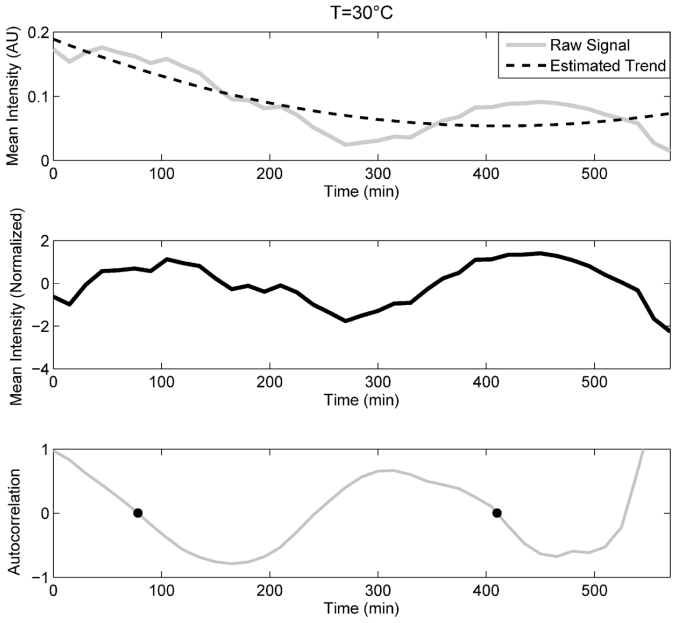

Fig. 3 Period estimation from the fluorescence intensity signal. In the top panel, the raw signal extracted from images is shown along with the estimated trend. In the middle panel, the trend was subtracted from the raw signal and the residual was scaled to unit power. The bottom panel shows the autocorrelation function of the treated signal. The distance between first and third zeros (black circles) corresponds to the period of oscillation in the cell.

the measured periods from each cell. For that, we find the maximum likelihood estimates for a single Gaussian (given by the mean and standard deviation of the measured periods) and for a mixture of two Gaussians, such that the mean and variance of the second are double that of the first (found using an iterative expectation maximization algorithm).[26] The appropriate model is selected by a likelihood ratio test with significance level of 0.01 between the two models. That is, we only select the 2-Gaussian model if the *p*-value of this test is smaller than 0.01. Finally, we performed the fitting with each subset of data lacking one of the measured periods (leave-one-out technique). This procedure results in N estimates each using $N-1$ measured periods from which the variance of the estimates is estimated.

Results

We measured the behaviour of the repressilator at 28 °C, 30 °C, 33 °C, and 37 °C. We also conducted measurements for lower and higher temperatures than these, but the number of functional repressilators was negligible or non-existing. We limited the measurements' length to 10 h, as cells tend to enter the stationary phase beyond this point, which halts the repressilator.[7] Cells with a non-functional repressilator, for this or other reasons, were discarded by the method used to determine if the GFP levels oscillate throughout the measurement period (see Methods).

We first tested if the distributions of lengths of the oscillations (Fig. 4) here referred to loosely as 'periods', differ with temperature. For that, we compared all pairs of distributions using the Kolmogorov–Smirnov (KS) test. All, except 33 °C *vs.* 37 °C, differ in a statistical sense (*p*-values smaller than 0.03), which implies that the circuit is sensitive to temperature.

Under all conditions, as visible from the distributions in Fig. 4, the period lengths vary widely. Given their mean and variability, a number of short-lasting periods (<100 min) are expected (visible in Fig. 4). To verify that these did not occur in a higher than expected frequency, for the condition '30 °C' (the one with most samples), we computed the probability of having such or a more extreme number of periods smaller than 100 min (*i.e.* a *p*-value) assuming the fitted model (see below and the Methods section). From the model, 2.93 'short periods' are expected while 3 were detected, which results in a *p*-value of 0.56 *i.e.*, the number of events observed is not unlikely.

The effects of temperature on the distribution of periods' length are visible in Fig. 4. The distribution appears to become bimodal for $T > 30$ °C. This bimodality, not possible if the oscillations in protein numbers were robust, appears to arise from 'failed oscillations' that occur with non-negligible probability. Namely, in some of the cells at $T > 30$ °C, the GFP levels appear to remain low for approximately one cycle and only increase again in the following cycle.

To test for bimodality, for each of the four distributions, we determined the maximum likelihood estimates for a single Gaussian and for a mixture of two Gaussians with the mean and variance of the second Gaussian being double those of the first. The preferred model (see Methods) in each condition is shown in Fig. 4 as well. For 33 °C and 37 °C, the model of two Gaussians was preferred.

Using the fitting, we estimated the number of failed oscillations in each cell, under each condition (see Methods). The fraction of successful oscillations (R) is shown in Table 1, for each condition. Beyond 30 °C, the repressilator loses much of its robustness, as several expected oscillations were not detected. This agrees with the observed decrease in functionality (F) for temperatures above 30 °C (Table 1).

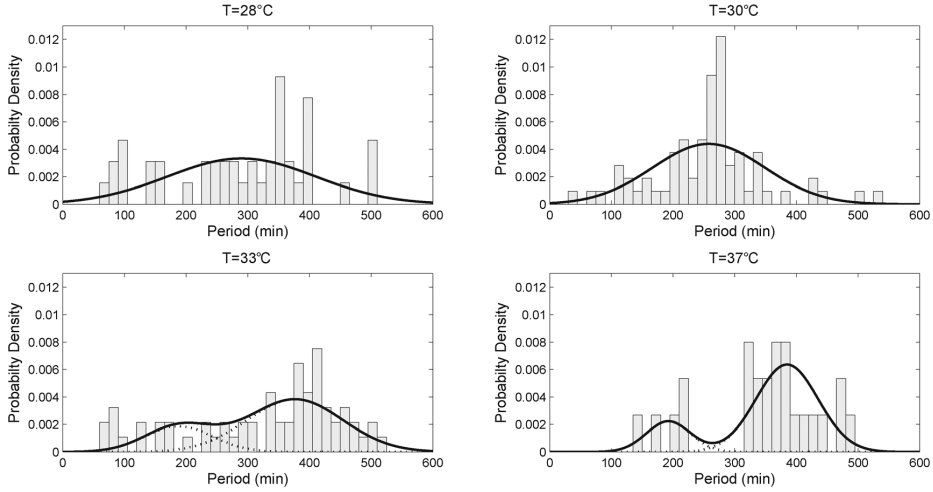

Fig. 4 Distribution of periods (magnitude scaled to represent probability density) for each temperature. Solid lines represent the probability densities of the fitted model with one or two Gaussians. Dashed lines represent the densities of individual components in the case of two Gaussians. For 28 °C and 30 °C, the *p*-values of the likelihood ratio tests are 0.08 and 1, respectively, indicating a lack of evidence for the two-Gaussian model, whereas for 33 °C and 37 °C, the *p*-values are 0.0065 and 0.0015, respectively, indicating that the two-Gaussian model should be favored over the one-Gaussian model.

Table 1 Kinetics of the repressilator at different temperatures. Temperature (T), fraction of functional cells (F), total number of cells exhibiting oscillations, fraction of robust oscillations (R), mean (m) and standard deviation (s) of the apparent period, and mean (μ) and standard deviation (σ) of the estimated true period are shown

T (°C)	F (%)	No. of cells oscillating	R (%)	m (min)	s (min)	μ (min)	σ (min)
28	20	43	100	290	120	290	120
30	30	71	100	258	91	258	91
33	15	62	26	328	126	188	59
37	5	25	20	347	92	192	36

Also in Table 1, we show the mean and standard deviation of both the apparent period and the true, estimated period. The mean true period, μ, always decreases with increasing temperature. On the other hand, the mean apparent period, m, is minimal at 30 °C.

Given this, we investigated whether the distributions of durations of true oscillations alone also differ with temperature, as the distributions of apparent oscillations do. Namely, we estimated the mean true period (Fig. 5) and then the one standard deviation of this estimate (error bars in Fig. 5). From Fig. 5, this mean always decreases significantly as temperature increases, except beyond 33 °C.

Next, we investigated the causes for the decrease in robustness with temperature. In particular, we investigated how temperature affects the functionality of the three component proteins of the repressilator, namely, CI, LacI, and TetR. First, studies suggest that as temperature increases from 30 °C to 42 °C, CI loses approximately half of its DNA-binding stability.[17] On the other hand, the DNA-binding affinity of LacI does not vary significantly between 28 °C and 37 °C.[27] Similarly, TetR's functionality is unaltered from 20 °C to 40 °C.[28] We thus hypothesized that a possible cause for the loss of robustness of the repressilator with increasing T was the weakening effectiveness of CI as a repressor.

There is another circuit, the CI–Cro genetic switch, of which CI is a component. If CI loses functionality with increasing temperature (partially or completely) the behaviour of this switch should change with temperature. To determine whether this is the case, we conducted *in vivo* measurements of RNA production, one event at a time, by one of the two genes of this switch. This particular gene is controlled by the promoter P_{RM}, and codes for CI as well as for a 48 MS2d binding array. The second gene of the switch, whose activity is not followed, is controlled by the promoter P_R and codes for Cro. Relevantly, Cro–DNA interactions do not vary significantly from 24–37 °C,[29] thus, behaviour changes in this switch with increasing temperature should mostly arise from the changes in CI–DNA interactions.

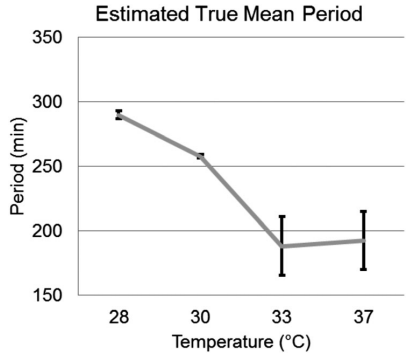

Fig. 5 Estimated mean values of the true period. Error bars indicate one standard deviations of the mean period estimated by the leave-one-out technique.

Table 2 Intervals between the appearances of novel, consecutive RNA molecules in individual cells. For condition, the table shows the number of intervals, mean (μ), standard deviation (σ) and, square of the coefficient of variation (CV^2) of the interval duration

T (°C)	No. intervals	μ (s)	σ (s)	CV^2
24	157	1242	1166	0.88
27	229	1452	1191	0.67
30	88	1130	1040	0.85
33	539	788	807	1.05
37	324	714	785	1.21

Table 3 P-values of the Kolmogorov–Smirnov test between distributions of intervals between consecutive RNA production events, under the control of P_{RM}, obtained at different temperatures. For p-values <0.01, the hypothesis that the two distributions are the same is rejected

T (°C)	24	27	30	33
27	0.149			
30		0.006		
33			0.009	
37				0.478

We measured intervals between consecutive productions of the RNA target for MS2-GFP in individual cells, from *in vivo* measurements 2 h long, with images taken every minute, at 24 °C, 27 °C, 30 °C, 33 °C and 37 °C. In Table 2, we show for each condition the number of samples (*i.e.* intervals) and the mean and standard deviation of the intervals' duration. As temperature increases, the kinetics of production of the target RNA changes. Specifically, aside from a decrease in the mean interval between consecutive transcription events, one observes that the production kinetics changes from sub-Poissonian ($CV^2 < 1$) for $T \leq 30$ °C, to super-Poissonian ($CV^2 > 1$) for $T > 30$ °C.

To verify if the change is significant, we compared the distributions of intervals in consecutive temperatures with the K–S test. The results in Table 3 indicate that the distributions at 24 °C and 27 °C cannot be statistically distinguished from one another. Similarly, the distributions at 33 °C and 37 °C cannot be distinguished. Meanwhile, the distributions from 27 °C and 30 °C, as well from 30 °C and 33 °C, differ from one another. Thus, there is a change in the dynamics of transcript production, and it occurs around 30 °C, which is similar to the point where changes in behaviour of the repressilator are observed.

Conclusions and discussion

We studied the behaviour of the repressilator at different temperatures. We observed that the fraction of functional cells

(*i.e.* exhibiting oscillations), the robustness of the oscillations in functional cells, and also the apparent and the real period all differ with temperature.

Because the robustness decreases at higher-than-optimal temperatures, the extraction of the period in this regime requires the identification of failed oscillations. Otherwise, the period will likely be overestimated. The extraction method here proposed should be applicable to other genetic clocks as well.

The apparent period was minimized at 30 °C. However, the results of employing the novel method of period extraction suggest that the increase in apparent period when increasing temperature beyond 30 °C is due to an increasing rate of failed oscillations. Meanwhile, the true period decreased significantly with increasing temperature (until 33 °C), in accordance with the response of other synthetic genetic clocks to increasing temperature.[30] This decrease is likely caused by the increased rate of the underlying thermodynamic processes (see ref. 30). In particular, we expect the decay rates of the proteins to increase, which decreases the period length.[35] The increased protein decay rates are expected from both increased rates of degradation and increased doubling rate of the cells. This allows the repressilator to be sensitive to temperature changes in the range tested.

We hypothesize that the design of genetic clocks that are insensitive to temperature will have to be able to compensate for increased speed of processes such as cell division, open complex formation,[13] among others.

Subsequently, based on previous studies on the functionality of the proteins of the repressilator,[17,27,28] we hypothesized that the loss of robustness with increasing temperature was associated with the temperature-dependent functionality of one component protein, CI. We tested this indirectly, by studying how temperature affects the CI–Cro switch. In particular, we conducted *in vivo* measurements, one event at a time, of the kinetics of production of an MS2-GFP tagged RNA that probed the transcription kinetics of the RNA coding for CI. From these, we observed that, when increasing temperature beyond 30 °C, the dynamics of production of the tagged RNA changed from sub-Poissonian to super-Poissonian, which suggests that the production of the tagged RNA became subject to repression.

Recent studies in *E. coli* suggest that, provided no repression, RNA production is a sub-Poissonian process, within the range of temperature tested here.[13,24,25,31] To be super-Poissonian, the promoter ought to have intervals of inactivity[21,34] (*e.g.* due to repressors) or due to another, similar mechanism. In the case of the CI–Cro switch, the occurrence of periods of inactivity of P_{RM} is expected if CI loses functionality, allowing Cro to be expressed.[32,33] Thus, these results suggest that CI loses functionality with increasing temperature.

The repressilator and the CI–Cro switch only share CI in common, while the other component proteins differ. Relevantly, the interactions between all these other proteins and their respective DNA binding sites are not temperature-dependent in the range studied.[27–29] Given this and all of the above, it is therefore reasonable to conclude that, in both circuits, the behavioural changes with temperature observed are primarily due to the temperature-dependence of CI's activity.[18,19]

Further, we hypothesize that it is possible to modify the repressilator so as to make it more robust to a wider range of temperatures. For that, the CI–DNA interaction should be replaced by a less temperature-dependent repression mechanism. This modification is not expected to compromise the sensitivity (which likely depends more heavily on the temperature-dependent cell division rate, among others).

It is worthwhile discussing the different effects of temperature on robustness and functionality. Namely, while functionality is maximized at 30 °C, robustness was only compromised at higher-than-optimal temperatures. In the latter regime, the two decreases are likely related. As robustness decreases, we expect a higher chance for repressilators to not function during the measurements. However, at lower-than-optimal temperatures, the loss in functionality is likely caused by other reasons, as the robustness was not compromised. Future research is needed to identify such causes.

Finally, the results presented here demonstrate that the behavioural changes in genetic circuits upon changing conditions depend not only on the topology of the circuit, but also on how each of its components responds to the environmental changes.

Acknowledgements

This work was supported by Academy of Finland (ASR), Finnish Funding Agency for Technology and Innovation (ASR), and Tampere City Science Foundation (AH). The funders had no role in study design, data collection and analysis, decision to publish, or preparation of the manuscript. We thank M. Elowitz and I. Golding for generously providing the genetic circuits.

Notes and references

1 C. H. Ko and J. S. Takahashi, *Hum. Mol. Genet.*, 2006, **15**, R271–R277.
2 Z. Neubauer and E. Calef, *J. Mol. Biol.*, 1970, **51**, 1–13.
3 D. L. Gally, J. A. Bogan, B. I. Eisenstein and I. C. Blomfield, *J. Mol. Biol.*, 1970, **51**, 1–13.
4 A. Becskei and L. Serrano, *Nature*, 2000, **405**, 590–593.
5 N. Nandagopal and M. B. Elowitz, *Science*, 2011, **333**, 1244–1248.
6 D. M. Wolf and A. P. Arkin, *Curr. Opin. Microbiol.*, 2003, **6**, 125–134.
7 M. B. Elowitz and S. Leibler, *Nature*, 2000, **403**, 335–338.
8 T. S. Gardner, C. Cantor and J. J. Collins, *Nature*, 2000, **403**, 339–342.
9 A. S. Khalil, T. K. Lu, C. J. Bashor, C. L. Ramirez, N. C. Pyenson, J. K. Joung and J. J. Collins, *Cell*, 2012, **150**, 647–658.
10 J. M. Callura, C. R. Cantor and J. J. Collins, *Proc. Natl. Acad. Sci. U. S. A.*, 2012, **109**, 5850–5855.
11 M. B. Elowitz and W. A. Lim, *Nature*, 2010, **468**, 889–890.
12 K. D. Litcofsky, R. B. Afeyan, R. J. Krom, A. S. Khalil and J. J. Collins, *Nat. Methods*, 2012, **9**, 1077–1080.

13 A.-B. Muthukrishnan, M. Kandhavelu, J. Lloyd-Price, F. Kudasov, S. Chowdhury, O. Yli-Harja and A. S. Ribeiro, *Nucleic Acids Res.*, 2012, **40**, 8472–8483.
14 D. M. Virshup and D. B. Forger, *Cell*, 2009, **137**, 602–604.
15 I. Mihalcescu, W. Hsing and S. Leibler, *Nature*, 2004, **430**, 81–85.
16 O. Oleksiuk, V. Jakovlejevic, N. Vladimirov, R. Carvalho, E. Paster, W. S. Ryu, Y. Meir, N. S. Wingreen, M. Kollmann and V. Sourjik, *Cell*, 2011, **145**(2), 312–321.
17 N. Jana, S. Roy, B. Bhattacharyya and N. C. Mandal, *Protein Eng.*, 1999, **12**(3), 225–233.
18 K. Koblan and G. Ackers, *Biochemistry*, 1991, **30**, 7822–7827.
19 K. Koblan and G. Ackers, *Biochemistry*, 1991, **30**, 7817–7821.
20 *Lambda II*, ed. R. W. Hendrix, J. W. Roberts, F. W. Stahl and R. A. Weisberg, Cold Spring Harbor Laboratory, Cold Spring Harbor, NY, 1983.
21 I. Golding, J. Paulsson, S. M. Zawilski and E. C. Cox, *Cell*, 2005, **123**, 1025–1036.
22 T. B. Chen, H. H. Lu, Y. S. Lee and H. J. Lan, *J. Biomed. Inf.*, 2008, **41**, 1021–1027.
23 N. Otsu, *IEEE Trans. Syst. Man Cybern.*, 1979, **9**, 62–66.
24 M. Kandhavelu, H. Mannerstrom, A. Gupta, A. Hakkinen, J. Lloyd-Price, O. Yli-Harja and A. S. Ribeiro, *BMC Syst. Biol.*, 2011, **5**, 149.
25 M. Kandhavelu, J. Lloyd-Price, A. Gupta, A.-B. Muthukrishnan, O. Yli-Harja and A. S. Ribeiro, *FEBS Lett.*, 2012, **586**, 3870–3875.
26 A. P. Dempster, N. M. Laird and D. B. Rubin, *J. R. Stat. Soc. Ser. B (Methodological)*, 1977, **39**(1), 1–38.
27 D. E. Frank, R. M. Saecker, J. P. Bond, M. W. Capp, O. V. Tsodikov, S. E. Melcher, M. M. Levandoski and M. T. Record Jr, *J. Mol. Biol.*, 1997, **267**, 1186–1206.
28 W. Hillen, G. Klock and I. Kaffenberger, *J. Biol. Chem.*, 1982, **257**, 6605–6613.
29 Y. Takeda, P. Ross and C. Mudd, *Proc. Natl. Acad. Sci. U. S. A.*, 1992, **89**, 8180–8184.
30 J. Stricker, S. Cookson, M. R. Bennet, W. H. Mather, L. S. Tsimring and J. Hasty, *Nature*, 2008, **456**, 516–520.
31 J. Mäkelä, M. Kandhavelu, S. Oliveira, J. Chandraseelan, J. Lloyd-Price, J. Peltonen, O. Yli-Harja and A. Ribeiro, *Nucleic Acids Res.*, 2013, **41**, 6544–6552.
32 L. Anderson and H. Yang, *Proc. Natl. Acad. Sci. U. S. A.*, 2008, **105**, 5827–5832.
33 S. Svenningsen, N. Costantino, D. Court and S. Adhya, *Proc. Natl. Acad. Sci. U. S. A.*, 2005, **102**, 4465–4469.
34 C. W. Gardiner, *Handbook of Stochastic Methods*, Springer, NY, 3rd edn, 2004.
35 A. Loinger and O. Biham, *Phys. Rev. E: Stat., Nonlinear, Soft Matter Phys.*, 2007, **76**, 051917.

Publication III

Chandraseelan, J. G., Oliveira, S. M. D., Häkkinen, A., Startceva, S and Ribeiro A. S. (2015). Synchrony between Genetic Repressilators in Sister Cells in Different Temperatures. International Science Index. 9(7). Paper presented at Proceedings of the International Conference on Computational and Molecular Systems Biology 2015, Zurich (Switzerland). World Academy of Science, Engineering and Technology.

Synchrony between Genetic Repressilators in Sister Cells in Different Temperatures

Jerome G. Chandraseelan, Samuel M. D. Oliveira, Antti Häkkinen, Sofia Startceva, and Andre S. Ribeiro

***Abstract*—**We used live *E. coli* containing synthetic genetic oscillators to study how the degree of synchrony between the genetic circuits of sister cells changes with temperature. We found that both the mean and the variability of the degree of synchrony between the fluorescence signals from sister cells are affected by temperature. Also, while most pairs of sister cells were found to be highly synchronous in each condition, the number of asynchronous pairs increased with increasing temperature, which was found to be due to disruptions in the oscillations. Finally we provide evidence that these disruptions tend to affect multiple generations as opposed to individual cells. These findings provide insight in how to design more robust synthetic circuits and in how cell division can affect their dynamics.

***Keywords*—**repressilator, robustness, synchrony, synthetic biology

I. Introduction

GENETIC circuits are capable of performing tasks such as time keeping [1], state holding [2], and signal modulation and multiplexing [3]. Naturally occurring circuits responsible for these critical tasks have evolved to be sensitive to specific inputs but robust to external fluctuations such as transient environmental changes [4]-[6]. Such behavior is necessary to regulate periodic cellular processes operating under a wide range of conditions, while maintaining efficiency to respond to environmental signals.

Synthetic versions of some important naturally occurring circuits have been engineered [7], [8]. These synthetic constructs aim to allow the programming of novel biological functions but also aid the understanding of the behavior of naturally occurring circuits, which may allow enhancing their performance as well. To match the performance of the natural circuits, the components of the synthetic circuits must be carefully selected such that both the desired behavior and level of robustness are attained [9]. For this purpose, synthetic circuits utilize chemical components whose physical and chemical properties are well characterized [10].

One example of a synthetic oscillator is the repressilator engineered by Elowitz *et al.* [7]. This circuit consists of three genes organized in a ring topology, each inhibiting the expression of a neighboring gene. These interactions form a negative feedback loop, which causes the protein levels of the component genes to oscillate over time. Additionally, one of the component genes is used to control a reporter gene producing green fluorescent proteins, which allows visualizing the system's behavior using fluorescence microscopy. Such oscillator could be used e.g. for time keeping, synchronization via phase-locking, or signal modulation and multiplexing [11].

Temperature is one environmental factor that is known to affect most cellular processes, e.g. by modulating the gene expression dynamics. Evidence suggests that natural time keeping circuits, such as circadian oscillators, have evolved to be robust against temperature fluctuations [4], [5], [12]. In contrast, previous studies of synthetic oscillators have found that the constructed circuits are not immune to temperature changes. In one study, the period of the oscillator was found to decrease monotonically with increasing temperature between 25 and 37 °C, causing over two-fold change, presumably because changes in temperature affect the thermodynamics of all the cellular processes [13]. Our previous study on the dynamics of the Elowitz repressilator provides evidence of a similar pattern, but also notes that the most cells exhibit disrupted oscillations for temperatures over 37 °C. Evidence was then provided that this is due to loss of functionality of one of the component proteins [14].

In this work, we use live *E. coli* cells containing a synthetic genetic repressilator [7] to study how the synchrony between sister cells changes as a function of temperature and the resulting changes in the robustness of these circuits. In our cells, the loss of synchrony is inevitable since, following cell division, it is not maintained by any process between the sister cells [7]. This would lead to tangible phenotypic differences between them, provided that the clocks were used to regulate some key cellular process. Here we quantify such degree of asynchrony as a function of temperature. The findings will be important in providing insight in designing more robust synthetic circuits, and in understanding the behavior of naturally occurring circuits.

Jerome G. Chandraseelan (e-mail: jerome.chandraseelan@tut.fi) and Samuel M. D. Oliveira (e-mail: samuel.oliveira@tut.fi) are with the Laboratory of Biosystem Dynamics (LBD), Department of Signal Processing, Tampere University of Technology, P.O. box 553, 33101 Tampere, Finland.

Antti Häkkinen is with the LBD and is supported by Jenny and Antti Wihuri foundation (e-mail: antti.hakkinen@tut.fi).

Sofia Startceva is with the LBD and is supported by TUT's Graduate School Grant (e-mail: sofiia.startceva@tut.fi).

Andre S. Ribeiro is with the LBD and supported by Academy of Finland (grant no. 257603) and Fundação para a Ciência e a Tecnologia (grant no. PTDC/BBB-MET/1084/2012) (corresponding author to provide phone: +358-40-8490736; e-mail: andre.ribeiro@tut.fi).

II. Materials and Methods

A. Cell Culturing and Microscopy

Cells of *E. coli lac*$^-$ strain MC 4100 containing the repressilator and the reporter plasmids were generously provided by M. B. Elowitz, Princeton University, NJ, USA. The cells were grown in minimal media with 2 mM $MgSO_4 \cdot 7H_2O$ (Sigma-Aldrich, USA), 7.6 mM $[NH_4]_2SO_4$ (Sigma Life Science, USA), 30 mM $FeSO_4 \cdot 7H_2O$ (Sigma Life Science, USA), 1 mM EDTA (Sigma Life Science, USA), and 60 mM KH_2PO_4 (Sigma Life Science, USA) (pH 6.8) supplemented with 0.5% glycerol (Sigma Life Science, USA) and 0.1% casaminoacids (Fluka Analytical, USA) overnight at 28, 30, or 37 °C with shaking at 300 rpm to an optical density of 0.1 at 600 nm. Next, cells were diluted into fresh media and a few ml of the culture was placed between a cover-slip and a slab of 2% low melting agarose in minimal media. During time lapse microscopy, the temperature of the samples was kept stable by a control chamber (FCS2, Bioptechs, PA, USA). Images were obtained every 15 min for 10 h using a Nikon Eclipse (TE2000-U, Nikon, Tokyo, Japan) inverted C2 confocal laser-scanning system with a 100 Apo TIRF (1.49 NA, oil) objective. GFP fluorescence was measured using a 488 nm laser (Melles-Griot) and a 515/30 nm detection filter. For image acquisition, Nikon EZ-C1 software was used.

B. Image Analysis

The cells were manually segmented in the fluorescence images in each frame of the time series (automatic segmentation is problematic due to the oscillatory signal). Afterwards, cell lineages were established such that a cell (segment) is associated to the cell with largest overlapping cell in the previous frame, after correcting for global translation between the two frames. A cell division was recorded in the case where two cells were associated with the same cell in the previous frame. Finally, the average fluorescence intensity was extracted from each frame and each cell for further analysis.

C. Functionality and Estimation of the Periods

Since a large fraction of the cells do not appear to exhibit oscillations [7], we used the criterion proposed by Elowitz *et al.* [7] to categorize the cells as functional or dysfunctional, and only included the functional cells in the further parts of our analysis. In this method, the power spectral density (estimated using discrete Fourier transform) of the signal is compared with that of a decaying exponential with a time constant of 90 min, the measured lifetime of the fluorescent protein [7]. Cells with spectra exhibiting peaks higher than 3.1 times the background spectral density at frequencies of 0.2 to 0.5 h^{-1} were classified as oscillatory. This method was applied to each branch of the lineage trees to determine the functionality of the youngest cells, whereas the other cells were considered to be functional if they had at least one functional child.

The period of oscillations were estimated using the zeros of the autocorrelation sequence of background-corrected intensity signals [14]. In this method, the raw intensity signal is fit with a quadratic polynomial of time, in least-squares sense, to estimate the background trend (caused e.g. by accumulation of GFP and photobleaching). Next, the background trend is subtracted, the residual is scaled to unit power, and the autocorrelation sequence is computed. The period can be estimated by locating the first and third zero of this sequence, as they are expected to occur at lags of 1/4 and 5/4 times the period.

D. Estimating Robustness and True Period Distributions

Particularly at higher temperatures, the period distributions were observed to exhibit bimodality [14]. This might be caused by either the repressilator or the reporter failing, causing an apparent doubling of the period [14]. Higher-order harmonics are not expected to be present due to the finite measurement time.

For this, we find the maximum likelihood estimates using a model of a single normal distribution (given by the mean and standard deviation of the data) and a mixture model of two normal distributions, with the mean and variance of the second equal to twice that of the first (found using an iterative expectation maximization algorithm [15]), using the measured periods in each condition. The appropriate model is selected using a likelihood ratio test with a significance level of 0.01, that is, the bimodal model is only selected if it fits significantly better than the unimodal one. Finally, in the bimodal case, the robustness of the population is determined from the total probability mass in the first normal distribution, and the robustness of the individual cells are determined by a maximum-a-posteriori classifier given the estimated parameters.

III. Results

We analyzed time series of cells with repressilators imaged in three different temperatures: 28, 30, and 37 °C. The time series were sampled every 15 min and were 10 h in duration. The image analysis process produced a total of 172, 186, and 683 cells in 28, 30, and 37 °C, respectively. Fig. 1 shows examples of confocal microscope images of a few cells and the corresponding extracted intensities.

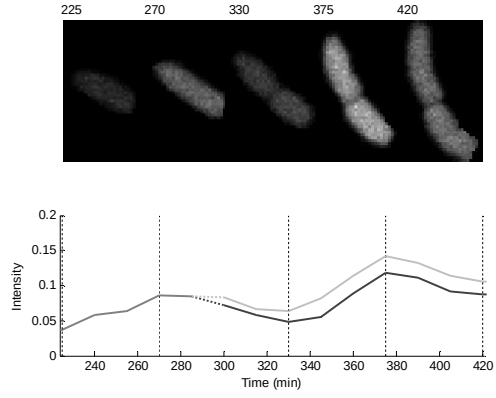

Fig. 1, Example images of related cells with repressilators in five different time points (top), and the corresponding mean intensities extracted from these cells (bottom). The vertical dashed lines indicate the time points corresponding to the images.

First, we computed the fraction of functional cells, estimated the period of each functional cell, and finally estimated the distribution of periods and robustness in each condition (see methods). Here functional cells are those that exhibit oscillations of "strong enough" power, and robust cells are those that exhibit oscillations at the fundamental frequency (and not some harmonic). Summary of the statistics is shown in Table I.

TABLE I
FUNCTIONALITY, PERIOD STATISTICS, AND ESTIMATED PERIOD DISTRIBUTION IN DIFFERENT TEMPERATURES

Statistic	28 °C	30 °C	37 °C
Functionality	0.64	0.83	0.80
Period mean	384	252	245
Period sd	84	93	98
Fit period mean	384	252	150
Fit period sd	84	93	51
Fit robustness	1	1	0.37

Units of time are in minutes. Period mean and standard deviation (sd) were extracted from the data, and estimated period mean, sd, and robustness were obtained by fitting the model (see methods).

The results indicate that the functionality is lower in the 28 °C condition (p-value of 1.56×10^{-4} in one-tailed binomial test with null hypothesis of equal distributions), and similar in the 30 °C and 37 °C conditions (p-value of 0.09). We also found that the mean period decreases with a temperature increase from 28 °C to 30 °C (p-value of 1.84×10^{-17} in one-tailed Welch's t-tests with null hypothesis of equal means), and is similar in 30 °C and 37 °C conditions (p-value of 0.28). The coefficients of variation (standard deviation over the mean) extracted from the periods are 0.22, 0.37, and 0.40 for 28, 30, and 37 °C, respectively, which suggests that the relative variations in the periods increase with temperature. These results are in agreement with previous findings [14].

Since only around 40% of the cells imaged under 37 °C were found to be robust, we further computed the statistics using only the robust cells in this condition. The mean (standard deviation) period of the robust cells is around 150 (51) min, resulting in a coefficient of variation of 0.34. In comparison to the whole population of the cells in the 37 °C case, the robust cells have significantly lower mean period compared to the 30 °C case (p-value of 2.50×10^{-15}), suggesting that an increase in temperature results in a decrease in the period of oscillations of "properly" operating repressilators throughout the whole region. In addition, the stochasticity in the period duration appears to be similar in the 30 and 37 °C conditions and lower in the 28 °C condition.

Next, in these data, we located each pair of sister cells in which both of the sister cells were functional. We found 32, 53, and 187 such pairs in 28, 30, and 37 °C conditions, respectively, and 35 such pairs in the robust cells of 37 °C condition.

We first tested if a robust cell is more (or less) likely to have a robust sister cell than is expected by chance, in the 37 °C condition. In our data, we found 112, 40, and 35 pairs where none, one, or both of the cells were robust, respectively, suggesting that the number of pairs where either none or both sisters are robust are overrepresented. More specifically, there is about a 0.64 chance for a robust cell to have a robust sister, and about a 0.85 chance for a non-robust cell to have a non-robust sister (cf. 0.37 in Table I). The significance of this correlation was confirmed by computing the p-value of one-tailed Fisher's exact test with the null hypothesis that being robust or not is independent in the sister cells, resulting in a p-value smaller than 1.29×10^{-10}.

Next, we computed the correlation between the intensity signals of each pair of sister cells. This correlation results from loss of synchrony caused both by division and variations in the behavior of the cells over their lifetime (i.e. variations/drift in the period and noise in the intensity signal). The distributions of correlation coefficient extracted from each pair of cells are shown in Fig. 2, and the mean and standard deviation of the coefficients is shown in Table II.

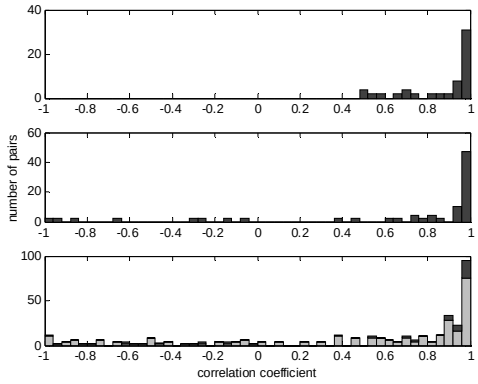

Fig. 2, Distributions of correlation coefficients between functional sister cells in 28 (to), 30 (middle), and 37 °C (bottom). In the 37 °C condition, the pairs where both cells are robust are represented in dark gray bars, while the others are represented in light gray.

TABLE II
CORRELATION BETWEEN SISTER CELLS IN VARIOUS TEMPERATURES

Statistic	28 °C	30 °C	37 °C	37 °C, robust
Correlation mean	0.87	0.66	0.42	0.63
Correlation sd	0.16	0.58	0.66	0.58

We found that as the temperature increases, the sister cells lose correlation, on average (p-values of 3.17×10^{-3} and 9.90×10^{-4} for 28 vs. 30 °C and 30 vs. 37 °C in one-tailed Welch's t-test with the null hypothesis that the means are

equal). This loss of correlation could be due to the increase in the noise of the period as a function of the temperature, which appears to follow a similar pattern. Accordingly, since the non-robust cells contribute much of the variation in the 37 °C condition, the correlation is restored to a level comparable to the 30 °C condition when only the robust cells are considered. Interestingly, Fig. 2 reveals that in each condition, most of the cells are very highly correlated. However, increases in the temperature results in pairs of cells with wider range of correlation coefficients, including a sizable number of pairs whose series are strongly anticorrelated.

IV. Conclusion

We used live *E. coli* cells containing genetic Repressilators to study how the synchrony between synthetic genetic repressilators contained in sister cells changes as a function of both the temperature and the affected robustness of the cells.

We found that the temperature affects both the mean and the variability of the synchrony between sister cells, as measured by the correlation coefficient between their intensity time series. While in each condition most pairs of sister cells are highly correlated, the number of uncorrelated and anticorrelated pairs grows with increasing temperature. These values result in an apparent reduction in the synchrony between the sister cells for the population as a whole.

However, in the 37 °C condition, the non-robust pairs (i.e. cells whose oscillations become disrupted) were found to be responsible for these unlikely pairs, and the synchrony of the cells that remain robust is comparable to the 30 °C case, as predicted by the changes in the stochasticity of the period. Finally, we found that a robust/non-robust cell is more likely to have a sister with similar than the opposite behavior, suggesting that the disruptions in the oscillators propagate to successive generations.

To explain these results, we provide evidence that the changes in the synchrony between the sister cells are reflected with changes in the stochasticity of the period of oscillations. Such stochasticity is expected to result in the sister cells randomly drifting to different behaviors over time. This hypothesis would explain the changes in synchrony both as a function of changes in the temperature and as a function of the changes in the robustness of the cells. However, we note that it remains unclear if other noise sources, such as the stochasticity of partitioning the repressilator or GFP plasmids, differ in the different conditions, and if they have a significant effect on the synchrony of cells of common ancestry.

These results further support the hypothesis that in higher temperatures the repressilators become disrupted, which might be due to the component protein CI losing functionality in these temperatures [14]. Furthermore, we have provided evidence that such failure would not only cause a disruption in the oscillatory signals, but also the loss of synchronization between similar the clock signals, which might be important if independent clocks are used to drive downstream circuits.

References

[1] J. C. Dunlap, “Molecular bases for circadian clocks,” in *Cell*, vol. 96, pp. 271-290, 1999.

[2] Z. Neubauer, and E. Calef, “Immunity phase-shift in defective lysogens: Non-mutational hereditary change of early regulation of λ prophage,” in J. Mol. Biol., vol. 51, pp. 1-13, 1970.

[3] R. E. Dolmetsch, K. Xu, R. S. Lewis, “Calcium oscillations increase the efficiency and specificity of gene expression,” in *Nature*, vol. 392, pp. 933-936, 1998.

[4] I. Mihalcescu, W. Hsing, and S. Leibler, “Resilient circadian oscillator revealed in individual cyanobacteria,” in *Nature*, vol. 430, pp. 81-85, 2004.

[5] D. M. Virshup, and D. B. Forger, “Keeping the beat in the rising heat,” in *Cell*, vol. 137, pp. 602-604, 2009.

[6] A. Ay, S. Knierer, A. Sperlea, J. Holland, and E. M. Ozbudak, “Short-lived Her proteins drive robust synchronized oscillations in the zebrafish segmentation clock,” in *Development*, vol. 140, pp. 3244-3253, 2013.

[7] M. B. Elowitz, and S. Leibler, “A synthetic oscillatory network of transcriptional regulators,” in *Nature*, vol. 403, pp. 335-338, 2000.

[8] T. S. Gardner, C. R. Cantor, J. J. Collins, “Construction of a genetic toggle switch in Escherichia coli,” in Nature, vol. 403, pp. 339-342, 2000.

[9] A. Becskei, and L. Serrano, “Engineering stability in gene networks by autoregulation,” in *Nature*, vol. 405, pp. 590-593, 2000.

[10] N. Nandagopal, and M. B. Elowitz, “Synthetic biology: Integrated gene circuits,” in *Science*, vol. 333, pp. 1244-1248, 2011.

[11] D. M. Wolf, and A. P.Arkin, "Motifs, modules and games in bacteria," in *Curr. Opin. Microbiol.*, vol. 6, pp. 125-134, 2003.

[12] K. Kruse, and J. Julicher, ”Oscillations in cell biology,” in *Curr. Opin. Cell Biol.*, vol. 17, pp. 20-26, 2005.

[13] J. Stricker, S. Cookson, M. R. Bennett, W. H. Mather, et al., “A fast, robust and tunable synthetic gene oscillator,” in *Nature*, vol. 456, pp. 516-519, 2008.

[14] J. G. Chandraseelan, S. M. D. Oliveira, A. Hakkinen, H. Tran, et al., “Effects of temperature on the dynamics of the LacI-TetR-CI repressilator,” in *Mol. Biosyst.*, vol. 9, pp. 3117-3123, 2013.

[15] A. P. Dempster, N. M. Laird, and D. B. Rubin, “Maximum likelihood from incomplete data via the EM algorithm,” in *J. Royal Stat. Soc. Ser. B (Methodological)*, vol. 39, pp. 1-38, 1977.

Publication IV

Oliveira, S. M. D *., Chandraseelan, J. G *., Häkkinen, A., Goncalves, N. S. M and Ribeiro A. S. (2015). Single-cell kinetics of the Repressilator when inserted into a single-copy plasmid. Mol. BioSyst., 2015, 11, 1939-1945. (* equal contribution).

Available online on the Royal Society of Chemistry's website, DOI: 10.1039/C5MB00012B

Molecular BioSystems

PAPER

Single-cell kinetics of a repressilator when implemented in a single-copy plasmid†

Samuel M. D. Oliveira,‡[a] Jerome G. Chandraseelan,‡[a] Antti Häkkinen,[a] Nadia S. M. Goncalves,[a] Olli Yli-Harja,[b] Sofia Startceva[a] and Andre S. Ribeiro*[a]

Cite this: *Mol. BioSyst.*, 2015, **11**, 1939

Received 8th January 2015,
Accepted 17th April 2015

DOI: 10.1039/c5mb00012b

www.rsc.org/molecularbiosystems

Synthetic genetic clocks, such as the Elowitz–Leibler repressilator, will be key regulatory components of future synthetic circuits. We constructed a single-copy repressilator (SCR) by implementing the original repressilator circuit on a single-copy F-plasmid. After verifying its functionality, we studied its behaviour as a function of temperature and compared it with that of the original low-copy-number repressilator (LCR). Namely, we compared the period of oscillations, functionality (the fraction of cells exhibiting oscillations) and robustness to internal fluctuations (the fraction of expected oscillations that would occur). We found that, under optimal temperature conditions, the dynamics of the two systems differs significantly, although qualitatively they respond similarly to temperature changes. Exception to this is in the functionality, in which the SCR is higher at lower temperatures but lower at higher temperatures. Next, by adding IPTG to the medium at low and high concentrations during microscopy sessions, we showed that the functionality of the SCR is more robust to external perturbations, which indicates that the oscillatory behaviour of the LCR can be disrupted by affecting only a few of the copies in a cell. We conclude that the SCR, the first functional, synthetic, single-copy, ring-type genetic clock, is more robust to lower temperatures and to external perturbations than the original LCR. The SCR will be of use in future synthetic circuits, since it complements the array of tasks that the LCR can perform.

Introduction

Efforts in synthetic biology dedicated to the engineering of artificial genetic circuits have focused on constructing functional switches (for decision making), clocks (for time keeping), and noise and frequency filters,[1] as these modules are likely candidate regulatory components of the activity of future, more complex synthetic circuits.

One of the first reported functional synthetic circuits is the 'repressilator',[2] a ring-oscillator with three genes, each expressing a protein that represses the next gene in the loop. From the study of the signal from GFP reporters in cells at 30 °C, it was shown that it oscillates (stochastically) at a slower rhythm than the cell cycle. Interestingly, for unknown reasons, only approximately 40% of the cells exhibit oscillations, *i.e.* are 'functional'. Further, even though the circuits' behaviour is uncoupled from the cell cycle in the previous phase,[2] these functional cells become non-functional in the stationary phase, suggesting that this synthetic network is not fully uncoupled from the regulatory mechanisms of cell growth. Finally, the oscillatory behaviour can be halted by external signals. *E.g.* most cells lose the functionality following the addition of 50 μM of isopropyl β-D-1-thio-galactopyranoside (IPTG) to the medium.[2]

A subsequent study[3] analysed the behaviour of the repressilator at temperatures below and above the optimal (from 28 °C to 37 °C, with 30 °C being considered as optimal), focusing on the period of oscillations, the functionality (the fraction of cells exhibiting oscillations) and the robustness (the fraction of expected oscillations that would occur) of the signal from the cells. Both the functionality (maximum at 30 °C) and the period length were found to be temperature-dependent. The minimum period length was observed at 30 °C. While the reason for longer periods at lower-than-optimal temperatures is likely the slower rate of most chemical processes, at temperatures beyond optimal, longer periods emerge due to the loss of functionality of one of the component proteins of the repressilator, CI.[3]

Originally, the repressilator was implemented on a low-copy plasmid (pZS1-lTlrLLtCL). Because of this (as the origin of replication is pSC101), each cell has, on average, 3–4 copies of the repressilator,[4] which are functionally coupled in that the proteins coded by a gene in one of the copies can act as repressors of the next gene in the loop in all other copies of

[a] *Laboratory of Biosystem Dynamics, Department of Signal Processing, Tampere University of Technology, P.O. Box 553, 33101 Tampere, Finland. E-mail: andre.ribeiro@tut.fi*
[b] *Computational Systems Biology Research Group, Department of Signal Processing, Tampere University of Technology, P.O. Box 553, 33101 Tampere, Finland*

† Electronic supplementary information (ESI) available. See DOI: 10.1039/c5mb00012b

‡ Equal contribution.

the plasmid in the cell. This coupling, according to simulations of stochastic models, is expected to reduce the fluctuations in period lengths that arise from the stochasticity in gene expression and in RNA and protein degradation.[5,6] So far, it is unknown whether the repressilator would function if implemented on a single-copy plasmid.

If functional, a single-copy repressilator (SCR) ought to be of use to ongoing efforts in synthetic biology. For example, by comparing its behaviour with that of the original LCR, we may obtain a better understanding of how the copy number variation in bacteria can lead to changes in bacterial growth rates[7,8] and phenotypic innovation,[9] among others. In the case of the repressilator, it is expected that the copy-number will affect the dynamics severely enough to allow the system to change from a single steady state to sustained oscillations.[10]

As these and other expectations are, so far, solely based on theoretical models,[7,10–13] we have implemented the Elowitz–Leibler repressilator[2] on a single-copy F-plasmid (pBAC2) in order to conduct an empirical analysis of the behavioural changes due to copy-number differences. This plasmid is well-known for its high hereditary, *i.e.* copy-number and stability.[14,15] For most of the cell cycle there is only one copy of the plasmid in the cell, which is replicated once, prior to cell division.

After verifying the functionality of our SCR, we compared its dynamics with the original LCR at optimal temperatures. Next, we compared their responses to changing temperatures. Finally, we studied their robustness to external perturbations.

The results provide new insights into the effects of coupling on genetic circuits in general, and clocks in particular. Understanding the functioning of natural, as well as synthetic clocks, such as the repressilator, will assist in the understanding of how cells regulate the timing of several processes[16] and contribute to ongoing efforts in synthetic biology to produce circuits useful in assisting medicine and biotechnology, particularly given the important role that synthetic clocks are expected to play as sensors and regulators in future synthetic circuits.

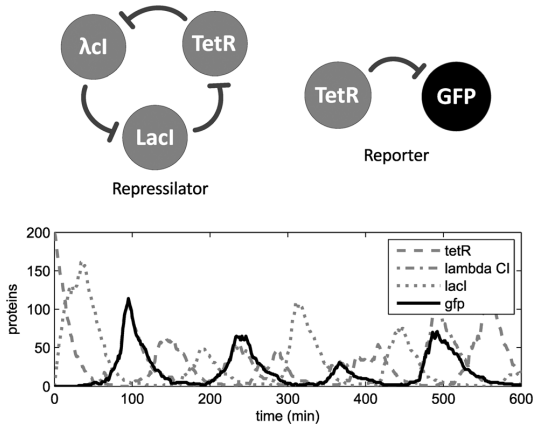

Fig. 1 Top: graphical representation of the 3-gene network (repressilator) along with the GFP reporter. Bottom: an example output from a stochastic model of the repressilator.[11] The black curve represents the output of the reporter while the grey curves represent the actual protein numbers of the three genes of the repressilator. The signals of the GFP reporter and λ CI are nearly superimposed, as expected.

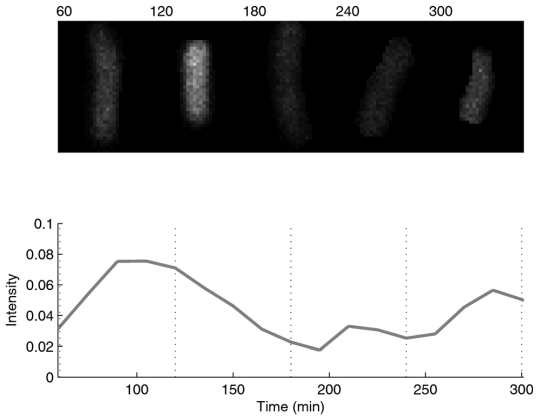

Fig. 2 Top: example images of a cell exhibiting oscillatory fluorescence levels. 5 frames are shown along with the time stamps in minutes. Images taken at 37 °C. Bottom: the mean fluorescence intensity level (in arbitrary units) over time of the cell shown above. The dashed lines indicate points at which the above frames were captured.

Methods

Design, validation, and functioning of single-copy repressilators

The repressilator consists of a three-gene network in a loop formation, with each gene repressing the next gene in the loop[2] (Fig. 1, top). Such a network is expected to exhibit periodic oscillations in the protein levels of the component genes (Fig. 1, bottom). To observe them, a GFP reporter is used, which is regulated by one of the proteins of the circuit.[2]

To build the SCR, we transferred the sequence coding for the repressilator from the original low-copy plasmid into a single-copy F-plasmid (pBAC2-lTlrLLtCL). The original GFP reporter system[2] was left unchanged. The construction history of the SCR is shown in Fig. S1 (ESI†). Images of the gels of the SCR plasmid and PCR are shown in Fig. S4 and S5 (ESI†), respectively. To further confirm the proper construction of the SCR plasmid we performed sequencing and qPCR (Fig. S6 and ESI,† respectively).

Finally, we conducted live cell microscopy to determine whether cells with the SCR exhibited a fluorescent signal whose intensity oscillates (for example Fig. 2 and Fig. S7, ESI†), similar to the original LCR. The observations confirmed the existence of oscillations.

Strains, genetic circuit assembly, and growth conditions

Cells of *E. coli* host strain *lac*$^-$ MC 4100, containing the low-copy repressilator (pZS1-lTlrLLtCL) and the reporter (pZE21-GFPaav)

plasmids, were generously provided by M. Elowitz (Princeton University, NJ, USA).[2] In cells of the same strain, MC4100, containing only the reporter system (also generously provided by M. Elowitz), controlled by the tetracycline repressor (*TetR*) and the promoter P_L tetO1,[2] we inserted the engineered single-copy F-plasmid containing the repressilator system (pBAC2-lTlrLLtCL) from pZS1-lTlrLLtCL (Fig. S1, ESI†).

The low-copy (LCR) and single-copy repressilator (SCR) strains were grown in agar lysogeny broth (LB) medium from glycerol stock (kept at −80 °C) for 12 hours until single colonies could be detected. Single colonies selected from the LB plates were transferred to LB-agar plates for 8 hours of fast growth. A single colony was then inoculated into a minimal medium for 10 hours at 28 °C, 30 °C, 33 °C or 37 °C with shaking at 250 rpm (6 rcf), to an optical density (OD) ≈ 0.1 at 600 nm. Next, cells were centrifuged at 8000 rpm (6093 rcf) for 1 minute and diluted into fresh minimal medium. In all steps, besides image acquisition, LCR cells' preparation contained 35 μg ml^{-1} of kanamycin and 20 μg ml^{-1} of ampicillin, while SCR cells' preparation contained 35 μg ml^{-1} of kanamycin and 35 μg ml^{-1} of chloramphenicol (all antibiotics from Sigma Aldrich, USA). For imaging, a few μl of the culture were placed between a cover-slip and a 2.5% low melting agarose gel pad of minimal medium with 1 mm thickness.

As mentioned above, the LCR and SCR differ in their antibiotic markers, as the SCR uses chloramphenicol instead of ampicillin. However, as we do not use either of antibiotics during the microscopy measurements and given the identical growth rates of the two strains during those measurements (see below), this difference is not expected to affect their dynamics.

Cell culturing optimization

To avoid plasmid instability[17–19] and to optimize culturing protocols[2,3] we proceeded as follows: (i) as in the original protocol,[2,3] cells were taken from a stock (at −80 °C) and streaked onto an LB agar medium with appropriate antibiotics for 14–16 hours; (ii) at this stage, we added to the original protocol an extra step of 8 hours of cell growth from single colonies in LB agar medium;[2,3] (iii) next, as in the original protocol, a few colonies from the second plate were inoculated in M63 liquid minimal medium with antibiotics for 10 hours. Finally, we placed cells at 28 °C, 30 °C, 33 °C, or 37 °C for 8 hours, after which we measured the optical density (OD). After these 8 hours of culturing OD_{600} ≈ 0.1–0.2 was reached under all conditions, as reported in ref. 3 No differences in behaviour were found between cells with the LCR and with the SCR during this procedure.

Microscopy

During time lapse microscopy, cells were kept at a stable temperature in a thermal chamber (Bioptechs, FCS2, PA, USA). Images of both LCR and SCR cells were obtained every 15 minutes for 10 hours using a Nikon Eclipse (Ti-E, Nikon, Japan) inverted microscope equipped with a C2+ confocal laser-scanning system and a 100× Apo TIRF (1.49 NA, oil) objective. Images were taken from multiple locations at each moment. GFP fluorescence was excited using a 488 nm argon ion laser (Melles-Griot) and measured using a 515/30 nm emission filter. The pixel dwell time was set to 2.4 μs, so that the total image acquisition time per location was ≈2.5 s. The laser shutter was open only during exposure to minimize photo-bleaching. We used NIS-Elements software (Nikon) for image acquisition.

Data and image analysis

For image and data analysis, we used custom software written in MATLAB 2011b (MathWorks). Cells with either the LCR or the SCR were manually segmented in the images.[3] Next, the segments were automatically tracked based on the overlapping areas of the segments in consecutive frames, and the total fluorescence intensity was extracted and used to calculate the mean pixel intensity of the cell at each moment.[3]

We used the following criterion to determine the functionality of the repressilator:[2,3] for cells presenting the fluorescence signal from start to end, a discrete Fourier transform was applied and divided by the transform of a decaying exponential of the measured lifetime of the fluorescent protein used (*GFPaav*), with a time constant of 90 min.[2] From these, cells with power spectra with peaks 3 times higher than the background, at frequencies of 0.2–0.5 per hour, were classified as oscillatory. As discussed in ref. 3, the bandwidth was larger than that reported in ref. 2 to detect failed oscillations, which create apparent periods close to the double mean and standard deviation.[3]

The same method as reported in ref. 3 was used to estimate the period of oscillations for each cell. It consists of subtracting the detected trend from a raw signal, followed by scaling the residual to unit power and computing an autocorrelation function. Afterwards, periods were estimated by locating the first and third zeros of the autocorrelation function, and computing their distance.

Robustness of the oscillations to internal fluctuations

It is known that some cells fail to report an oscillation at times, particularly at temperatures higher than 30 °C.[3] This occurs either because no oscillation occurred or because the reporter failed to report it. Typically, such 'halted' signals resume in the next cycle. Regardless of the cause, these events are evidence for the lack of robustness to internal fluctuations of the repressilator–reporter system. To quantify this phenomenon and assess its temperature dependence in each system, we defined robustness to internal fluctuations as the fraction of expected oscillations that do occur according to the reporter (*i.e.* the ratio between true and apparent cycles). To find the fraction of 'apparent' and 'true' cycles in functional cells under each condition, distributions of period lengths were analysed (Fig. S2 and S3, ESI†).

As reported in ref. 3, these distributions were fitted to either a single Gaussian or to a mixture of two Gaussians. In the distributions where bimodality was observed, the 'apparent' and 'true' periods were extracted from the fitting of a 2-Gaussian model such that the mean and the variance of the second period were twice that of the first (found using an iterative expectation

maximization algorithm).[20] The appropriate model was selected by a likelihood ratio test with a significance level of 0.01 between the two models. That is, we only select the 2-Gaussian model if the *p*-value of this test is smaller than 0.01. This methodology was used here solely to quantify the robustness of the repressilator–reporter system to internal fluctuations.

External perturbation of the activity of the repressilator

In one experiment, we assessed the robustness of the SCR and LCR to external perturbations by introducing a certain concentration of IPTG into the medium, 180 minutes after starting the microscopy measurements (to allow at least one cycle of oscillation). IPTG induces the P_L lacO1 promoter and, as such, it should disrupt the functioning of the repressilator. We performed three such experiments. First, we perturbed cells with the SCR and cells with the LCR by adding 50 μM of IPTG to the medium at 30 °C, to compare the robustness of these two circuits to external perturbations. Next, we perturbed cells with the SCR by adding 1 mM of IPTG to the medium, so as to compare the effects of 'weak' (50 μM) and 'strong' (1 mM) perturbations on the SCR dynamics. In all tests, pre-warmed fresh M63 medium containing IPTG at the desired concentration was added to the medium using a peristaltic pump at the rate of 0.3 ml min^{-1}. Images were taken every 15 minutes for 6 hours (3 hours prior to perturbation and 3 hours after the perturbation).

Results

Effects of the plasmid copy number under optimal conditions

We imaged cells with the SCR and LCR at 30 °C, the temperature at which the LCR exhibits shorter period and higher functionality and robustness,[3] due to, among others, the temperature dependence of CI[3,21–23] (see results in Table 1). It is noted that in both cases, cells grow at a relatively slow rate under the microscope (division time of ~60 min). Thus, it is reasonable to assume that, in the case of SCR cells, most of the time only one copy of the repressilator is present in the cells. Nevertheless, in all cases, the SCR cells contain significantly fewer copies of repressilators than the LCR cells (see below).

From these data, we assessed if the dynamics of the LCR and SCR differed significantly by performing a Kolmogorov–Smirnov (K–S) test of statistical significance to determine whether the two sets of time lengths of oscillations could be obtained from equal distributions. We obtained a *p*-value of 0.006, from which we concluded that the dynamics of the circuits differs statistically (typically, the null hypothesis is rejected at a significance level of 0.01). From this difference, and since the repressilator circuits in the SCR and LCR implementation do not differ, it is possible to conclude that more than one copy of the 3–4 copies[4] of the LCR present in each cell is active.

Interestingly, this difference in the period distributions (particularly the higher variance) is not reflected in the robustness of the oscillations of the SCR, which does not differ from the robustness of the LCR. Also, the SCR exhibits higher functionality at 30 °C than the LCR (similar values to those previously reported in ref. 2). Finally, the period of the SCR is longer and noisier (higher CV^2).

Table 1 Kinetics of the LCR and the SCR at 30 °C. The table shows the fraction of functional cells (*F*), the number of cells exhibiting oscillations, the fraction of robust oscillations in functional cells (*R*), the mean (*m*) and standard deviation (*s*) of the period, and the squared coefficient of variation (CV^2) of the period in functional cells

Copy no.	*F* (%)	No. of oscillating cells	*R* (%)	*m* (min)	*s* (min)	CV^2
LCR	42	37	100	251	89	0.126
SCR	48	59	100	313	122	0.152

Table 2 Kinetics of the LCR and the SCR at various temperatures. The temperature (*T*), the fraction of functional cells (*F*), the number of cells exhibiting oscillations, the fraction of robust oscillations (*R*), the mean (*m*) and standard deviation (*s*) of the period are shown

Copy no.	*T* (°C)	*F* (%)	No. of oscillating cells	*R* (%)	*m* (min)	*s* (min)
LCR	28	30	41	100	393	40
LCR	30	42	37	100	251	89
LCR	33	35	38	43	275	100
LCR	37	30	38	34	291	111
SCR	28	32	46	100	342	124
SCR	30	48	59	100	313	122
SCR	33	24	84	39	364	161
SCR	37	21	49	31	404	145

Dynamics at different temperatures

Next, we measured the behaviour of the LCR and of the SCR at 28 °C, 30 °C, 33 °C, and 37 °C (Table 2). We also conducted measurements at lower and higher temperatures than these, but the number of functional repressilators was negligible. We limited the measurement period to 10 h, as cells tend to enter the stationary phase at this stage, halting the repressilator.[2,3]

From the images, for each condition, we extracted the fraction of functional cells (*F*), the number of cells exhibiting the oscillatory fluorescent signal, the robustness (*R*) of the oscillations in 'functional' cells, and the mean and standard deviation of the period (*m* and *s*). The results are shown in Table 2.

In Table 3, we show the results from K–S tests of statistical significance to determine whether the distributions of periods from the LCR and the SCR could be obtained from equal distributions, at each temperature. This table indicates that the two circuits exhibit different dynamics at all temperatures. Nevertheless, Table 2 indicates that both circuits respond similarly (but not identically) to temperature changes, in the range tested. Specifically, one similarity is that in both circuits

Table 3 *p*-values of the K–S test between distributions of periods from different copy number plasmids. For *p*-values < 0.01, the null hypothesis that the two distributions are equal is rejected

T (°C)	28	30	33	37
p-value	5.02×10^{-4}	0.006	0.36×10^{-4}	7.04×10^{-7}

Table 4 p-values of the Kolmogorov–Smirnov test between distributions of the LCR and SCR periods from different temperatures. For p-values < 0.01, the null hypothesis that the two distributions are equal is rejected

Copy no.	28 °C *vs.* 30 °C	30 °C *vs.* 33 °C	33 °C *vs.* 37 °C
LCR	3.09×10^{-14}	0.13	0.33
SCR	0.44	6.70×10^{-5}	0.30

the mean period is minimized at 30 °C. Another is that the robustness of both circuits is hampered at temperatures beyond 30 °C, due to the loss of effectiveness of CI as a repressor.[21–23] Finally, in both systems, the functionality is maximized at 30 °C.

On the other hand, as indicated in Table 2, one main difference in how the two circuits respond to temperature changes is that the functionality of the SCR has a steeper decrease with increasing temperature. This causes the SCR's functionality to be lowered at higher temperatures (33 °C and 37 °C). The other significant difference is in how the oscillations change with temperature. While in the LCR the steepest change in the mean period length occurs when raising the temperature from 28 °C to 30 °C (decrease of 142 min), in the SCR it occurs when raising the temperature from 30 °C to 33 °C (increase by 51 min). We verified this by K–S tests of statistical significance to determine whether the sets of oscillation lengths at different temperatures could be obtained from equal distributions, for both the LCR and the SCR (Table 4). From these, one observes a p-value smaller than 0.01 in the LCR only when comparing data from 28 °C and 30 °C, while in the SCR such observation only occurs when comparing data from 30 °C and 33 °C, in agreement with the observed changes in the oscillations' mean time length with temperature.

Perturbing the functioning by IPTG induction

One important property of genetic clocks is their robustness and/or responsiveness to external perturbations. In natural systems, depending on the tasks that they are involved in, it is expected that the genetic clocks have evolved specific robustness and/or responsiveness to perturbations. *E.g.*, some clocks likely evolved robustness to weak, spurious perturbations but responsiveness to strong perturbations (such as due to an environmental shift). For similar reasons, these properties are also important in the case of synthetic circuits, as they will define their applicability.

We compared the robustness of the LCR and the SCR to a 'weak' perturbation, by addition of a small amount of IPTG to the medium. Also, we compared the robustness of the SCR to a 'weak' and to a 'strong' perturbation. For this, after starting measurements as before, we introduced IPTG into the medium at the end of the third hour of the measurements, as this is approximately the time length of one oscillation (see the Methods section). The expected effect of this permanent perturbation is the continuous induction of the P_L lacO1 promoter (*i.e.* up-regulation of *TetR*) in the repressilator. Consequently, P_L tetO1 ought to become permanently repressed. Since this promoter also drives the reporter, the reporter signal should become negligible, following the perturbation, if the perturbation succeeds in disrupting the oscillations.

First, we compared the effects of perturbation (50 μM of IPTG) on the dynamics of the LCR with of the SCR. For that, we assessed the functionality (see the Methods section) in the first 3 hours prior to perturbation and in the subsequent 3 hours after the perturbation. We found that the functionality of cells with the LCR equalled 93.3% in the first 3 hours, and 1.64% in the subsequent 3 hours (61 cells imaged) (*i.e.* 98% of the cells were perturbed). Meanwhile, the functionality of cells containing the SCR equalled 100.0% in the first 3 hours, and 8.96% in the subsequent 3 hours (145 cells imaged) (*i.e.* 91% of the cells were perturbed). Thus, surprisingly, we conclude that the LCR is less robust to this perturbation than the SCR. As a side note, the reason why the functionality values are much higher than those shown in Table 2 is the shorter duration of the present measurements and the criteria of the functionality (see the Methods section).

Next, we compared the effects of a 'strong' *versus* a 'weak' perturbation in cells containing the SCR (by adding 1 mM or 50 μM of IPTG to the medium, respectively), at the end of the third hour of the measurements (112 cells imaged). We measured a functionality of 100.0% in the first 3 hours as before, but only 0.89% in the later 3 hours (99.1% of the cells were perturbed). We conclude that, as predicted in simulations of models of this and similar circuits,[6,11] the robustness of the SCR's functionality to external perturbations decreases with the strength of the perturbation, in this case defined by the concentration of IPTG in the medium.

Assessing the robustness to perturbations

Given that the LCR and the SCR exhibit different dynamics at any of the temperatures tested, we concluded that more than one repressilator circuit is active in cells with the LCR. Also, it is reasonable to assume that, following the introduction of IPTG into themedia with LCR cells, in each cell, it is always equally or more likely that at least one circuit is affected by IPTG than all of its circuits. Finally, it is reasonable to assume that for the same perturbation, it is more likely that at least one circuit is perturbed in cells with the LCR than in cells with the SCR, due to the larger number of circuits.

Given the above and the observation that cells with the LCR exhibit weaker robustness to the external perturbations than cells with the SCR, it is possible to conclude that, in cells with the LCR, not all copies of the repressilator need to be perturbed in order to disrupt the periodic signal. This is expected, given that all circuits of the LCR are necessarily dynamically coupled in a cell (as demonstrated by the existence of a periodic signal prior to perturbation), since they produce and are affected by identical proteins, which are equally available to interact with any of the circuits.

To exemplify this, we implemented stochastic models of the SCR and the LCR (based on a model proposed by Zhu *et al.*[11]). The methods are described in the ESI.† We simulated the two models for each of the 1000 instances (cells) and extracted the functionality of each cell prior to and after perturbation. In the model with three repressilator copies the functionality is

reduced from 81.7% to 1.09% as a result of the perturbation, while in the model of the SCR the corresponding numbers are 96.3% and 9.60%. The functionalities do not differ significantly from the measurements in either case (p-values larger than 0.01), as determined by a set of Fisher's exact tests. Meanwhile, the LCR and SCR models differ significantly (p-values are 5.2×10^{-27} and 6.5×10^{-19} for before and after perturbation, respectively).

Conclusions and discussion

We inserted the genetic repressilator of Elowitz and Leibler[2] into a single-copy F-plasmid to obtain, to our knowledge, the first functional, synthetic, single-copy, ring-type genetic clock.

The SCR was found to exhibit stronger fluctuations (the lower copy number is expected to decrease the rhythmicity of the coupled system[24]) and longer mean periods and, as such, to differ in dynamics from the LCR. Regardless, the signal of the SCR is stable enough so as to maintain its main feature, periodicity. Interestingly, this difference in dynamics is a demonstration that the stability of the signal of the original LCR relies, to some extent, on the existence of more than one functional copy of the repressilator in each cell. In addition, as these multiple copies exhibit a periodic signal, one can conclude that they are dynamically coupled (as expected, given the indistinguishability between the proteins they produce and are regulated by).

On the other hand, the response of the two systems to temperature changes is similar. In both circuits, the mean period is minimized and the functionality is maximized at 30 °C. Also, both systems lose robustness at temperatures above 30 °C. These behaviours have been explained in a previous study.[3]

There are only two differences in their response to temperature changes. First, the functionality appears to have a more rapid decrease with increasing temperature in the SCR. Second, the most temperature-sensitive regions of the two systems differ (between 28 °C *vs.* 30 °C in the LCR and between 30 °C *vs.* 33 °C in the SCR). At present, we do not have sufficient information to further investigate the causes of these two differences between the SCR and the LCR, particularly since it is presently unknown which underlying parameters regulate the functionality. Our study suggests that the number of functional circuits in a cell is likely one of these parameters.

Finally, we studied the effects of external perturbations on the robustness of the repressilator as a function of the copy numbers and the perturbation strength. First, we observed that the LCR is less robust to a constant perturbation (50 μM of IPTG in the medium) than the SCR, which shows that not all copies of a repressilator in a cell have to be perturbed in order to disrupt the periodic signal. This result was exemplified using a model, which assumed perfect coupling within a cell and no differences in the promoter strength of the two circuits. Consequently, we find it reasonable to hypothesize that the measured differences between the dynamics of the LCR and the SCR are solely due to the differences in copy-numbers.

From the perturbation studies, we also observed that the SCR is sensitive to the strength of the perturbation, which is particularly relevant in that it increases the number of possible future applications for this circuit.

Overall, we find that the differences in robustness to external perturbations as well as the differences in the dynamics of the two circuits reported here justify the need for a version of the synthetic repressilator implemented on a single-copy plasmid. In particular, its higher robustness to external perturbations and higher functionality at lower temperatures allow the SCR to be more useful than the LCR under certain conditions (*i.e.* by being a more robust clock). This is important for future efforts of synthetic biology aiming to engineer artificial genetic circuits whose proper functioning requires robust time tracking.

Finally, our study also provides much needed empirical data for developing more accurate models of coupled genetic circuits which, so far, have relied on arbitrary parameter values (see *e.g.* ref. 5, 6, 25 and 26). In this regard, the observed fluctuations in the length of the oscillations strongly supports the need to use detailed stochastic modelling strategies[27,28] to accurately mimic the behaviour of the circuits.

Acknowledgements

This work is supported by Academy of Finland [126803 to A.S.R.], Fundacao para a Ciencia e a Tecnologia [PTDC/BBB-MET/1084/2012 A.S.R.], and Jenny and Antti Wihuri Foundation [A.H.]. We thank the Helsinki Bio-center for sequencing services. The funders had no role in study design, data collection and analysis, decision to publish, or preparation of the manuscript.

Notes and references

1 M. D. Wolf and A. P. Arkin, *Curr. Opin. Microbiol.*, 2003, **6**, 125–134.
2 M. Elowitz and S. Leibler, *Nature*, 2000, **403**, 335–338.
3 J. G. Chandraseelan, S. M. D. Oliveira, A. Häkkinen, H. Tran, I. Potapov, A. Sala, M. Kandhavelu and A. S. Ribeiro, *Mol. BioSyst.*, 2013, **9**, 3117–3123.
4 R. Lutz and H. Bujard, *Nucleic Acids Res.*, 1997, **25**(6), 1203–1210.
5 A. Ribeiro, *Phys. Rev. E: Stat., Nonlinear, Soft Matter Phys.*, 2007, **75**, 061903.
6 A. Ribeiro and S. A. Kauffman, *J. Theor. Biol.*, 2007, **247**, 743–755.
7 J. A. Klappenbach, J. M. Dunbar and T. M. Schmidt, *Appl. Environ. Microbiol.*, 2000, **66**, 1328–1333.
8 B. S. Stevenson and T. M. Schmidt, *Appl. Environ. Microbiol.*, 2004, **70**, 6670–6677.
9 M. Lynch and J. S. Conery, *Science*, 2000, **290**, 1151–1155.
10 Y. Mileyko, R. I. Joh and J. S. Weitz, *Proc. Natl. Acad. Sci. U. S. A.*, 2008, **105**(43), 16659–16664.
11 R. Zhu, A. S. Ribeiro, D. Salahub and S. A. Kauffman, *J. Theor. Biol.*, 2007, **246**, 725–745.

12 A. S. Ribeiro, *Phys. Rev. E: Stat., Nonlinear, Soft Matter Phys.*, 2007, **75**(6), 061903.
13 A. S. Ribeiro, *Phys. Rev. E: Stat., Nonlinear, Soft Matter Phys.*, 2007, **76**(5), 051915.
14 G. Gordon, D. Sitnikov, C. Webb, A. Teleman, A. Straight, R. Losick, A. Murray and A. Wright, *Cell*, 1997, **90**, 1113–1121.
15 T. Ogura and S. Hiraga, *Proc. Natl. Acad. Sci. U. S. A.*, 1983, **80**, 4784–4788.
16 D. Bray, *Nature*, 1995, **376**, 307–312.
17 V. Dinçbaş, A. Hortaçsu and A. Çamurdan, *Biotechnol. Prog.*, 1993, **9**, 218–220.
18 M. Smith and M. Bidochka, *Can. J. Microbiol.*, 1998, **44**, 351–355.
19 X. Chen, Z. Xu, P. Cen and W. Wong, *Biochem. Eng. J.*, 2006, **28**, 215–219.
20 A. P. Dempster, N. Laird and D. B. Rubin, *J. R. Stat. Soc.*, 1977, **39**, 1–38.
21 N. K. Jana, S. Roy, B. Bhattacharyya and N. C. Mandal, *Protein Eng.*, 1999, **12**, 225–233.
22 K. S. Koblan and G. K. Ackers, *Biochemistry*, 1991, **30**, 7817–7821.
23 K. S. Koblan and G. K. Ackers, *Biochemistry*, 1991, **30**, 7822–7827.
24 J. Garcia-Ojalvo, M. B. Elowitz and S. H. Strogatz, *Proc. Natl. Acad. Sci. U. S. A.*, 2004, **101**, 10955–10960.
25 A. Goldbeter and O. Pourquié, *J. Theor. Biol.*, 2008, **252**, 574–585.
26 D. Gonze, *BioSystems*, 2010, **99**, 60–69.
27 H. H. McAdams and A. Arkin, *Proc. Natl. Acad. Sci. U. S. A.*, 1997, **94**, 814–819.
28 A. S. Ribeiro, R. Zhu and S. A. Kauffman, *J. Comput. Biol.*, 2006, **13**, 1630–1639.

Electronic Supplementary Material (ESI) for Molecular Biosystems.
This journal is © The Royal Society of Chemistry 2014

Electronic supplementary information

Single-cell kinetics of the Repressilator when inserted into a single-copy plasmid

Samuel M.D. Oliveira[a,*], Jerome G. Chandraseelan[a,*], Antti Häkkinen[a], Nadia S.M. Goncalves[a], Olli Yli-Harja[b], Sofia Startceva[a], and Andre S. Ribeiro[a,+]

[a]Laboratory of Biosystem Dynamics, Tampere University of Technology, P.O. Box 553, 33101 Tampere, Finland
[b]Computational Systems Biology Research Group, Department of Signal Processing, Tampere University of Technology, P.O. Box 553, 33101 Tampere, Finland.

*** Equal contributions**

+ Corresponding author
Andre S. Ribeiro
Tampere University of Technology,
P.O. Box 553, 33101 Tampere, Finland
E-mail: andre.ribeiro@tut.fi.
Tel: +358408490736

Supplementary Methods

Media and chemicals

We used Lysogeny Broth (LB) and minimal nutrient (M63) media with the following components (i) and (ii), respectively: (i) 10g/L of Tryptone (Sigma Aldrich, USA), 5g/L of yeast extract (LabM, UK) and 10g/L of NaCl (LabM, UK); (ii) 2 mM $MgSO_4.7H_2O$ (Sigma-Aldrich, USA), 7.6 mM $(NH_4)_2SO_4$ (Sigma Life Science, USA), 30 µM $FeSO_4 \cdot 7H_2O$ (Sigma Life Science, USA), 1 mM EDTA (Sigma Life Science, USA), 60 mM KH_2PO_4 (Sigma Life Science, USA) pH 6.8 with Glycerol 0.5% (Sigma Life Science, USA) and Casaminoacids 0.1% (Fluka Analytical, USA).

Isopropyl β-D-1-thiogalactopyranoside (IPTG) was used for studying the effects of external perturbations on the Repressilator. All antibiotics used for SCR and LCR strain culturing were purchased from Sigma-Aldrich (USA): (i) 35 mg/mL kanamycin and 35 mg/mL chloramphenicol; (ii) 35 mg/mL kanamycin and 20 µg/mL Ampicillin. Agarose (Sigma Life Science, USA) was used for the microscopic slide gel preparation.

Bacterial strains and single-copy repressilator plasmid construction and validation

Cells of *E. coli lac*$^-$ strain MC 4100 with the repressilator (pZS1-lTlrLLtCL), here denoted by low-copy repressilator (LCR), and the reporter plasmid (pZE21-GFPaav) were generously provided by M. Elowitz, Princeton University, NJ, USA. Cloning and measurements were performed on this strain.

To construct the single-copy F-plasmid repressilator (SCR) system pBAC2-lTlrLLtCL, we amplified the functional repressilator cassette from the original plasmid (*de novo*

SmaI restriction sites were added to the end of the cassette during this procedure). The primers used were:

1-Rep.SmaI-Fw: 5' CCCGGGTCGAGAATTGTGAGCG 3'
2-Rep.SmaI-Rev: 5' CCCGGGTCAAGCTGCTAAAGCGTAG 3'

The vector, pTB-BAC2 F-plasmid, containing the origin of replication and Chloramphenicol resistance gene, was amplified using PCR, also amplified with *SmaI* restriction enzyme sites, using the following primers:

3-Sc.ori.Cam-SmaI-Fw: 5' CCCGGGTTCGAACGCGTATGCATGAG 3'
4-Sc.ori.Cam-SmaI-Rev: 5' CCCGGGTTAGGGCCGTCGACCAA 3'

The amplified sequences of the repressilator and pTB-BAC2 vector were digested using SmaI and then ligated. The plasmid was then transferred into *lacI*$^-$ *E. coli* MC4100 containing the reporter plasmid.

We validated the SCR construction by performing gel electrophoresis (Fig. S4, for the construction; Fig. S5 for the final product) to confirm the presence of the Repressilator circuit in the single-copy plasmid.

Sequencing the plasmid for confirmation

A fraction (covering the vector and insert) of the new plasmid was amplified using PCR, from the Chloramphenicol resistance gene in the vector to the tetR region of the Repressilator, and sequenced using appropriate primers. The primers used for the amplification were:

5-CmR-1-F: 5' CCGCTGGCGATTCAGGTTC 3'
6-tetR-3-R: 5' AGCAAAGCCCGCTTATTTTTTACATG 3'

The alignment of the sequence obtained from sequencing against the expected original Repressilator sequence[2] using NCBI BLAST (S. F. Altschul et al., J. Mol. Biol. 1990, 215: 403-410) is shown in Fig. S6B. Further, the complete sequence of the single-copy repressilator plasmid is shown in Fig. S6C.

qPCR verification of RNA expression

qPCR was used to further validate the presence of each gene in the SCR plasmid in the host cell. For that, *lacI*$^-$ *E. coli* MC 4100 cells, containing the SCR with the reporter system, were grown following the culturing protocols described in the methods section of the manuscript. After 10 hours of culturing in 5 mL liquid M63 medium at shaking 250 rpm, one sample was taken and rifampicin was immediately added to prevent further transcription. RNA protect reagent was used to fix the cells before their enzymatic lysis with Tris-EDTA lysozyme buffer (pH 8.3). The RNA was isolated from cells using RNeasy mini-kit (Qiagen) following manufacturer's instructions. Total of 1 µg of RNA was used as a starting material. To ensure purity of the RNA, the RNA samples were treated with DNase free of RNase to remove residual DNA. Next, the RNA was reverse transcribed into cDNA using iSCRIPT reverse transcription super mix (Biorad). Finally, qPCR was performed using Power SYBR-green master mix (Life Technologies) with primers for the amplification of the target and the reference genes at a concentration of 200 nM. Reactions were carried out in 20 µL triplicates with 500 nM per primer. The following primers were used for quantification:

-For *lacI* gene:
7-lacI.pro-Fw: 5' GTGGTGTCGATGGTAGAACG 3'
8-lacI.pro-Rev: 5' CTGTTGATGGGTGTCTGGTC 3'

- For *tetR* gene:
9-tetR.pro-Fw: 5' CGCTGTGGGGCATTTTAC 3'
10-tetR.pro-Rev: 5' AAGAAGGCTGGCTCTGCAC 3'

- For *cI* gene:
11-cI.pro-Fw: 5' GATGCGGAGAGATGGGTAAG 3'
12-cI.pro-Rev: 5' ACTCATCACCCCCAAGTCTG 3'

The length of the amplicons was kept at 90 bp. The sequences of the primers of the reference gene 16S rRNA (EcoCyc Accession Number: EG30090) were obtained from Thermo Scientific:

13-Fw: 5' CGTCAGCTCGTGTTGTGAA 3'
14-Rev: 5' GGACCGCTGGCAACAAAG 3'

The level of each target gene was normalized with the level of the 16S rRNA for all samples. The PCR cycling protocol used was 94 °C for 15 s, 51 °C for 30 s, and 72 °C for 30 s, up to 39 cycles. We used no-RT enzyme and no-Template as controls. The C_q values were obtained from the CFX Manager™ Software and the fold change of the genes were analysed using the Livak method (K.J. Livak, and T.D. Schmittgen, Methods, 2001, 25, 402-408).

For the SCR, we obtained the following cycle threshold (C_t) values: 18.7 (lacI), 17.3 (tetR), and 21.6 (cI). Meanwhile, in the no-Template control these numbers equalled 26.6, 33.2, and 31.4, respectively. These result in fold changes no smaller than 200, which indicates that the RNAs are being expressed in the SCR.

Stochastic model of the Repressilator and of coupled Repressilators

We implemented stochastic models of the LCR and of the SCR based on a model proposed by Zhu and others[11]. The models are implemented using the stochastic simulation algorithm, which is a Monte Carlo simulation of the stochastic chemical kinetics governed by the chemical master equation. Gene expression is modelled by the following reactions:

$$\varnothing \xrightarrow{N_i \cdot k_i} P_i \qquad k_i = \frac{a_i}{1 + \left(\frac{P_{\sigma(i)}}{H_i} \right)^{b_i}}$$

$$P_i \xrightarrow{d_i} \varnothing$$

where the first reaction represents the production of the proteins P_i (for $i = 1,2,3,4$), and the second their degradation. Here, N_i represents the copy number of the gene, k_i is the effective rate of protein production for a single gene (accounting for e.g. transcription and translation rates and the messenger RNA degradation of that gene), and d_i^{-1} is the protein lifetime. In our model P_1, P_2, P_3 and P_4 correspond to TetR, λ cI, LacI and the GFP reporter, respectively, and

the repressor indices are $\sigma(1)=3$, $\sigma(2)=1$, $\sigma(3)=2$ and $\sigma(4)=1$. The production rate k_i of each gene is modulated by the concentration of the corresponding repressor proteins. In the expression, a_i represents the maximum expression rate, b_i is the Hill coefficient, and H_i is the repressor level that results in half the repression. This model of regulation is appropriate when the repressor binding/unbinding events occur at much faster rates than gene expression.

We model the perturbation caused by the introduction of IPTG in the system at a certain point in time. In our model, IPTG allows the lac promoter to express regardless of the presence of the LacI repressors. This is modelled by the following reaction:

$$\varnothing \xrightarrow{N_1 \cdot I \cdot a_0} P_1$$

where I is a binary variable denoting the presence of IPTG and a_0 is the leak expression rate of the lac promoter when IPTG is present (i.e. when $I = 1$). This rate also accounts for the IPTG concentration, which is not modelled explicitly.

In the above model, we used copy numbers $N_i = 1$ for the SCR and $N_i = 3$ for the LCR[4]. The following parameters were used: $a_i = 1000$ min^{-1}, $b_i = 3$, $H_i = 1$, $d_i^{-1} = 10$ min and $a_0 = 3.5$ min^{-1}. The protein lifetimes were set in accordance with measurements (Taniguchi et al., Science 2010, **329**, 533-538), and a Hill coefficient of $b_i = 3$ was used, since many proteins function in a multimeric form (Xia et al., Proc. Natl. Sci. U.S.A. 2007, **104**, 17329–17334). The parameters a_i and a_0 were tuned for the model dynamics to agree with the empirical data.

We simulated the above model for a duration of 10 h, such that the system state in the measurement window is largely unaffected by the initial protein concentrations (set to $P_i = 0$) (in the measurements, a similar procedure occurs, as cells prior to imaging are cultured for ~10 hours). After this, we simulate the model for further 6 h, sampling the state every 15 min. As in the measurements, the perturbation is performed 3 h after the sampling was started. In each simulation (cell), the two 3 h series prior to and after the perturbation are analysed separately to determine the functionality using the same methods as for the measurement data. A total of 1000 instances of both the SCR and the LCR were simulated to compute the statistics.

Supplementary Figures

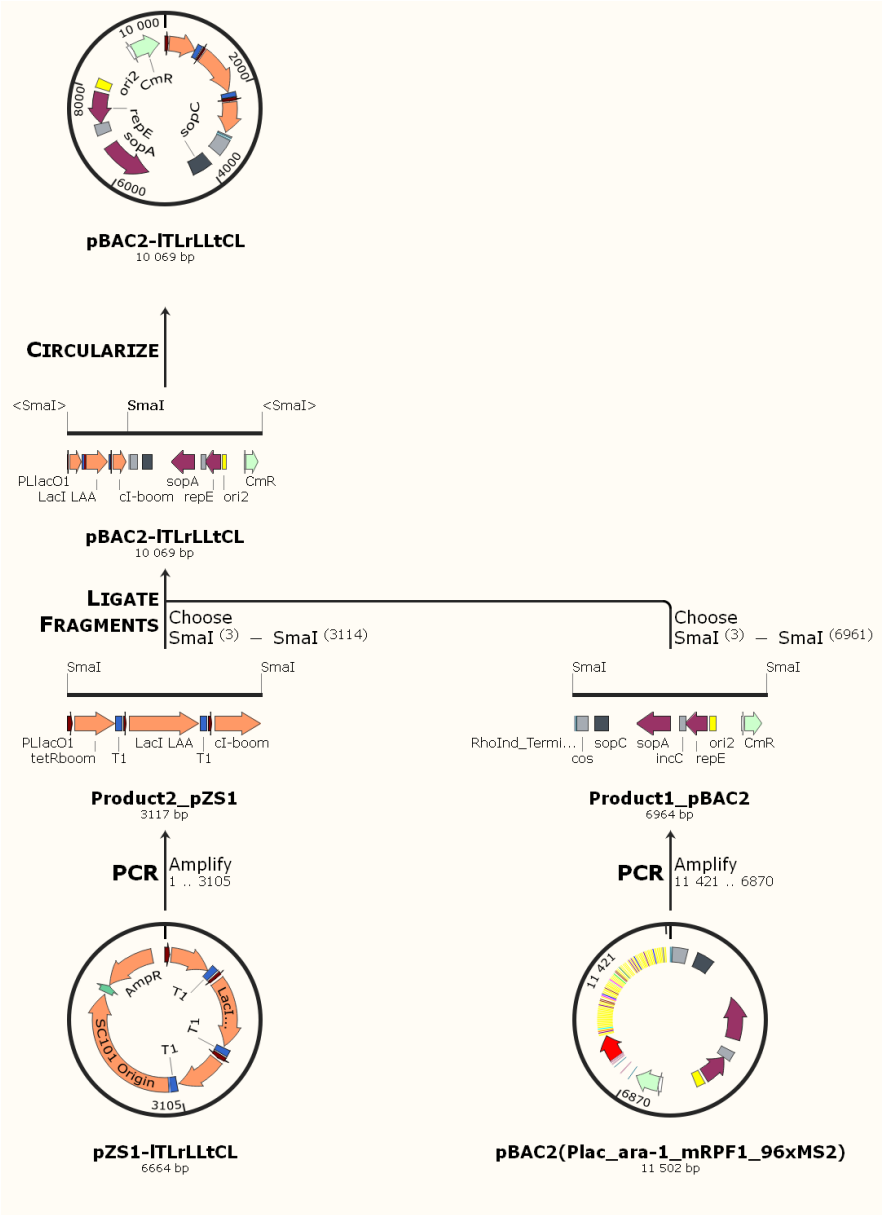

Fig. S1 Illustration of the construction of the SCR plasmid. The pBAC2-lTlrLLtCL plasmid was engineered by inserting the repressilator cassette into pBAC2 ($P_{lac/ara-1}$-mRFP1-MS2-96x) vector (generously provided by Ido Golding, University of Illinois, USA), containing the single-copy origin of replication. The construction history was generated and adapted using SnapGene® 1.5.2.

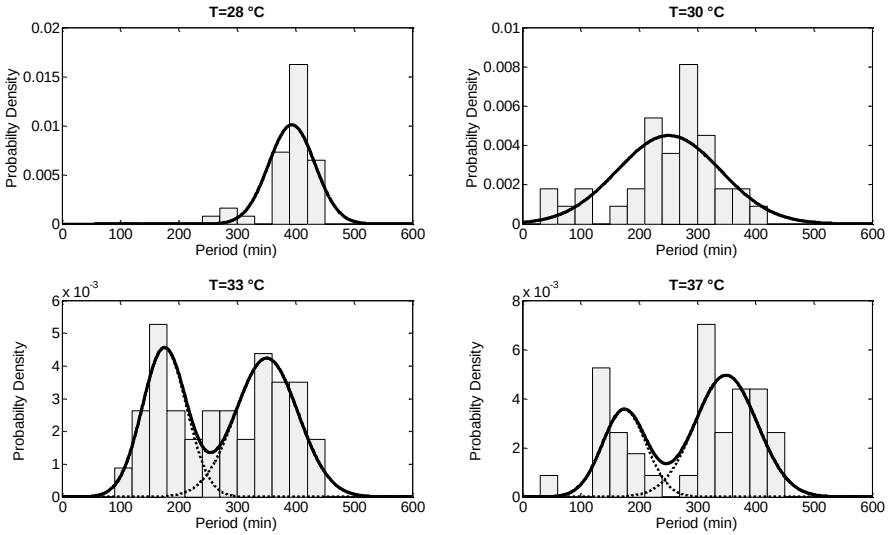

Fig. S2 LCR period distributions at different temperatures. Solid lines represent the probability densities of the fitted model with one or two Gaussians as determined by the likelihood ratio tests. Dashed lines represent the densities of the individual components in the case of two Gaussians. Magnitudes were scaled to represent a probability densities.

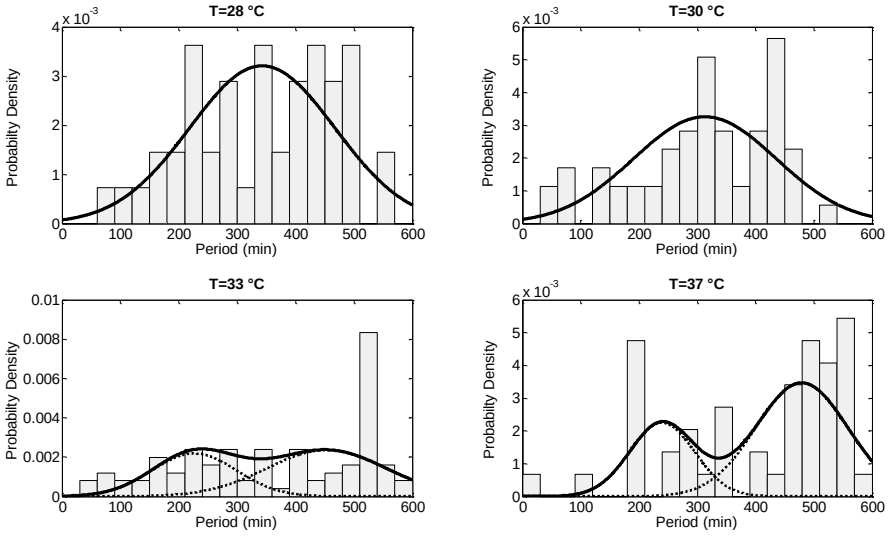

Fig. S3 SCR period distributions at different temperatures. Solid lines represent the probability densities of the fitted model with one or two Gaussians as determined by the likelihood ratio tests. Dashed lines represent the densities of the individual components

in the case of two Gaussians. Magnitudes were scaled to represent a probability densities.

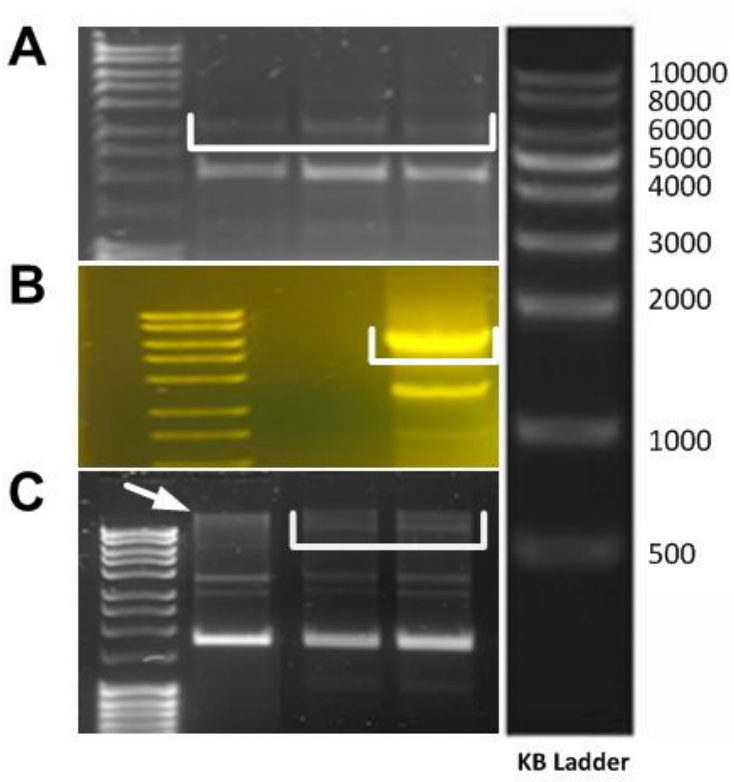

Fig. S4 Split gels for the intermediate steps of the SCR plasmid construction. (A) PCR fragment of 3114 bp amplified from the original pZS1-lTlrLLtCL with appropriate primers, in triplicate (bracket). (B) Lane containing pTB-BAC2 backbone amplified region with the single-copy origin of replication (6961 bp) (bracket). (C) Lane 1: plasmid profile of the strain containing only the reporter plasmid (white arrow). Lanes 2 and 3: two replicates of the plasmid profile of the strain with the reporter and the final construct pBAC2-lTlrLLtCL (SCR plasmid, 10069 bp) (bracket). The numbers of the DNA ladders on the left side of Figures A, B and C are shown on an identical ladder on the right side of the figure.

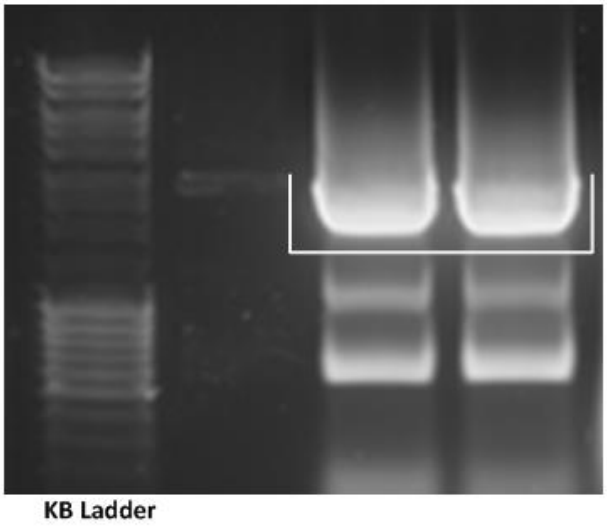

Fig. S5 Split gel of the final product of the SCR plasmid construction. Lane 1: unused. Lanes 2 and 3: PCR amplification of the Repressilator circuit (3114 bp) from the SCR plasmid, pBAC2-lTlrLLtCL, with appropriate primers (bracket). The ladder is identical to those in Fig. S4.

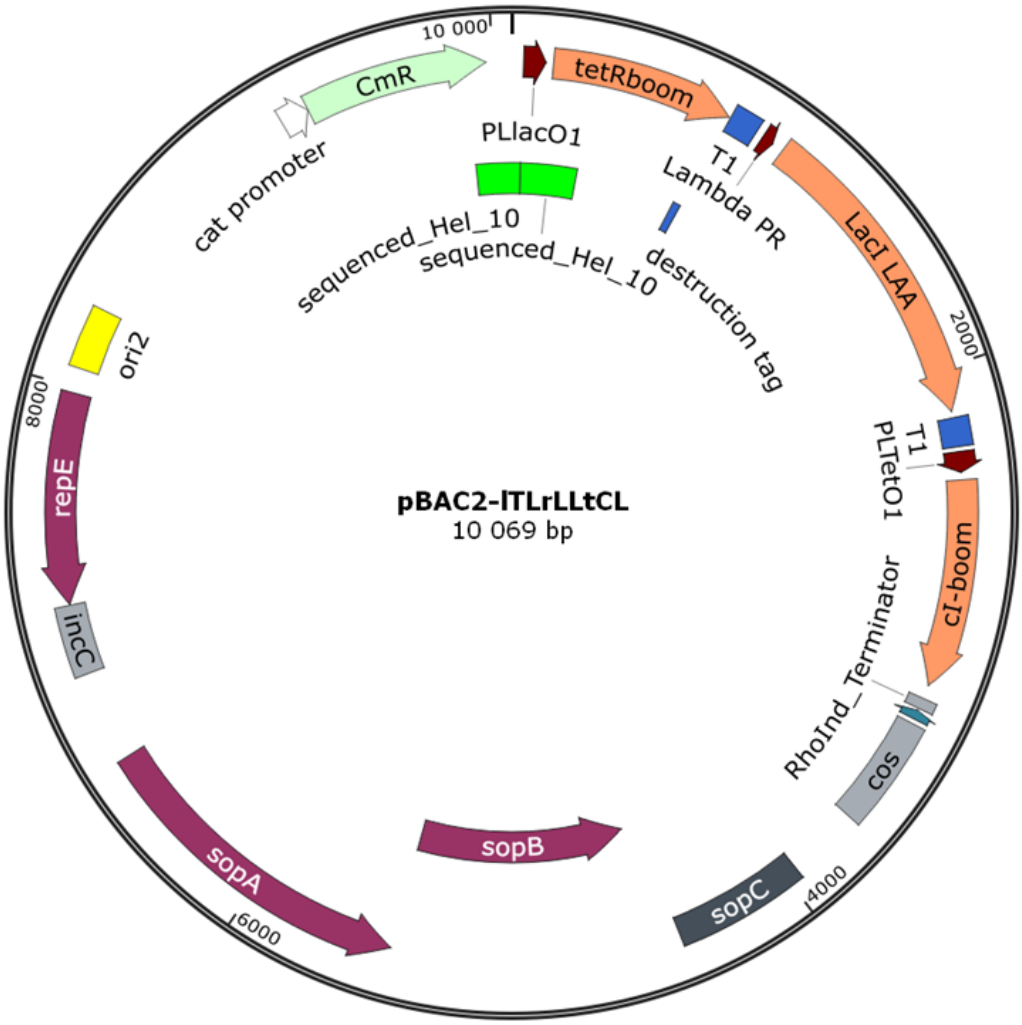

Fig. S6A. Complete map of the single-copy plasmid pBAC2-ITLrLLtCL containing the Repressilator. The green region ('sequenced_Hel_10') corresponds to the sequence in Fig. S6B.

```
Query 1125 GATGGCTTCCATGTCGGCAGAATGCTTAATGAATTACAACAGTACTGCGATGAGTGGCAG  1184
           |||||||| ||||||||||||||||||||||||||||||||||||||||||||||||||
Sbjct  4   GATGGCTT-CATGTCGGCAGAATGCTTAATGAATTACAACAGTACTGCGATGAGTGGCAG  62

Query 1185 GGCGGGGCGTAAttttttAAGGCAGTTATTGGTGCCCTTAAACGCCTGGTTGCTACGCC  1244
           ||||||||||||||||||||||||||||||||||||||||||||||||||||||||||||
Sbjct 63   GGCGGGGCGTAATTTTTTTAAGGCAGTTATTGGTGCCCTTAAACGCCTGGTTGCTACGCC  122

Query 1245 TGAATAAGTGATAATAAGCGGATGAATGGCAGAAATTCGATGATAAGCTGTCAAACATGA  1304
           ||||||||||||||||||||||||||||||||||||||||||||||||||||||||||||
Sbjct 123  TGAATAAGTGATAATAAGCGGATGAATGGCAGAAATTCGATGATAAGCTGTCAAACATGA  182

Query 1305 GAATTGGTCGACGGCCCTAACCCGGGTCGAGAATTGTGAGCGGATAACAATTGACATTGT  1364
           ||||||||||||||||||||||||||||||||||||||||||||||||||||||||||||
Sbjct 183  GAATTGGTCGACGGCCCTAACCCGGGTCGAGAATTGTGAGCGGATAACAATTGACATTGT  242

Query 1365 GAGCGGATAACAAGATACTGAGCACATCAGCAGGACGCACTGACCGAATTCATTAAAGAG  1424
           ||||||||||||||||||||||||||||||||||||||||||||||||||||||||||||
Sbjct 243  GAGCGGATAACAAGATACTGAGCACATCAGCAGGACGCACTGACCGAATTCATTAAAGAG  302

Query 1425 GAGAAAGGTACCATGTCCAGATTAGATAAAAGTAAAGTGATTAACAGCGCATTAGAGCTG  1484
           ||||||||||||||||||||||||||||||||||||||||||||||||||||||||||||
Sbjct 303  GAGAAAGGTACCATGTCCAGATTAGATAAAAGTAAAGTGATTAACAGCGCATTAGAGCTG  362

Query 1485 CTTAATGAGGTCGGAATCGAAGGTTTAACAACCCGTAAACTCGCCCAGAAGCTAGGTGTA  1544
           ||||||||||||||||||||||||||||||||||||||||||||||||||||||||||||
Sbjct 363  CTTAATGAGGTCGGAATCGAAGGTTTAACAACCCGTAAACTCGCCCAGAAGCTAGGTGTA  422

Query 1545 GAGCAGCCTACATTGTATTGGCATGTAAAAAATAAGCGGGCTTTGCT  1591
           |||||||||||||||||||||||| ||||||||||||||||||||
Sbjct 423  GAGCAGCCTACATTGTATTGGCATGTGAAAAATAAGCGGGCTTTGCT  469
```

Fig. S6B. Alignment of sequence obtained from sequencing, using the primer CmR-1-F, against the expected sequence of the original Repressilator[2]. The alignment shows that the single-copy vector is present and the Repressilator has been inserted into it.

GGGTCGAGAATTGTGAGCGGATAACAATTGACATTGTGAGCGGATAACAAGATACT
GAGCACATCAGCAGGACGCACTGACCGAATTCATTAAAGAGGAGAAAGGTACCATG
TCCAGATTAGATAAAAGTAAAGTGATTAACAGCGCATTAGAGCTGCTTAATGAGGTC
GGAATCGAAGGTTTAACAACCCGTAAACTCGCCCAGAAGCTAGGTGTAGAGCAGCC
TACATTGTATTGGCATGTAAAAAATAAGCGGGCTTTGCTCGACGCCTTAGCCATTGA
GATGTTAGATAGGCACCATACTCACTTTTGCCCTTTAGAAGGGGAAAGCTGGCAAG
ATTTTTTACGTAATAACGCTAAAAGTTTTAGATGTGCTTTACTAAGTCATCGCGATGG
AGCAAAAGTACATTTAGGTACACGGCCTACAGAAAAACAGTATGAAACTCTCGAAAA
TCAATTAGCCTTTTTATGCCAACAAGGTTTTTCACTAGAGAATGCATTATATGCACTC
AGCGCTGTGGGGCATTTTACTTTAGGTTGCGTATTGGAAGATCAAGAGCATCAAGT
CGCTAAAGAAGAAAGGGAAACACCTACTACTGATAGTATGCCGCCATTATTACGAC
AAGCTATCGAATTATTTGATCACCAAGGTGCAGAGCCAGCCTTCTTATTCGGCCTTG
AATTGATCATATGCGGATTAGAAAAACAACTTAAATGTGAAAGTGGGTCTGCAGCAA
ACGACGAAAACTACGCTTTAGCAGCTTAATCTAGAGGCATCAAATAAAACGAAAGG
CTCAGTCGAAAGACTGGGCCTTTCGTTTTATCTGTTGTTTGTCGGTGAACGCTCTCC
TGAGTAGGACAAATCCGCCGCCCTAGACCTAGCTGCAGGTCGAGGATAAATATCTA
ACACCGTGCGTGTTGACTATTTTACCTCTGGCGGTGATAATGGTTGCATGTACTAGA
ATTCATTAAAGAGGAGAAAGGTACCATATGGTGAATGTGAAACCAGTAACGTTATAC
GATGTCGCAGAGTATGCCGGTGTCTCTTATCAGACCGTTTCCCGCGTGGTGAACCA
GGCCAGCCACGTTTCTGCGAAAACGCGGGAAAAAGTGGAAGCGGCGATGGCGGA
GCTGAATTACATTCCCAACCGCGTGGCACAACAACTGGCGGGCAAACAGTCGTTGC
TGATTGGCGTTGCCACCTCCAGTCTGGCCCTGCACGCGCCGTCGCAAATTGTCGC
GGCGATTAAATCTCGCGCCGATCAACTGGGTGCCAGCGTGGTGGTGTCGATGGTA
GAACGAAGCGGCGTCGAAGCCTGTAAAGCGGCGGTGCACAATCTTCTCGCGCAAC
GCGTCAGTGGGCTGATCATTAACTATCCGCTGGATGACCAGGATGCCATTGCTGTG
GAAGCTGCCTGCACTAATGTTCCGGCGTTATTTCTTGATGTCTCTGACCAGACACC
CATCAACAGTATTATTTTCTCCCATGAAGACGGTACGCGACTGGGCGTGGAGCATC
TGGTCGCATTGGGTCACCAGCAAATCGCGCTGTTAGCGGGCCCATTAAGTTCTGTC
TCGGCGCGTCTGCGTCTGGCTGGCTGGCATAAATATCTCACTCGCAATCAAATTCA
GCCGATAGCGGAACGGGAAGGCGACTGGAGTGCCATGTCCGGTTTTCAACAAACC
ATGCAAATGCTGAATGAGGGCATCGTTCCCACTGCGATGCTGGTTGCCAACGATCA
GATGGCGCTGGGCGCAATGCGCGCCATTACCGAGTCCGGGCTGCGCGTTGGTGC
GGATATCTCGGTAGTGGGATACGACGATACCGAAGACAGCTCATGTTATATCCCGC
CGTTAACCACCATCAAACAGGATTTTCGCCTGCTGGGGCAAACCAGCGTGGACCG
CTTGCTGCAACTCTCTCAGGGCCAGGCGGTGAAGGGCAATCAGCTGTTGCCCGTC
TCACTGGTGAAAAGAAAAACCACCCTGGCGCCCAATACGCAAACCGCCTCTCCCCG
CGCGTTGGCCGATTCATTAATGCAGCTGGCACGACAGGTTTCCCGACTGGAAAGC
GGGCAGGCAGCAAACGACGAAAACTACGCTTTAGCAGCTTAAAAGCTTAATTAGCT
GAGTCTAGAGGCATCAAATAAAACGAAAGGCTCAGTCGAAAGACTGGGCCTTTCGT
TTTATCTGTTGTTTGTCGGTGAACGCTCTCCTGAGTAGGACAAATCCGCCGCCCTA
GACCTAGCTGCAGGTCGAGTCCCTATCAGTGATAGAGATTGACATCCCTATCAGTG
ATAGAGATACTGAGCACATCAGCAGGACGCACTGACCGAATTCATTAAAGAGGAGA
AAGGTACCATGAGCACAAAAAAGAAACCATTAACACAAGAGCAGCTTGAGGACGCA
CGTCGCCTTAAAGCAATTTATGAAAAAAAGAAAAATGAACTTGGCTTATCCCAGGAA
TCTGTCGCAGACAAGATGGGGATGGGGCAGTCAGGCGTTGGTGCTTTATTTAATGG
CATCAATGCATTAAATGCTTATAACGCCGCATTGCTTGCAAAAATTCTCAAAGTTAG
CGTTGAAGAATTTAGCCCTTCAATCGCCAGAGAAATCTACGAGATGTATGAAGCGG
TTAGTATGCAGCCGTCACTTAGAAGTGAGTATGAGTACCCTGTTTTTTCTCATGTTC
AGGCAGGGATGTTCTCACCTGAGCTTAGAACCTTTACCAAAGGTGATGCGGAGAGA

TGGGTAAGCACAACCAAAAAAGCCAGTGATTCTGCATTCTGGCTTGAGGTTGAAGG
TAATTCCATGACCGCACCAACAGGCTCCAAGCCAAGCTTTCCTGACGGAATGTTAA
TTCTCGTTGACCCTGAGCAGGCTGTTGAGCCAGGTGATTTCTGCATAGCCAGACTT
GGGGGTGATGAGTTTACCTTCAAGAAACTGATCAGGGATAGCGGTCAGGTGTTTTT
ACAACCACTAAACCCACAGTACCCAATGATCCCATGCAATGAGAGTTGTTCCGTTGT
GGGGAAAGTTATCGCTAGTCAGTGGCCTGAAGAGACGTTTGGCGCAGCAAACGAC
GAAAACTACGCTTTAGCAGCTTGACCCGGGTTCGAACGCGTATGCATGAGCTCTTA
ATTAACTCCGGATCTAGAGCCCGCCTAATGAGCGGGCTTTTTTTTCTTAAGGCCGC
ATCGAATATAACTTCGTATAATGTATGCTATACGAAGTTATTAGCGATGAGCTCGGA
CTTCCATTGTTCATTCCACGGACAAAAACAGAGAAAGGAAACGACAGAGGCCAAAA
AGCTCGCTTTCAGCACCTGTCGTTTCCTTTCTTTTCAGAGGGTATTTTAAATAAAAAC
ATTAAGTTATGACGAAGAAGAACGGAAACGCCTTAAACCGGAAAATTTTCATAAATA
GCGAAAACCCGCGAGGTCGCCGCCCCGTAACCTGTCGGATCACCGGAAAGGACC
CGTAAAGTGATAATGATTATCATCTACATATCACAACGTGCGTGGAGGCCATCAAAC
CACGTCAAATAATCAATTATGACGCAGGTATCGTATTAATTGATCTGCATCAACTTAA
CGTAAAAACAACTTCAGACAATACAAATCAGCGACACTGAATACGGGGCAACCTCA
TGTCCGAGCTCGCGAGCTCGTCGACAGCGACACACTTGCATCGGATGCAGCCCGG
TTAACGTGCCGGCACGGCCTGGGTAACCAGGTATTTTGTCCACATAACCGTGCGCA
AAATGTTGTGGATAAGCAGGACACAGCAGCAATCCACAGCAGGCATACAACCGCAC
ACCGAGGTTACTCCGTTCTACAGGTTACGACGACATGTCAATACTTGCCCTTGACA
GGCATTGATGGAATCGTAGTCTCACGCTGATAGTCTGATCGACAATACAAGTGGGA
CCGTGGTCCCAGACCGATAATCAGACCGACAACACGAGTGGGATCGTGGTCCCAG
ACTAATAATCAGACCGACGATACGAGTGGGACCGTGGTCCCAGACTAATAATCAGA
CCGACGATACGAGTGGGACCGTGGTTCCAGACTAATAATCAGACCGACGATACGA
GTGGGACCGTGGTCCCAGACTAATAATCAGACCGACGATACGAGTGGGACCATGG
TCCCAGACTAATAATCAGACCGACGATACGAGTGGGACCGTGGTCCCAGTCTGATT
ATCAGACCGACGATACGAGTGGGACCGTGGTCCCAGACTAATAATCAGACCGACG
ATACGAGTGGGACCGTGGTCCCAGACTAATAATCAGACCGACGATACGAGTGGGA
CCGTGGTCCCAGTCTGATTATCAGACCGACGATACAAGTGGAACAGTGGGCCCAG
AGAGAATATTCAGGCCAGTTATGCTTTCTGGCCTGTAACAAAGGACATTAAGTAAAG
ACAGATAAACGTAGACTAAAACGTGGTCGCATCAGGGTGCTGGCTTTTCAAGTTCC
TTAAGAATGGCCTCAATTTTCTCTATACACTCAGTTGGAACACGAGACCTGTCCAGG
TTAAGCACCATTTTATCGCCCTTATACAATACTGTCGCTCCAGGAGCAAACTGATGT
CGTGAGCTTAAACTAGTTCTTGATGCAGATGACGTTTTAAGCACAGAAGTTAAAAGA
GTGATAACTTCTTCAGCTTCAAATATCACCCCAGCTTTTTTCTGCTCATGAAGGTTAG
ATGCCTGCTGCTTAAGTAATTCCTCTTTATCTGTAAAGGCTTTTTGAAGTGCATCACC
TGACCGGGCAGATAGTTCACCGGGGTGAGAAAAAAGAGCAACAACTGATTTAGGCA
ATTTGGCGGTGTTGATACAGCGGGTAATAATCTTACGTGAAATATTTTCCGCATCAG
CCAGCGCAGAAATATTTCCAGCAAATTCATTCTGCAATCGGCTTGCATAACGCTGAC
CACGTTCATAAGCACTTGTTGGGCGATAATCGTTACCCAATCTGGATAATGCAGCCA
TCTGCTCATCATCCAGCTCGCCAACCAGAACACGATAATCACTTTCGGTAAGTGCA
GCAGCTTTACGACGGCGACTCCCATCGGCAATTTCTATGACACCAGATACTCTTCG
ACCGAACGCCGGTGTCTGTTGACCAGTCAGTAGAAAAGAAGGGATGAGATCATCCA
GTGCGTCCTCAGTAAGCAGCTCCTGGTCACGTTCATTACCTGACCATACCCGAGAG
GTCTTCTCAACACTATCACCCCGGAGCACTTCAAGAGTAAACTTCACATCCCGACCA
CATACAGGCAAAGTAATGGCATTACCGCGAGCCATTACTCCTACGCGCGCAATTAA
CGAATCCACCATCGGGGCAGCTGGTGTCGATAACGAAGTATCTTCAACCGGTTGAG
TATTGAGCGTATGTTTTGGAATAACAGGCGCACGCTTCATTATCTAATCTCCCAGCG
TGGTTTAATCAGACGATCGAAAATTTCATTGCAGACAGGTTCCCAAATAGAAAGAGC
ATTTCTCCAGGCACCAGTTGAAGAGCGTTGATCAATGGCCTGTTCAAAAACAGTTCT

CATCCGGATCTGACCTTTACCAACTTCATCCGTTTCACGTACAACATTTTTTAGAACC
ATGCTTCCCCAGGCATCCCGAATTTGCTCCTCCATCCACGGGGACTGAGAGCCATT
ACTATTGCTGTATTTGGTAAGCAAAATACGTACATCAGGCTCGAACCCTTTAAGATC
AACGTTCTTGAGCAGATCACGAAGCATATCGAAAAACTGCAATGCGGAGGTGTAGT
CAAACAACTCAGCAGGCGTGGGAACAATCAGCACATCAGCAGCACATACGACATTA
ATCGTGCCGATACCCAGGTTAGGCGCGCTGTCAATAACTATGACATCATAGTCATG
AGCAACAGTTTCAATGGCCAGTCGGAGCATCAGGTGTGGATCGGTGGGCAGTTTA
CCTTCATCAAATTTGCCCATTAACTCAGTTTCAATACGGTGCAGAGCCAGACAGGAA
GGAATAATGTCAAGCCCCGGCCAGCAAGTGGGCTTTATTGCATAAGTGACATCGTC
CTTTTCCCCAAGATAGAAAGGCAGGAGAGTGTCTTCTGCATGAATATGAAGATCTG
GTACCCATCCGTGATACATTGAGGCTGTTCCCTGGGGGTCGTTACCTTCCACGAGC
AAAACACGTAGCCCCTTCAGAGCCAGATCCTGAGCAAGATGAACAGAAACTGAGGT
TTTGTAAACGCCACCTTTATGGGCAGCAACCCCGATCACCGGTGGAAATACGTCTT
CAGCACGTCGCAATCGCGTACCAAACACATCACGCATATGATTAATTTGTTCAATCG
TATAACCAACACGTTGCTCAACCCGTCCTCGAATTTCCATATCCGGGTGCGGTAGT
CGCCCTGCTTTCTCGGCATCTCTGATAGCCTGAGAAGAAACCCCAACTAAATCCGC
TGCTTCACCTATTCTCCAGCGCCGGGTTATTTTCCTCGCTTCCGGGCTGTCATCATT
AAACTGTGCAATGGCGATAGCCTTCGTCATTTCATGACCAGCGTTTATGCACTGGTT
AAGTGTTTCCATGAGTTTCATTCTGAACATCCTTTAATCATTGCTTTGCGTTTTTTTAT
TAAATCTTGCAATTTACTGCAAAGCAACAACAAAATCGCAAAGTCATCAAAAAACCG
CAAAGTTGTTTAAAATAAGAGCAACACTACAAAAGGAGATAAGAAGAGCACATACCT
CAGTCACTTATTATCACTAGCGCTCGCCGCAGCCGTGTAACCGAGCATAGCGAGCG
AACTGGCGAGGAAGCAAAGAAGAACTGTTCTGTCAGATAGCTCTTACGCTCAGCGC
AAGAAGAAATATCCACCGTGGGAAAAACTCCAGGTAGAGGTACACACGCGGATAGC
CAATTCAGAGTAATAAACTGTGATAATCAACCCTCATCAATGATGACGAACTAACCC
CCGATATCAGGTCACATGACGAAGGGAAAGAGAAGGAAATCAACTGTGACAAACTG
CCCTCAAATTTGGCTTCCTTAAAAATTACAGTTCAAAAAGTATGAGAAAATCCATGCA
GGCTGAAGGAAACAGCAAAACTGTGACAAATTACCCTCAGTAGGTCAGAACAAATG
TGACGAACCACCCTCAAATCTGTGACAGATAACCCTCAGACTATCCTGTCGTCATG
GAAGTGATATCGCGGAAGGAAAATACGATATGAGTCGTCTGGCGGCCTTTCTTTTT
CTCAATGTATGAGAGGCGCATTGGAGTTCTGCTGTTGATCTCATTAACACAGACTTG
CAGGAAGCGGCGGCGGAAGTCAGGCATACGCTGGTAACTTTGAGGCAGCTGGTAA
CGCTCTATGATCCAGTCGATTTTCAGAGAGACGATGCCTGAGCCATCCGGCTTACG
ATACTGACACAGGGATTCGTATAAACGCATGGCATACGGATTGGTGATTTCTTTTGT
TTCACTAAGCCGAAACTGCGTAAACCGGTTCTGTAACCCGATAAAGAAGGGAATGA
GATATGGGTTGATATGTACACTGTAAAGCCCTCTGGATGGACTGTGCGCACGTTTG
ATAAACCAAGGAAAAGATTCATAGCCTTTTTCATCGCCGGCATCCTCTTCAGGGCGA
TAAAAAACCACTTCCTTCCCCGCGAAACTCTTCAATGCCTGCCGTATATCCTTACTG
GCTTCCGCAGAGGTCAATCCGAATATTTCAGCATATTTAGCAACATGGATCTCGCAG
ATACCGTCATGTTCCTGTAGGGTGCCATCAGATTTTCTGATCTGGTCAACGAACAGA
TACAGCATACGTTTTTGATCCCGCGAGAGACTATATGCCGCCTCAGTGAGGTCGTT
TGACTGGACGATTCGCGGGCTATTTTTACGTTTCTTGTGATTGATAACCGCTGTTTC
CGCCATGACAGATCCATGTGAAGTGTGACAAGTTTTTAGATTGTCACACTAAATAAA
AAAGAGTCAATAAGCAGGGATAACTTTGTGAAAAAACAGCTTCTTCTGAGGGCAATT
TGTCACAGGGTTAAGGGCAATTTGTCACAGACAGGACTGTCATTTGAGGGTGATTT
GTCACACTGAAAGGGCAATTTGTCACAACACCTTCTCTAGAACCAGCATGGATAAA
GGCCTACAAGGCGCTCTAAAAAAGAAGATCTAAAAACTATAAAAAAAATAATTATAAA
AATATCCCCGTGGATAAGTGGATAACCCCAAGGGAAGTTTTTTCAGGCATCGTGTG
TAAGCAGAATATATAAGTGCTGTTCCCTGGTGCTTCCTCGCTCACTCGAGGGCTTC
GCCCTGTCGCTCGACTGCGGCGAGCACTACTGGCTGTAAAAGGACAGACCACATC

ATGGTTCTGTGTTCATTAGGTTGTTCTGTCCATTGCTGACATAATCCGCTCCACTTC
AACGTAACACCGCACGAAGATTTCTATTGTTCCTGAAGGCATATTCAAATCGTTTTC
GTTACCGCTTGCAGGCATCATGACAGAACACTACTTCCTATAAACGCTACACAGGC
TCCTGAGATTAATAATGCGGATCTCTACGATAATGGGAGATTTTCCCGACTGTTTCG
TTCGCTTCTCAGTGGATAACAGCCAGCTTCTCTGTTTAACAGACAAAAACAGCATAT
CCACTCAGTTCCACATTTCCATATAAAGGCCAAGGCATTTATTCTCAGGATAATTGTT
TCAGCATCGCAACCGCATCAGACTCCGGCATCGCAAACTGCACCCGGTGCCGGGC
AGCCACATCCAGCGCAAAAACCTTCGTGTAGACTTCCGTTGAACTGATGGACTTAT
GTCCCATCAGGCTTTGCAGAACTTTCAGCGGTATACCGGCATACAGCATGTGCATC
GCATAGGAATGGCGGAACGTATGTGGTGTGACCGGAACAGAGAACGTCACACCGT
CAGCAGCAGCGGCGGCAACCGCCTCCCCAATCCAGGTCCTGACCGTTCTGTCCGT
CACTTCCCAGATCCGCGCTTTCTCTGTCCTTCCTGTGCGACGGTTACGCCGCTCCA
TGAGCTTATCGCGAATAAATACCTGTGACGGAAGATCACTTCGCAGAATAAATAAAT
CCTGGTGTCCCTGTTGATACCGGGAAGCCCTGGGCCAACTTTTGGCGAAAATGAGA
CGTTGATCGGCACGTAAGAGGTTCCAACTTTCACCATAATGAAATAAGATCACTACC
GGGCGTATTTTTTGAGTTATCGAGATTTTCAGGAGCTAAGGAAGCTAAAATGGAGAA
AAAAATCACTGGATATACCACCGTTGATATATCCCAATGGCATCGTAAAGAACATTT
TGAGGCATTTCAGTCAGTTGCTCAATGTACCTATAACCAGACCGTTCAGCTGGATAT
TACGGCCTTTTTAAAGACCGTAAAGAAAAATAAGCACAAGTTTTATCCGGCCTTTATT
CACATTCTTGCCCGCCTGATGAATGCTCATCCGGAATTCCGTATGGCAATGAAAGA
CGGTGAGCTGGTGATATGGGATAGTGTTCACCCTTGTTACACCGTTTTCCATGAGC
AAACTGAAACGTTTTCATCGCTCTGGAGTGAATACCACGACGATTTCCGGCAGTTTC
TACACATATATTCGCAAGATGTGGCGTGTTACGGTGAAAACCTGGCCTATTTCCCTA
AAGGGTTTATTGAGAATATGTTTTTCGTCTCAGCCAATCCCTGGGTGAGTTTCACCA
GTTTTGATTTAAACGTGGCCAATATGGACAACTTCTTCGCCCCCGTTTTCACCATGG
GCAAATATTATACGCAAGGCGACAAGGTGCTGATGCCGCTGGCGATTCAGGTTCAT
CATGCCGTTTGTGATGGCTTCCATGTCGGCAGAATGCTTAATGAATTACAACAGTAC
TGCGATGAGTGGCAGGGCGGGGCGTAATTTTTTTAAGGCAGTTATTGGTGCCCTTA
AACGCCTGGTTGCTACGCCTGAATAAGTGATAATAAGCGGATGAATGGCAGAAATT
CGATGATAAGCTGTCAAACATGAGAATTGGTCGACGGCCCTAACCC

Fig S6C. The complete sequence of the single-copy plasmid containing the Repressilator, as determined by sequencing.

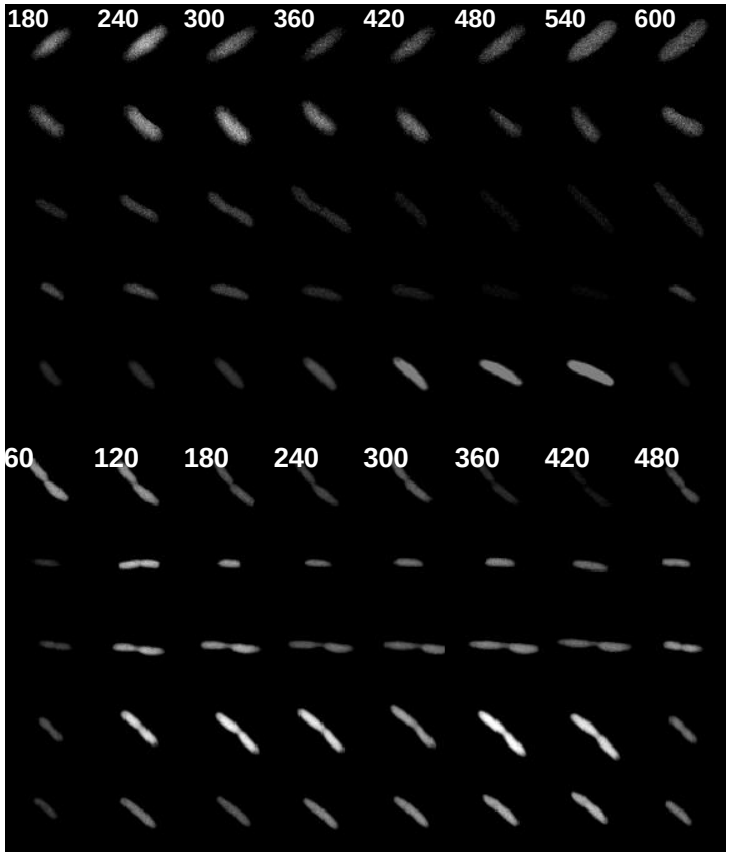

Fig S7. Example images of cells at 30 °C exhibiting oscillatory fluorescence levels. For each cell, 8 frames are shown along with the time after starting the imaging in minutes. From top to bottom, the first 5 cells contain a LCR while the last 5 cells contain a SCR.

Tampereen teknillinen yliopisto
PL 527
33101 Tampere

Tampere University of Technology
P.O.B. 527
FI-33101 Tampere, Finland

ISBN 978-952-15-3560-4
ISSN 1459-2045